Development of Polymeric Porous Scaffolds Using an Ice Particulate Template for Tissue Engineering

Young-Gwang Ko
(Doctoral Program in *Materials Science and Engineering*)

Submitted to the Graduate School of
Pure and Applied Sciences
in Partial Fulfillment of the Requirements
for the Degree of Doctor of Philosophy in
Engineering

at the
University of Tsukuba

Content

List of abbreviations

ANOVA	Analysis of variance
ATR-FT-IR	Attenuated total reflection-fourier transform-infrared spectroscopy
DAPI	4',6-diamidino-2-phenylindole
DMEM	Dulbecco's modified eagle medium
ECM	Extracellular matrix
EDTA	Ethylenediaminetetraacetic acid
FBS	Fetal bovine serum
GA	Glutaraldehyde
GAG	Glycosaminoglycan
HA	Hyaluronic acid
HE staining	Hematoxylin and eosin staining
hEGF	Human epidermal growth factor
HEPES	N-2-hydroxyethylpiperazine-N'-2-ethanesulfonic acid
hFGF-B	Human recombinant fibroblast growth factor-basic
NHDF	Neonatal human dermal fibroblast
PBS solution	Phosphate buffered saline solution
PCL	Polycaprolactone
PFA film	Perfluoroalkoxy film
PGA	Poly(glycolic acid)
PLA	Poly(lactic acid)
PLGA	Ploy(lactic-co-glycolic acid)
PLLA	Poly(L-lactic acid)
PVDC film	Polyvinylidene chloride film
SD	Standard deviation
SEM	Scanning electron microscope
WSC	Water-soluble carbodiimide
WST-1 reagent	Water-soluble tetrazolium salt-1 reagent

Chapter 1

General introduction

1.1 Tissue engineering

Tissue engineering has been developed as one of the most promising alternative therapies to the conventional drug administration, artificial prosthesis and organ transplantation. Tissue engineering involves the expansion of cells from a small biopsy, followed by culturing of the cells in temporary three-dimensional scaffolds to form the new tissues or organs.

1.1.1 Background of tissue engineering

Medicine of modern age provides effective therapy for diseases and defects using advanced medical technology. Although their therapeutic advances provide many successful results, there are still some limitations. First, severely damaged tissues can not be regenerate to normal function completely. For example, failure of tissues from extensive burn and big accidents result in difficulty of full recovery. Second, transplantation of tissues or organs for patients is limited because of shortage of donors. Numerous patients die each year while waiting for organ transplantation due to lack of donor organs and efficient substitutes. Third, infection and device rejection from artificial replacements are also serious concerns after surgical operations. Therefore, new approaches are required to solve these problems. The emerging field of tissue engineering may help to solve these problems. Engineered tissues are effective, unlimited and biocompatible [1,2].

The origin of the term “tissue engineering”, and of the concept can be traced to bioengineering pioneer Y.-C. Fung of the University of California at San Diego (UCSD), who led the UCSD team that submitted an unsuccessful proposal to the National Science Foundation (NSF) in 1985 for an Engineering Research Center Program award under the title “Center for the Engineering of Living Tissues”. Fung proposed the term again at a 1987 panel meeting that was considering future directions for the NSF’s Directorate for Engineering Bioengineering and Research to Aid the Handicapped Program, strong interest in the concept within NSF led to a special panel meeting on tissue engineering at NSF in the fall of 1987 and then to the Lake Granlibakken, CA workshop of 1988, the first formal scientific meeting of this emerging field. This workshop, and succeeding symposia in 1990 and 1992, helped “seed” the scientific literature with this new concept. More widespread awareness of the term tissue engineering appears to have followed with the 1993 publication of a review article in *Science* by Robert Langer and Joseph Vacanti, a paper which cites, among others,

funding support from NSF [3-5].

The definitions of the concept presented in the published proceedings of the Granlibakken workshop and in the Langer and Vacanti review have provided the framework within which most researchers who published later have situated their work. Langer and Vacanti defined tissue engineering as "an interdisciplinary field that applies the principles of engineering and life sciences toward the development of biological substitutes that restore, maintain, or improve tissue function", and identified three general strategies employed in tissue engineering: use of isolated cells or cell substitutes, use of tissue-inducing substances, and use of cells placed on or within matrices. However, actual usage of the term reflects an ongoing ambiguity in scope and focus, notably with respect to how far applications can stray into purely molecular (rather than cellular) approaches and still be considered tissue engineering, and with respect to the role of hybrid and external organ replacement devices [4].

1.1.2 Main factors of tissue engineering

Tissue engineering aims to develop biomedical substitutes to replace or to regenerate damaged tissues or organs by combination of cells, scaffolds and growth factors using biology and engineering principles as shown in Figure 1.1. Tissue engineering is an interdisciplinary research that combines (1) cell biology for analysis of cellular functions such as differentiation and growth, (2) immunology and molecular genetics for design of cells in acceptable immune system, (3) materials science for cell attachment and support of cellular matrix during spreading and tissue formation of desired shapes, (4) engineering of the scaffold fabrication for a biomimic porous structure. The fabrication process of a scaffold is crucial factor for successful cell distribution and tissue formation, (5) controlled release system of bioactive molecular is an additional factor, (6) design of cell culture environment is key point of three-dimensional tissue regeneration such as a dynamic seeding method and a bioreactor system.

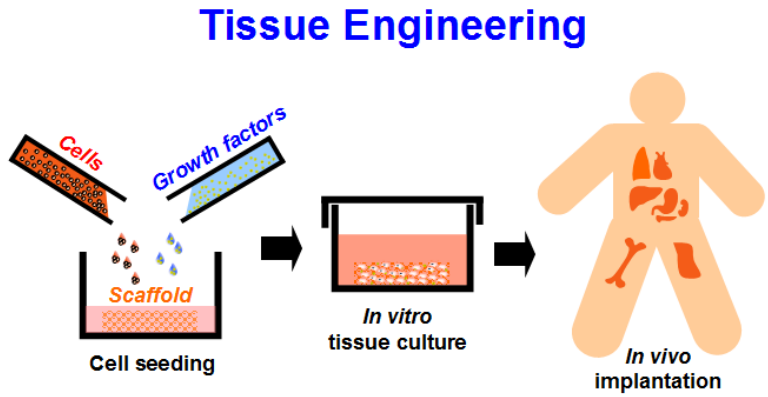

Figure 1.1 The basic concept of tissue engineering based upon the scaffold guided tissue regeneration. This method involves seeding cells in a porous scaffold with growth factors, then in vitro culturing to reconstruct new tissues and organs for in vivo implantation.

1.1.2.1 Cells

Tissue engineering utilizes living cells as engineering materials. Examples include using living fibroblasts in

skin replacement or repair, living chondrocytes in cartilage replacement or repair, or other types of cells used in other ways. Beginning to engineer a tissue or organ, a type of cell should be considered for specific function of substitutes. Quantity, pathogens and contamination of cells are ensured as well as decision of the cell source that is autologous, allogeneic, xenogeneic before design of experiments. As shown in Table 1.1, each cell source has their origin. Cells are often categorized by their source: autologous cells are obtained from the same individual to which they will be reimplanted. Autologous cells have the fewest problems with rejection and pathogen transmission, however in some cases might not be available. For example, in genetic disease suitable autologous cells are not available. Also very ill or elderly persons, as well as patients suffering from severe burns, may not have sufficient quantities of autologous cells for tissue engineering. Moreover, since this category of cells needs to be harvested from the patient, there are also some concerns related to the necessity of performing such surgical operations that might lead to donor site infection or chronic pain. Autologous cells also must be cultured from biopsies before they can be used, this takes time, so autologous solutions may not be very quick. Recently there has been a trend towards the use of autologous mesenchymal stem cells (MSCs) from bone marrow and fat. These cells can differentiate into a variety of tissue types, including bone, cartilage, fat, and nerve. A large number of cells can be easily and quickly isolated from fat, thus opening the potential for large numbers of cells to be quickly and easily obtained. Allogeneic cells come from the body of a donor of the same species. While there are some ethical constraints to the use of human cells for in vitro studies, the employment of dermal fibroblasts from human foreskin has been demonstrated to be immunologically safe and thus a viable choice for tissue engineering of skin. Xenogenic cells are these isolated from individuals of another species. In particular, animal cells have been used quite extensively in experiments aimed at the construction of cardiovascular implants. Syngenic or isogenic cells are isolated from genetically identical organisms, such as twins, clones, or highly inbred research animal models. However, there is considerable interest in the use of embryonic stem (ES) cells as a primary source for regeneration of tissues. This approach has made rapid progress in regenerative medicine. In addition, induced pluripotent stem (iPS) cells that are a type of pluripotent stem cell artificially derived from a non-pluripotent cell, typically an adult somatic cell, by inducing a "forced" expression of certain genes have been invented by Shinya Yamanaka's team at the Kyoto University. Stem cells are undifferentiated cells with the ability to divide in culture and give rise to different forms of specialized cells. According to their source, stem cells are divided into "adult" and "embryonic" stem cells, the first class being multipotent and the latter mostly pluripotent, some cells are totipotent, in the earliest stages of the embryo. While there is still a large ethical debate related with the use of embryonic stem cells, it is thought that stem cells may be useful for the repair of diseased or damaged tissues, or may be used to grow new organs. There are about 210 known distinct human cell types. To regenerate full function of tissues, however, it is necessary to understand how stem cell differentiates into a specific cell and development of cell population technology for clinical application and cell delivery technology to targeted area on time [1,2].

Table 1.1 Description of cell source

Source	**Description**
Autologous	from the same individual (patient's own cell)
Allogeneic	from the body of a donor of the same species
Xenogeneic	from individuals of another species
Syngenic	from genetically identical organisms, such as twins, clones, or highly inbred research animal models

1.1.2.2 Scaffolds

A second factor for tissue engineering is a three-dimensional architecture that is mimicked native microenvironment for implantation or seeding cells into an artificial structure. The design and engineering of scaffold should be considered carefully for each specific tissue. Scaffolds have critical interrelationship of effect on functions of cells and tissues. The scaffolds provide a three-dimensional structure for cell adhesion, proliferation, differentiation, and secretion of extracellular matrices to guide new tissue formation and regeneration. An ideal scaffold should meet the requirements as shown in Figure 1.2. The requirements include biocompatibility, biodegradability, suitable surface property, biochemical property, biomechanical property, 3D porous structure with adequate pore size to facilitate cell seeding, high interconnectivity and open surface pore structure [5].

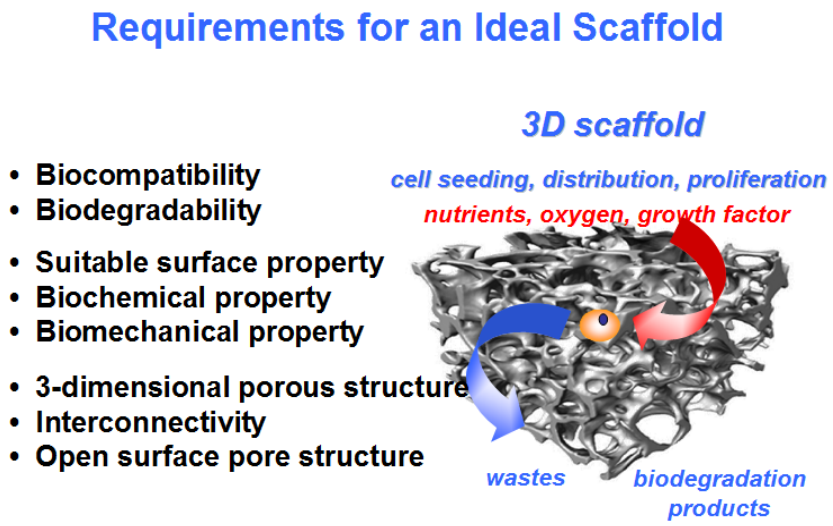

Figure 1.2 Requirements for an ideal scaffold upon scaffold guided tissue engineering.

1.1.2.3 Growth factors

A third factor is growth factors to control cell growth and differentiation. To realize this issue, bioactive molecules can be introduced in cell culture system or in a scaffold as a chemical immobilization. Growth factors are proteins that bind to receptors on the cell surface, with the primary result of activating cellular proliferation and/or differentiation. Many growth factors are quite versatile, stimulating cellular division in numerous different cell types, while others are specific to a particular cell-type. The common growth factors include vascular endothelial cell growth factor (VEGF: stimulates the growth of new blood vessels), fibroblast growth factor (FGF: protein is associated with the ECM and promotes proliferation of many cells), epithelial cell growth factor (EGF: promotes proliferation of mesenchymal, glial and epithelial cells), transforming growth factor beta (TGF-beta: suppresses cytokine production, promotes wound healing, inhibits macrophage and lymphocyte proliferation), keratinoctye growth factor (KGF), hepatocyte growth factor (HGF), platelet derived growth factor (PDGF: promotes proliferation of connective tissue, glial and smooth muscle cells) and bone morphogenetic protein (BMP) etc. These growth factors tend to exist in multiple isoforms, each with its specific biological activity. Purified forms of growth factor and biological peptides have

been investigated in recent years as therapeutic treatments of stimulating blood vessel formation, inhibiting blood vessel and so on. However, this therapeutic approach has struggled with determination and delivery of optimal dose, the ability to sustain and localize the growth factor release at the desired site, and the inability to turn on and off as needed during the tissue repair. The other approach is physical stimulation of cell-scaffold construct as native environment [2].

1.2 Design of three-dimensional scaffolds

A scaffold was focused on this study among three factors of tissue engineering due to its importance upon scaffold guided tissue regeneration. Three-dimensional scaffolds serve as temporary substrates for supporting and guiding tissue formation in various in vitro and in vivo tissue regeneration. Recent years have seen the emergence of scaffolds designed explicitly to control various aspect of the tissue formation process. This section summarizes current scaffold design approaches and essential principles that can guide the rational multifunctional design for tissue engineering [5-19].

1.2.1 Biocompatibility

The definition of biocompatibility is the ability of a material to perform with an appropriate host response in a specific application. In general, the scaffold should be fabricated from a highly biocompatible material which does not have the potential to elicit an immunological or clinically detectable primary or secondary foreign body reaction. The scaffold for tissue engineering requires biocompatibility. The biocompatibility of a scaffold or matrix for tissue-engineering products refers to the ability to perform as a substrate that will support the appropriate cellular activity, including the facilitation of molecular and mechanical signaling systems, in order to optimize tissue regeneration, without eliciting any undesirable effects in those cells, or inducing any undesirable local or systemic responses in the eventual host.

1.2.2 Biodegradability

Biodegradation means gradual breakdown of a material mediated by specific biological system. A polymer scaffold material should be chosen to degrade at a controlled rate to match the tissue regeneration speed as the specific tissue cells seeded into the three-dimensional construct attach, spread and increase in quantity (number of cells/per void volume) as well as in quality. Tissue engineering scaffolds serve a temporary device to facilitate tissue regeneration process. The scaffold of cell construct should be degraded according to filling the void space of artificial matrix completely. Their degradation byproducts also should be nontoxic and adsorbed completely.

1.2.3 Biochemical property

Cells interact with scaffolds primarily through the material surface, which can be dominated by the surface chemical and topological features. The surface chemistry is dictated by the biochemical compositions of the bulk and substances resulting from the surface adsorption or chemical reactions. Besides mediating cell behavior and functions inside scaffolds, controlled surface properties are of central importance in directing the inflammatory and immunological responses. Controlled surface properties may be useful for ameliorating the foreign-body reaction at the host-scaffold interaction in vivo.

1.2.4 Biomechanical property

The scaffold should have appropriate biomechanical property to support proliferated cells and extra cellular matrix. Weak scaffold has difficulty of handling and serious deformation of shape. It is important to determine if constructs are capable of withstanding the forces associated with locomotion in vivo, and whether construct properties compare to the corresponding native tissue. Optimized mechanical property of a scaffold as defined microenvironments depends on specified tissues. Because tissues of the human body have specific mechanical properties ranging from soft (brain, about 0.5 kPa), to moderately stiff (skin and muscles, around 10 kPa) and stiff (precalcified bone, >30 kPa). For tissue engineering approach in which cells must re-synthesize a functional ECM within a scaffold, the mechanical property of the construct will indicate whether the native structure is being replicated.

1.2.5 Pore architecture

Pore structure and interconnectivity should be controllable in reproducible manner. Specific scaffolds have proper pore size, interconnectivity and specific morphology. Pore morphology relates to porosity and surface area. Most of cells need enough area for cell spreading and enough space for nutrient delivery and transportation of metabolic wastes. Optimal pore sizes exist for regenerating specific types of tissues. Open and interconnected porous structures are required for smooth cell seeding and uniform cell distribution in the scaffolds for functional tissue engineering. Partially closed surface pore structures inhibit cell penetration into the inner body of the scaffolds and result in uneven cell distribution. On the other hand, straight-through pore structures present the problems of cell leakage and low cell loading in the scaffolds. The creation of a porous structure that can facilitate both cell seeding and cell distribution is highly desirable.

1.2.6 Mass transportation and vascularization

For the long term cell culture and tissue engineering of large and complex tissues, channels of mass transportation and vascularization are necessary. Difficulty in nutrient and oxygen diffusion will result in necrosis of inner tissue. For this reason, well designed channels are required to engineer large and complex tissues.

1.3 Biomaterials used for scaffold fabrication

Biomedical materials can be divided into three main types governed by the tissue response. In broad terms, inert (more strictly, nearly inert) materials illicit no or minimal tissue response. Active materials encourage bonding to surrounding tissue with, for example, new bone growth being stimulated. Degradable, or resorbable materials are incorporated into the surrounding tissue, or may even dissolve completely over a period of time. Metals are typically inert, ceramics may be inert, active or resorbable and polymers may be inert or resorbable [1,2]. However, these materials can also induce inflammation when the scaffold is implanted in the body sometimes.

The selection of biomaterials plays a key role in the design and development of tissue engineering product. While the classical selection criterion for a safe, stable implant dictates choosing a passive, inert materials, it is now understood that any such device will elicit a cellular response. It is important for tissue engineering product developer to have several biomaterials options available for each application cells under a unique environment. Such applications include (1) support for new tissue growth such as cell-cell communication and availability to nutrients, growth factors

and pharmaceutically active agents, (2) prevention of cellular activity such as surgically induced adhesion, (3) guided tissue response, (4) enhancement of cell attachment and subsequent cellular activation with cell proliferation and ECM production, (5) inhibition of cellular attachment or activation such as platelet attachment to a vascular graft, (6) prevention of a biological response such as blocking antibodies against homograft or xenograft cells used in organ replacement therapies.

1.3.1 Natural polymers

Polymeric materials are extensively used for their flexibility and stability, but have also been used for low friction articulating surfaces. Biodegradable polymers are applicable to those of tissue engineering products which tissue repair or remodeling is the goal, but no where long-term materials stability is required.

Collagen is a major component of mammalian connective tissue, animal protein, accounting for approximately 30% of all protein in the human body. There are 29 types of collagen. Over 90% of the collagen in the body is type I, II, III, and IV. Types I, II and III are the most abundant and form fibrils of similar structure. Type IV collagen forms a two-dimensional reticulum and is a major component of the basal lamina. Type I collagen is most abundant source for isolation from mammalian that is found in tendons, skin, artery walls, the endomysium of myofibrils, fibrocartilage, and the organic part of bones and teeth. However type II collagen is the most abundant collagen in articular cartilage. Type I collagen sponges retain better mechanical integrity than type II collagen materials. Type I collagen can serve good substrate for cell attachment and growth because of extensive integrin-binding domains (ligands). Type Ⅰ collagen has been used extensively in the formation of biomedical materials due to superior biocompatibility.

Glycosaminoglycan (GAG), which consists of repeating disaccharide units in linear arrangement, usually includes an uronic acid component (glucuronic acid) and hexosamin component (N-acetyl-D-glucosamin). The predominant types of GAGs attached to naturally occurring core proteins of proteoglycans include chondroitin sulfate, dermatan sulfate, keratan sulfate, and heparan sulfate. The GAGs are attached to the core protein by specific carbohydrates sequences containing three or four monosaccharides.

Chitosan is a natural cationic polymer (positive charge) that is a linear amino polysaccharide composed of approximately 20% β-1,4-linked N-acetyl-D-glucosamine and approximately 80% β-1,4-linked D-glucosamine prepared by the partial deacetylation of chitin in hot alkali. Chitosan has been studied for tissue engineering applications because of its biocompatibility, biodegradability, antibacterial property, reactive groups.

Hyaluronic acid (HA) is a hydrophilic and natural glycosaminoglycan that is found in human skin, cartilage, intra-articular joint fluid and vitreous humor. It is one of the base connective materials in extracellular matrix. HA plays an important role in the lubrication of soft tissues, cushion cells, water absorbance, cell differentiation, migration and cell growth. HA-based scaffolds have been widely used in the tissue engineering of skin, cartilage tissue, bone and soft tissue filler. The other natural polymers are silk fibroin, gelatin, alginate etc.

1.3.2 Synthetic polymers

A commonly used synthetic material is poly(lactic acid) (PLA). This is polyester which degrades within the human body to form lactic acid, a naturally occurring chemical which is easily removed from the body. Similar materials are poly(glycolic acid) (PGA) and polycaprolactone (PCL), their degradation mechanism is similar to that of PLA, but they exhibit respectively a faster and a slower rate of degradation compared to PLA. Poly(lactic acid) or

polylactide (PLA) is a biodegradable, thermoplastic, aliphatic polyester derived from renewable resources, such as corn starch (in the U.S.) or sugarcanes (rest of world). Although PLA has been known for more than a century, it had only been of commercial interest some years ago, in light of its biodegradability. PLA is currently used in a number of biomedical applications, such as sutures, stents, dialysis media and drug delivery devices. It is also being evaluated as a material for tissue engineering. Because it is biodegradable, it can also be employed in the preparation of bioplastic, useful for producing loose-fill packaging, compost bags, food packaging, and disposable tableware.

Polyglycolide or Poly(glycolic acid) (PGA) is a biodegradable, thermoplastic polymer and the simplest linear, aliphatic polyester. It can be prepared starting from glycolic acid by means of polycondensation or ring-opening polymerization. PGA has been known since 1954 as a tough fiber-forming polymer. Owing to its hydrolytic instability, however, its use has initially been limited. Currently polyglycolide and its copolymers (poly(lactic-*co*-glycolic acid) with lactic acid, poly(glycolide-*co*-caprolactone) with ε-caprolactone, and poly (glycolide-*co*-trimethylene carbonate) with trimethylene carbonate) are widely used as a material for the synthesis of absorbable sutures and are being evaluated in the biomedical field. The traditional role of PGA as a biodegradable suture material has led to its evaluation in other biomedical fields. Implantable medical devices have been produced with PGA, including anastomosis rings, pins, rods, plates and screws. It has also been explored for tissue engineering or controlled drug delivery. Tissue engineering scaffolds made with polyglycolide have been produced following different approaches, but generally most of these are obtained through textile technologies in the form of non-woven meshes.

Polycaprolactone (PCL) is a biodegradable polyester with a low melting point of around 60°C and a glass transition temperature of about −60°C. PCL is prepared by ring opening polymerization of ε-caprolactone using a catalyst such as stannous octanoate. The most common use of polycaprolactone is in the manufacture of speciality polyurethanes. Polycaprolactones impart good water, oil, solvent and chlorine resistance to the polyurethane produced. PCL is degraded by hydrolysis of its ester linkages in physiological conditions (such as in the human body) and has therefore received a great deal of attention for use as an implantable biomaterial. In particular it is especially interesting for the preparation of long term implantable devices, owing to its degradation which is even slower than that of polylactide.

Poly(lactic-*co*-glycolic acid) (PLGA) has been frequently used to prepare medical devices, owing to its biodegradability and biocompatibility. PLGA has been successful as a biodegradable polymer because it undergoes hydrolysis in the body to produce the original monomers, lactic acid and glycolic acid. These two monomers under normal physiological conditions, are by-products of various metabolic pathways in the body. Since the body effectively deals with the two monomers, there is very minimal systemic toxicity associated with using PLGA for drug delivery or biomaterial applications. The other synthetic polymers as biomaterials are PHBV, PVA, PU, PS etc.

1.3.3 Ceramics

Ceramic biomaterials are generally used for their hardness and wear resistance for applications such as articulating surfaces in joints and in teeth as well as bone bonding surfaces in implants.

Hydroxylapatite, also called hydroxyapatite, is a naturally occurring mineral form of calcium apatite with the formula $Ca_5(PO_4)_3(OH)$, but is usually written $Ca_{10}(PO_4)_6(OH)_2$ to denote that the crystal unit cell comprises two entities. Hydroxylapatite is the hydroxyl endmember of the complex apatite group. Hydroxylapatite can be found in teeth and bones within the human body. Thus, it is commonly used as a filler to replace amputated bone or as a coating to promote bone ingrowth into prosthetic implants.

Tricalcium phosphate is a compound with formula $Ca_3(PO_4)_2$. It is also known as calcium orthophosphate, tertiary calcium phosphate, tribasic calcium phosphate, or "bone ash" (calcium phosphate being one of the main

combustion products of bone). It can be used as a tissue replacement for repairing bony defects when autogenous bone graft is not feasible or possible. It may be used alone or in combination with a biodegradable, resorbable polymer such as polyglycolic acid. It may also be combined with autologous materials for a bone graft.

The incorporation of a tricalciumphosphate (TCP), hydroxyapatite (HAp) and basic salts into a polymer matrix produces a hybrid/composite material. These inorganic fillers allow to tailor the desired degradation and resorption kinetics of the polymer matrix. A composite material would also improve biocompatibility and hard tissue integration in a way that ceramic particles, which are embedded into the polymer matrix, allow for increased initial flash spread of serum proteins compared to the more hydrophobic polymer surface. In addition, the basic resorption products of HA or TCP would buffer the acidic resorption by-products of the aliphatic polyester and may thereby help to avoid the formation of an unfavorable environment for the cells due to a decreased pH. The other ceramics are alumina, zirconia, carbon, etc.

1.3.4 Metals

Metallic biomaterials are used for load bearing applications and must have sufficient fatigue strength to endure the rigors of daily activity.

Titanium is a chemical element with the symbol Ti and atomic number 22. Sometimes called the “space age metal”, it has a low density and is a strong, lustrous, corrosion-resistant (including sea water, aqua regia and chlorine) transition metal with a silver color. Because it is biocompatible (non-toxic and is not rejected by the body), titanium is used in a gamut of medical applications including surgical implements and implants such as hip balls and sockets (joint replacement) that can stay in place for up to 20 years. Titanium has the inherent property to osseointegrate, enabling use in dental implants that can remain in place for over 30 years. This property is also useful for orthopedic implant applications.

316L stainless steel metallurgy, stainless steel, also known as inox steel or inox, is defined as a steel alloy with a minimum of 10.5 or 11% chromium content by mass. It is more resistant to general corrosion and pitting than conventional nickel chromium stainless steels such as 302-304. It has been used as surgical and medical tools, and surgical implants. The other metallic biomaterials are Co-Cr Alloys, Ti6Al4V etc.

1.4 Methods of scaffold fabrication

A number of different methods have been described in literature for preparing porous structures to be employed as tissue engineering scaffolds. Each of these techniques presents its own advantages, but none is devoid of drawbacks. This section reviews commonly used methods for scaffold fabrication (Figure 1.3-1.9) [5,20-26].

1.4.1 Solvent casting/particulate leaching

This technique was developed to control precious shape of scaffolds. This method to create pores involves the use of a water-soluble porogen such as salt and sugar. The first step in this process is to dissolve the polymer (PLLA or PLGA) in organic solvent such as chloroform or methylene chloride and then cast it onto a petri dish filled with the porogen. After evaporation of the solvent, the polymer/salt composite is leached in water to remove the porogen. The resulting scaffold porosity can be controlled by the amount of salt added, while the pore size is dependent on the size of the salt crystals. With 70 wt% salt and above, the pores exhibited high interconnectivity. Foams fabricated in this

manner have been used extensively with various cell types and have shown no adverse effects on new tissue formation. However, due to concerns that the side of the foam exposed to air had a different morphology (rougher) than that exposed to the petri dish, a modification of this technique has been developed. In this case, pieces of the polymer/salt composite are compression molded into cylindrical form at temperatures just above the melting (PLLA) or glass transition temperature (PLGA). The cylinder is then cut into discs of desired thickness before leaching in water. This allows more precise control of scaffold thickness and increases uniformity of the foam surface. However, thermal degradation of the polymer during the compression molding step could be a concern. With any solvent casting/particulate leaching procedure, organic solvents are used, which in many cases precludes the possibility of adding pharmacological agents to the scaffold during fabrication. Also, the leaching step for water-soluble porogens significantly increases the scaffold preparation time [20].

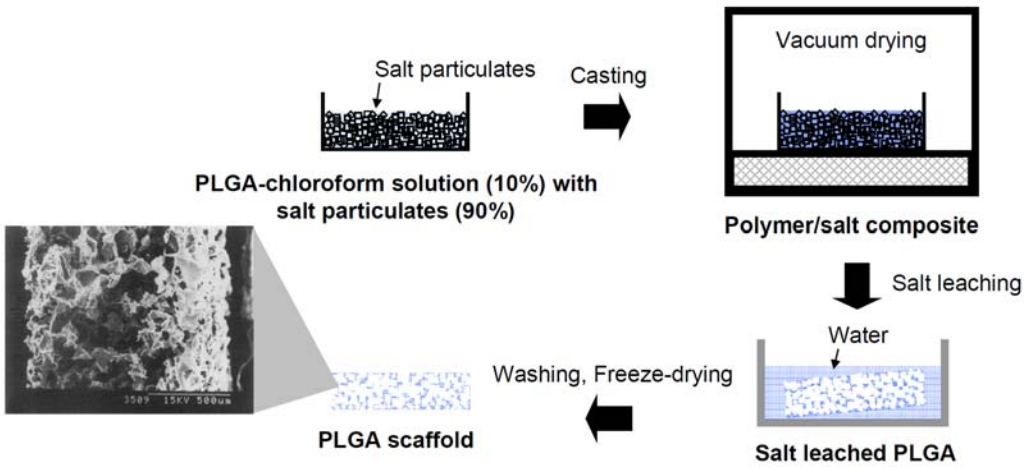

Figure 1.3 Schematic of solvent casting/salt leaching technique and the SEM image of a PLGA scaffold.

1.4.2 Freeze-drying

This method uses a principle of crystallization of solvent at freezing temperature to make pores. When preparing scaffolds by freezing followed by lyophilization, pore structure after drying is a replica of the ice crystal morphology after freezing. Therefore, the pore structure of the scaffold can be controlled directly using the employed freezing process and the heat transfer processes associated with it. Differences in heat transfer rates during the freezing process of the suspension have a great effect on the microstructure of the fabricated scaffolds. Sublimed ice crystals generate pores and sizes of pores are controlled by solution parameters such as freezing rate, temperature, concentration, alignment of ice crystals and additives (e.g, ethanol, acetic acid). Freeze-drying method is simple and reproducible. Scaffolds prepared by freeze-drying are highly interconnected pores with high porosity. This method has been applied for many biocompatible natural and synthetic polymers. However, surface pores are partially closed [21].

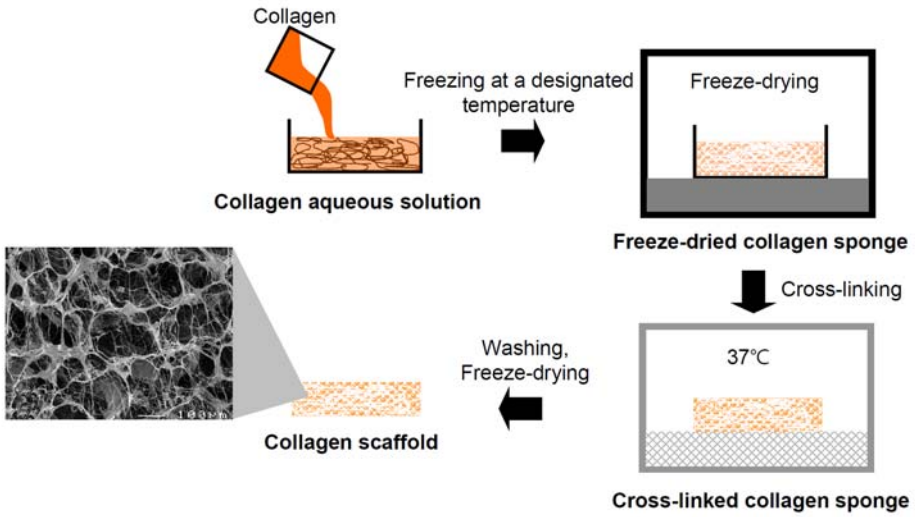

Figure 1.4 Schematic of freeze-drying technique and the SEM image of a collagen scaffold.

1.4.3 Phase separation

This method uses the principle of phase separation of two solid. In brief, a biocompatible polymer such as PLGA is dissolved in an appropriate solvent. While stirring, the bioactive molecules are added and dispersed into a homogeneous mixture and cooled below the solvent melting point until the liquid phase separate. The polymer and solvent are quenched with liquid nitrogen, resulting two-phase solid. The solvent is removed by sublimation, which yields a porous scaffold with bioactive molecules embedded inside the polymer. Porosity and structure are affected by the cooling rate and the melting temperature of the solvent relative to the polymer [22].

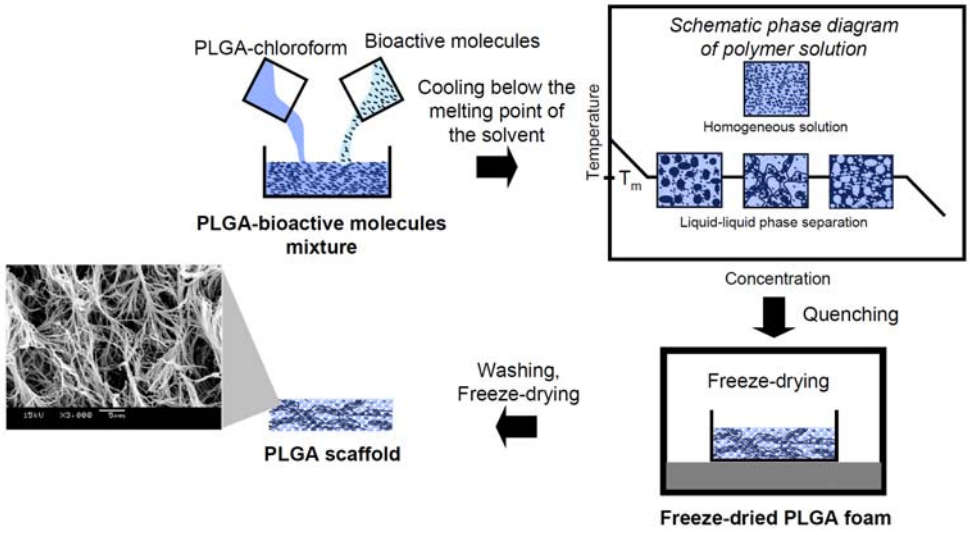

Figure 1.5 Schematic of phase separation technique and the SEM image of a PLLA scaffold.

1.4.4 Gas foaming

This method uses gas to form porous structure instead of organic solvent systems. Briefly, compressed polymer blocks are placed in high pressure CO_2 to saturate the polymer with gas. A thermodynamic instability then was created by decreasing the gas pressure to ambient pressure. This led to the nucleation and growth of CO_2 pores within the polymer matrices as the amount and rate of pressure. This method requires no leaching step and uses no harsh chemical solvents. But this method involves high temperature in the disk formation that prohibits the bioactive molecules and results in largely unconnected and closed surface pore structure. Incorporation of a particle leaching method on gas forming help to get opened pores on the surface of a scaffold [23].

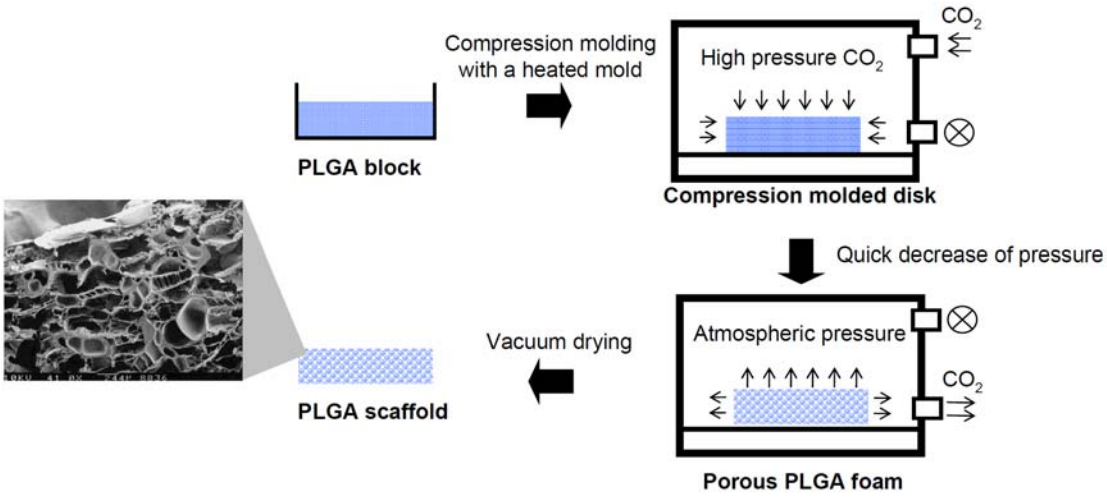

Figure 1.6 Schematic of gas foaming technique and the SEM image of a PLGA scaffold.

1.4.5 Electrospinning

This method uses electrostatic force to create nano- or microscale nonwoven fibers. It can be use to fabricate biomimetic scaffolds. Briefly, the instruments consisted of high-voltage power supply, a syringe pump and collector units. Polymers are dissolved in appropriate solvent. The polymer solution is loaded in a syringe attached metal capillary at a constant feeding rate by a syringe pump. High voltage generator is connected to metal capillary and grounded collecting surface. When the electric force is reached to appropriate value, charged polymer solution form spinning jet to ground surface. At the same time, solvent evaporates. Thereby, ultrafine fibers could formed by the narrowing of the ejected jet fluid as it underwent increasing surface charge density due to evaporation of the solvent. Electrospun nanofibrous mats were carefully detached from the collector and dried in vacuum to remove the solvent molecules completely. Diameter of fibers is controlled by adjusting polymer concentration, solvent properties, feeding rate, applying voltage, capillary diameter, ground surface material, a distance between the capillary and the ground surface collector, and so on [24].

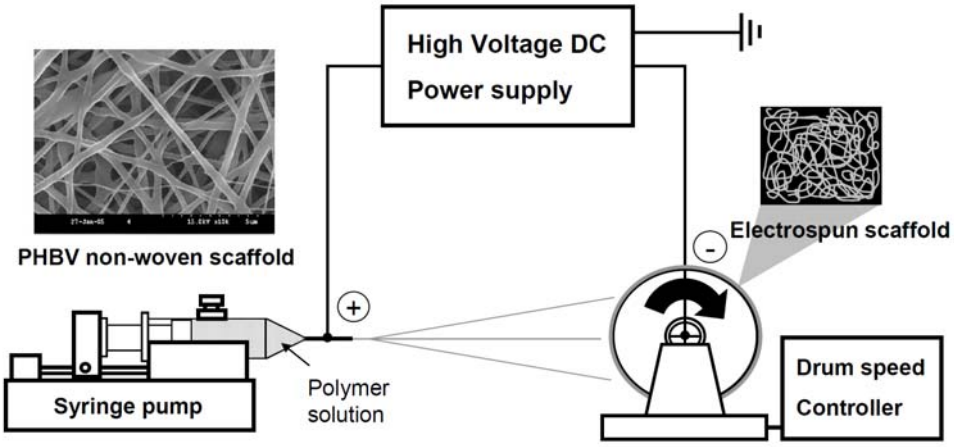

Figure 1.7 Schematic of electrospinning technique and the SEM image of a PHBV (poly(hydroxybutrate-co-hydroxyvalerate)) scaffold.

1.4.6 Fiber bonding

This method uses polymer fibers that have high surface area to volume ratio as a scaffold. Nonbonded fiber meshes do not have a proper mechanical integrity for in vivo tissue regeneration. To overcome this problem, fiber bonding method has been developed to bind the fibers together at points of intersection. In brief, PGA fibers are immersed in a PLLA solution. When the solvent evaporates, the network of PGA fibers is embedded in PLLA. The composite is then heated to above the melting temperature of both polymers. The PLLA melts first and fills all voids left by the fibers. This helps retain the spatial arrangement of fibers so that when the PGA begins to melt, the fiber structure does not collapse. Instead, in order to minimize interfacial energy, fibers at the cross-points become "welded" (melted) together, forming a highly porous foam. The PLLA is then removed by dissolution with methylene chloride [5]. This method improves the mechanical properties of fabric scaffolds. The fiber bonding scaffold fabrication technique is desirable for its simplicity, the retention of the fibers original properties, the use of only biocompatible materials and structural advantages. The disadvantages of fiber bonding are the shortage of control over porosity and pore size, the availability of suitable solvents, immiscibility of the two polymers in the melt state, and the required relative melting temperature of the polymers.

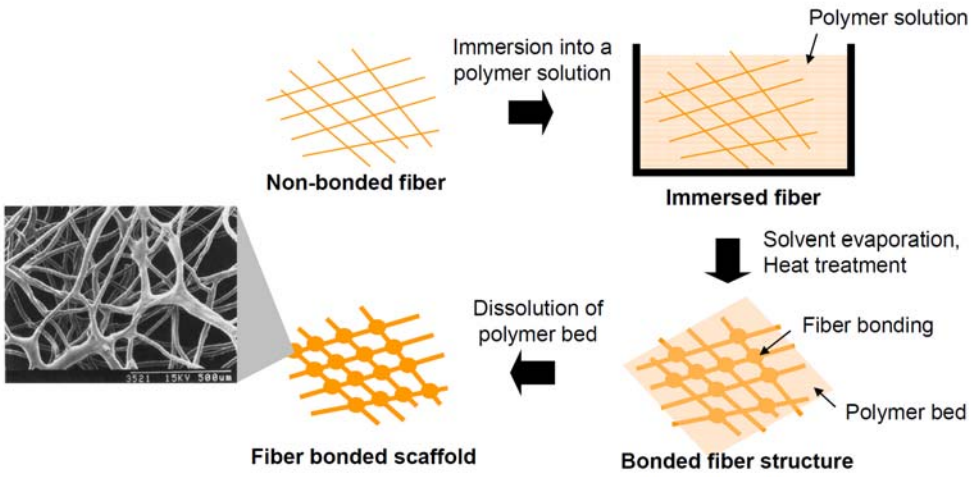

Figure 1.8 Schematic of fiber bonding technique and the SEM image of a PGA scaffold.

1.4.7 Prototyping

This method requires a computer model of the desired scaffold architecture from computer-assisted design (CAD) or computer tomography (CT). Prototyping technique results in a three-dimensionally accurate structure with a fully interconnected network of pores with complex architectures on the micron scale. Prototyping of solid free-form includes three-dimensional printing, laser sintering, and sterolithogarpy. A popular method of fabrication by rapid prototyping is sterolithography. It uses light to polymerize, cross-link, or harden a photosensitive material. Typically, a fine layer of a solution of biocompatible polymer, photo-cross-linkg initiating agent, porogen, and an appropriate solvent is placed beneath the laser. The CAD software guides the laser in the desired pattern for the designed scaffold. The laser's ultraviolet light reacts with photo-initiator to form chemical bonds between polymer chains in the specified locations. Subsequent layers of polymer solution are added and photo-cross-linked. The final product is washed to remove unreacted polymer and yield a three-dimensional structure with specific microarchitectures. Figure 1. 9 shows the schematic of three dimensional fiber deposition device consisting of three main components (1) a molten co-polymer dispensing unit consisting of a syringe and nozzle, (2) a positional control unit consisting of stepper-motor drivers linked to a personal computer containing software for generating a stepper motor driven, and (3) X-Y-Z table and fiber deposition paths. The molten polymer could be extrude from the nozzle with regulated pressure and displacement of polymer strands could be controlled by a custom deposition program via the printer port. By lowering the X-Y table one layer-step in the z-direction, successive layers of rapidly solidifying fibers were laminated to previous layers with 100% interconnecting pore volume. Fiber layers could be continuously deposited resulting in scaffolds up to 4mm thick [25,26].

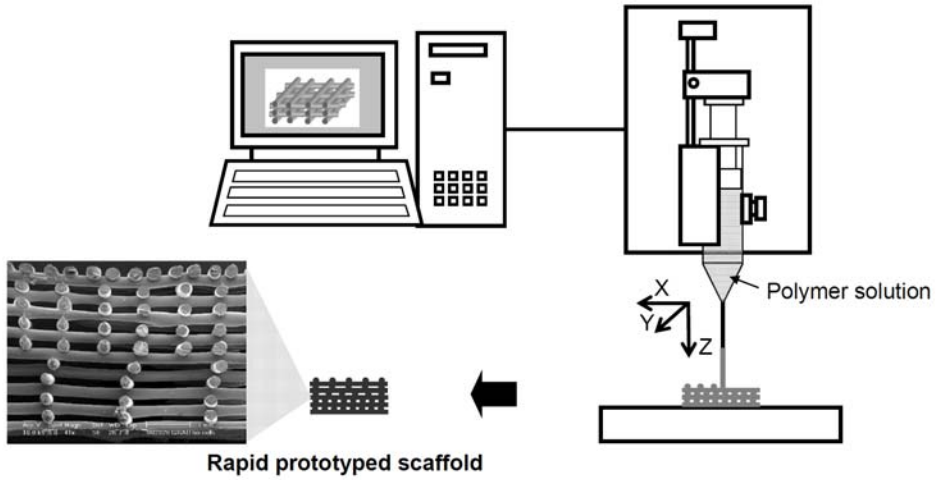

Figure 1.9 Schematic of rapid prototyping technique and the SEM image of a PEGT/PBT co-polymer scaffold.

1.5 Cell culture technique

After scaffold fabrication, cells should be implanted to the three-dimensional scaffolds. In this step, before cell seeding, we have to decide a cell type, dimension of a scaffold, culture dish, cell number, cell seeding method, cell culture environment and culture period. Design of cell culture is essential procedure in tissue engineering. In many cases, creation of functional tissues and biological structures in vitro requires extensive culturing to promote survival, growth and inducement of functionality. In general, the basic requirements of cells must be maintained in culture, which include oxygen, pH, humidity, temperature, nutrients and osmotic pressure maintenance. Tissue engineered cultures also present additional problems in maintaining culture conditions such as necrosis. In standard cell culture, diffusion is often the sole means of nutrient and metabolite transport. However, as a culture becomes larger and more complex, such as the case with engineered organs and whole tissues, other mechanisms must be employed to maintain the culture.

Another issue with tissue culture is introducing the proper signals or stimuli required to induce functionality. In many cases, simple maintenance culture is not sufficient. Growth factors, hormones, specific metabolites or nutrients, chemical and physical stimuli are sometimes required. For example, certain cells respond to changes in oxygen tension as part of their normal development, such as chondrocytes, which must adapt to low oxygen conditions or hypoxia during skeletal development. Others, such as endothelial cells, respond to shear stress from fluid flow, which is encountered in blood vessels [1,2].

1.6 Motivation and objective

Porous scaffolds play an important role in tissue engineering as a temporary support to cell adhesion, proliferation, and differentiation and to guide the formation of new tissues and organs into desired shape and complicated structures. Open surface pores and interconnected porous structures are required for smooth cell seeding and uniform cell distribution in the scaffolds for functional tissue engineering. The creation of a porous structure that

can facilitate both cell seeding and cell distribution is highly desirable. Scaffolds prepared by the methods listed in this chapter have various problems concerning the surface pores, interconnectivity and cell seeding efficiency. To solve these problems, development of an optimal scaffold design and new method for scaffold preparation is strongly required.

Therefore, we proposed new design as an innovative scaffold structure that having large sunken pores of top layer and highly interconnected inner bulk pores. And we developed a novel scaffold fabrication method by using embossed ice particulates as a template for preparation of a new type of three-dimensional open porous scaffolds to facilitate cell seeding, cell distribution and homogeneous tissue formation for tissue engineering. The ice particulate template was used as a porogen material due to several advantages. The ice particulate template can initiate the formation of a connected ice crystal network inside the aqueous polymer solution during the freezing process and the ice crystal network can be easily removed by lyophilization. The low temperature manipulation without usage of any organic solvents can preserve the biological activity of functional drugs and proteins incorporated in the scaffolds. The collagen, chitosan, hyaluronic acid and collagen-glycosaminoglycan were applied as polymeric materials for the preparation of open porous scaffolds by the ice particulate template method in each chapter. Subsequently, the pore structures, cell distribution, cell viability and tissue formation were characterized using respective scaffolds to discuss the effect of their pore structures and feasibility for tissue engineering.

1.7 References

1 Atala, A., Lanza, R., editors., Methods of tissue engineering. California:*Academic Press* (2002).

2 Lanza, R., Langer, R., Vacanti, J., editors., Principles of tissue engineering-3rd ed. MA:*Elsevier Academic Press*: 309-320 (2007).

3 Viola, J., Lal, B., Grad, O., The emergence of tissue engineering as a research field for The National Science Foundation. MA:*Abt Associates Inc*: 5-7 (2003).

4 Langer, R., Vacanti, J. P., Tissue engineering. *Science* **260**, 920-926 (1993).

5 Mikos, A. G., Temenoff, J. S., Formation of highly porous biodegradable scaffolds for tissue engineering. *Electronic J Biotech* **3**, 1-6 (2000).

6 O'Brien, F. J., Harley, B. A., Yannas, I. V., Gibson, L. J., The effect of pore size on cell adhesion in collagen-GAG scaffolds. *Biomaterials* **26**, 433-441 (2005).

7 Harley, B. A. C., Kim, H. D., Zaman, M. H., Yannas, I. V., Lauffenburger, D. A., Gibson, L. J., Microarchitecture of three-dimensional scaffolds influences cell migration behavior via junction interactions. *Biophysic J* **95**, 4013-4024 (2008).

8 Lu, Q., Ganesan, K., Simionescu, D. T., Vyavahare, N. R., Novel porous aortic elastin and collagen scaffolds for tissue engineering. *Biomaterials* **25**, 5227-5237 (2004).

9 Yannas, I. V., Burke, J. F., Gordon, P. L., Huang, C., Rubenstein, R. H., Design of an artificial skin. Ⅱ. Control of chemical composition. *J Biomed Mater Res* **14**, 107-131 (1980).

10 Dagalakis, N., Flinkt, J., Stasikelis, P., Burke, J. F., Yannas I. V. Design of an artificial skin. Part Ⅲ. Control of pore structure. *J Biomed Mater Res* **14**, 511-528 (1980).

11 Hiraoka, Y., Kimura, Y., Ueda, H., Tabata, Y., Fabrication and biocompatibility of collagen sponge reinforced with poly(glycolic acid) fiber. *Tissue Eng* **9**, 1101-1112 (2003).

12 Lee, M., Dunn, J. C. Y., Wu, B. M., Scaffold fabrication by indirect three-dimensional printing. *Biomaterials* **26**, 4281-4289 (2005).

13 Lee, S. J., Kim, S. Y., Lee, Y. M., Preparation of porous collagen/hyaluronic acid hybrid scaffolds for biomimetic

functionalization through biochemical binding affinity, *J Biomed Mater Res B* **82B**, 506-518 (2007).

14 Lien, S. M., Ko, L. Y., Huang, T. J., Effect of pore size on ECM secretion and cell growth in gelatin scaffold for articular cartilage tissue engineering. *Acta Biomater* **5**, 670-679 (2009).

15 Salem, A. K., Stevens, R., Pearson, R. G., Davies, M. C., Tendler, S. J. B., Roberts, C. J., et al., Interactions of 3T3 fibroblasts and endothelial cells with defined pore features. *J Biomed Mater Res* **61**, 212-217 (2002).

16 Chen, G., Sato, T., Ohgushi, H., Ushida, T., Tateishi, T., Tanaka, J., Culturing of skin fibroblasts in a thin PLGA-collagen hybrid mesh. *Biomaterials* **26**, 2559-2566 (2005).

17 Kumbar, S. G., Nukavarapu, S. P., James, R., Nair, L. S., Laurencin, C. T., Electrospun poly(lactic acid-co-glycolic acid) scaffolds for skin tissue engineering. *Biomaterials* **29**, 4100-4107 (2008).

18 Hollister, S. J., Porous scaffold design for tissue engineering. *Nature Mater* **4**, 518-590 (2005).

19 Atthoff, B., Aulin, C., Adelöw, C., Hilborn, J., Polarized protein membrane for high cell seeding efficiency. *J Biomed Mater Res B* **83B**, 472-480 (2007).

20 Mikos, A. G., Thorsen, A. J., Czerwonka, L. A., Bao, Y., Langer, R., Winslow, D. N., Vacanti, J. P., Preparation and characterization of poly(L-lactic acid) foams. *Polymer* **35**, 1068-1077 (1994).

21 Faraj, K. A., Kuppevelt, T. H. V., Daamen, W. F., Construction of collagen scaffolds that mimic the three-dimensional architecture of specific tissues. *Tissue Eng* **13**, 2387-2394 (2007).

22 Yang, F., Murugan, R., Ramakrishna, S., Wang, X., Ma, Y. X., Wang, S., Fabrication of nano-structured porous PLLA scaffold intended for nerve tissue engineering. *Biomaterials* **10**, 1891-1900 (2004).

23 Harris, L. D., Kim, B. S., Mooney, D. J., Open pore biodegradable matrices formed with gas foaming. *J Biomed Mater Res* **42**, 396-402 (1998).

24 Kwon, O. H., Lee, I. K, Ko, Y.-G., Meng, W., Jung, K.-H., Kang I.-K., Ito Y., Electrospinning of microbial polyester for cell culture. *Biomed Mater* **2**, 52-58 (2007).

25 Hsu, S. H., Yen, H. J., Tseng, C. S., Cheng, C. S., Tsai, C. L., Evaluation of the growth of chondrocytes and osteoblasts seeded into precision scaffolds fabricated by fused deposition manufacturing. *J Biomed Mater Res B* **80B**, 519-527 (2007).

26 Woodfield, T. B. F., Malda, J., de Wijn, J., Peters, F., Riesle, J., van Blitterswijk, C. A., Design of porous scaffolds for cartilage tissue engineering using a three-dimensional fiber-deposition technique. *Biomaterials* **25**, 4149-4161 (2004).

Chapter 2

Preparation of collagen sponges using an ice particulate template

2.1 Summary

In this chapter, preparation of the open porous collagen scaffolds using an ice particulate template was demonstrated. Preparation of scaffolds with controlled porous structures is very important for tissue engineering and regenerative medicine. A new type of collagen sponges was prepared by using embossing ice particulates as a template. The new collagen sponge had a hierarchical structure of large open pores on the top surface and interconnected small pores in the inner bulk body. The shape, size, and density of the surface large pores were determined by the ice particulates that were used as templates while the interconnected small pores were determined by the freezing temperature. The open and interconnected porous structure of the new collagen sponge facilitated cell seeding, cell penetration, and distribution throughout the scaffold, and accelerated the regeneration of new tissue. The use of ice particulates as a template will be a useful method for the creation of an open and interconnected porous structure.

2.2 Introduction

Porous scaffolds have broad application in tissue engineering and regenerative medicine. The scaffolds provide a three-dimensional structure for cell adhesion, proliferation, differentiation, and secretion of extracellular matrices to guide new tissue formation and regeneration [1-8]. Open and interconnected porous structures are required for smooth cell seeding and uniform cell distribution in the scaffolds for functional tissue engineering. Many methods have been developed to control the porous structures. They include particle leaching [9], freeze-drying [10,11], phase separation [12], gas foaming [13], electrospinning [14], fiber bonding [15], and rapid prototyping [16]. However, scaffolds prepared by the first five methods have the problem of partially closed surface pore structures that inhibit cell penetration into the inner body of the scaffolds and result in uneven cell distribution. Scaffolds prepared by the latter two methods have straight-through pore structures that present the problems of cell leakage and low cell loading in the scaffolds. The creation of a porous structure that can facilitate both cell seeding and cell distribution is highly desirable. This chapter introduces a novel method of using embossing ice particulates as a template to fabricate a new type of collagen sponge that has large open surface pores on its top surface and highly interconnected small pores beneath the top surface to facilitate cell seeding and cell distribution within the sponge for rapid tissue regeneration.

2.3 Materials and methods

2.3.1 Preparation of ice particulate template

An ice particulate template was prepared by forming water droplets on a copper plate and freezing them (Figure 2.1a). At first, a copper plate (width x height x thickness: 80 x 100 x 5 mm) was wrapped with perfluoroalkoxy (PFA) film (Universal Co., Ltd.). A silicone frame (inner dimension: width x height x thickness: 65 x 85 x 1 mm) was placed onto the PFA-wrapped copper plate to hold the collagen solution in the defined dimension. Subsequently, hemispheric water droplets were formed by spraying pure water onto the PFA film. The diameter of the water droplets could be controlled by the spraying times (10, 20, and 30 times). The diameter of the water droplets increased with an increase in the spraying time. The first two steps were carried out at room temperature. Finally, the set was frozen in a freezer (-30°C) for 5 hours to form embossing ice particulates on the PFA-wrapped copper plate. The ice-particulate template was moved to a low temperature chamber (WT-201, ESPEC Corp.) that was set at a designated temperature (-1, -3, -5, or -10°C) and kept for 1 hour to allow the ice-particulate template to reach the designated temperature before use.

2.3.2 Preparation of collagen sponges

The new-type collagen sponges were fabricated using the embossing ice particulates as templates (Figure 2.1). To investigate the effect of diameter of ice particulates on the porous structure, three types of templates with ice particulates of three different diameters were used and the freezing temperature was at -3°C. First, the temperature of the low-temperature chamber was set at -3°C. The ice particulate templates frozen at -30°C were moved to the low-temperature chamber and balanced for 1 hour. And then, a 1 mm-thick silicone frame was placed on the template to control the thickness of the loaded aqueous collagen solution. An aqueous solution of collagen (1.0 wt %, Nippon Meat Packers, Inc. Osaka, Japan) was poured onto the embossed ice template inside the silicone frame. The surface of the aqueous collagen solution was covered with a glass plate wrapped with polyvinylidene chloride film. The aqueous collagen solution was stored at -1°C for 24 hours for cooling before being poured onto the template. The temperature of the aqueous collagen solution should be set at a temperature that will not melt the embossing ice particulates and will not freeze the aqueous collagen solution. In this study, a temperature of -1°C was chosen. At this temperature, the aqueous collagen solution was in a supercooled state and did not freeze in the absence of a nucleating agent. The temperature of the low-temperature chamber was kept at -3°C to initiate the growth of ice crystals. The collagen aqueous solution and the templates were kept in the low-temperature chamber for 1 hour to allow the formation of ice crystals and then moved to a freezer of -80°C for 5 hours to ensure complete freezing of the aqueous collagen solution. The frozen collagen together with the ice particulates were then detached from the copper plate and PFA film, and freeze-dried for 24 hours in a freeze-drying machine (VirTis AdVantage Benchtop Freeze Dryers, SP Industries Incorporation). Finally, the freeze-dried collagen sponges were cross-linked by glutaraldehyde (GA) vapor that was saturated with 25% aqueous glutaraldehyde solution at 37°C in a closed box. The cross-linking lasted for 4 hours. After cross-linking, any non-reacted glutaraldehyde was removed from the collagen sponges by washing with pure water and the non-reacted aldehyde groups were blocked by treatment with 0.1M aqueous glycine solution. The collagen sponges were washed with pure water and freeze-dried again to obtain the new-type collagen sponges. Control collagen sponge was prepared by using the same procedure without use of the ice particulate template.

To investigate the effect of temperature on pore structure, a template with ice particulates 398 μm in diameter was used and the chamber temperature was set at -1, -3, -5, or -10°C. The freezing temperature was the same as the

chamber temperature. All the other conditions were the same as those stated above.

2.3.3 Scanning electron microscopy

The microstructures of the new-type collagen sponges and control collagen sponge were observed using a scanning electron microscope (SEM, JSM-5610, JEOL) at a 10 kV acceleration voltage. Specimens were coated with platinum by a sputter coater (ESC-101, Elionix) before observation. The mean pore diameter of the scaffolds was calculated by the equivalent area diameter equation for the measurement of polygonal pores using image analysis software (MetaVue, Universal Imaging Corp.). The equivalent area diameter (D) was calculated using the following formula: $D^2 = 4A/\pi$, where A is the pore area and π is the ratio of the circumference of a circle to its diameter. Three representative images of each specimen from three replicates were used for measuring pore diameters with more than 100 pores.

2.3.4 Cell culture and evaluation of cell seeding efficiency

Neonatal human dermal fibroblasts (NHDF, Cascade Biologics Incorporation) were used for the cell culture experiment. The fibroblasts were subcultured in 106S medium supplemented with 2 (v/v)% fetal bovine serum (FBS), 10 ng/mL human recombinant epidermal growth factor (hEGF), and 3 ng/mL human recombinant fibroblast growth factor-basic (hFGF-B). Cell culture was maintained in an incubator equilibrated with 5% CO_2 at 37°C. The fibroblasts were subcultured once after reaching confluence. The subcultured fibroblasts were harvested using HEPES buffer containing 0.025% (w/v) trypsin (2000 U/g) and 0.01% (w/v) EDTA. After being washed with the serum medium, the cells were suspended in the serum medium at a concentration of 2 x 10^6 cells/ml.

The new-type collagen sponge prepared with ice particulates 398 μm in diameter at -3°C and control collagen sponge were used for cell culture. The sponges were cut into disks (diameter: 16 mm) for cell culture. The collagen sponge disks were sterilized by 70% aqueous ethanol solution for 10 minutes and then rinsed three times with phosphate buffered saline (PBS) and once with cell culture medium. The sterilized collagen sponge disks were placed in the wells of 24-well cell culture plates. The cell suspension was dropped onto the collagen sponge disks (500 μL/disk) to seed the cells in each scaffold and incubated for 1 hour. After culture for 1 hour, the collagen sponge disks were transferred to new wells. The cells in the old medium and those that adhered to each of the old wells of the old 24-well cell culture plates were collected by trypsin treatment and counted. The cell number of each well was taken as the number of unattached cells. The difference between the number of seeded cells and number of unattached cells was considered as the number of attached cells held by the sponges. The cell seeding efficiency of each sponge was calculated by dividing the number of adhered cells by the number of seeded cells as following equation. To obtain averages and standard deviations, three sponge disks were used for the measurements.

$$\text{Percent cell seeding efficiency } (\%) = \left(\frac{N_s - N_u}{N_s}\right) \times 100,$$

where N_s is number of seeded cells and N_u number of unattached cells.

2.3.5 Analysis of cell adhesion and distribution

Cell adhesion and distribution in the collagen sponges were observed by a SEM. Cells were seeded in three pieces of each collagen sponge disk and incubated for 1 hour. The cell/sponge constructs were transferred to other dishes, rinsed three times with PBS, and fixed with 2.5% glutaraldehyde (GA) solution at room temperature for 1 hour. The fixed cells/scaffold constructs were washed three times with pure water. Next, they were frozen in a −10◦C chamber for 1 hour and a deep freezer (−80◦C) for another hour, and lyophilized in a freeze dryer for 24 hours. The dried samples were cross-sectioned and coated with platinum for SEM observation to examine cellular penetration and distribution in the scaffolds.

2.3.6 Viability evaluation

After culture in the new-type collagen sponge and control collagen sponge for 2 weeks, cell viability was evaluated using a live/dead assay kit (Cellstain-Double Staining Kit, Dojindo Laboratories, Tokyo, Japan). The constructs were washed three times with PBS and incubated in 2 μM calcein-AM (stain live cells) and 4 μM propidium iodide (PI) (stain dead cells) in serum-free DMEM for 40 min. The constructs were then immersed in serum-free medium in a 35 mm tissue culture dish after being rinsed with PBS. The staining was observed under a fluorescence microscope (BX51, Olympus Corp.).

2.3.7 Histological analysis

After the fibroblasts were cultured in the collagen sponges for 2 weeks, the regenerated tissues were washed with PBS and fixed in 10% neutral buffered formalin, embedded in paraffin, and sectioned (10 μm). The cross-sections were stained with hematoxylin and eosin to analyze cellular distribution and proliferation. They were mounted and then analyzed with an optical microscope (IX71, Olympus Corp.).

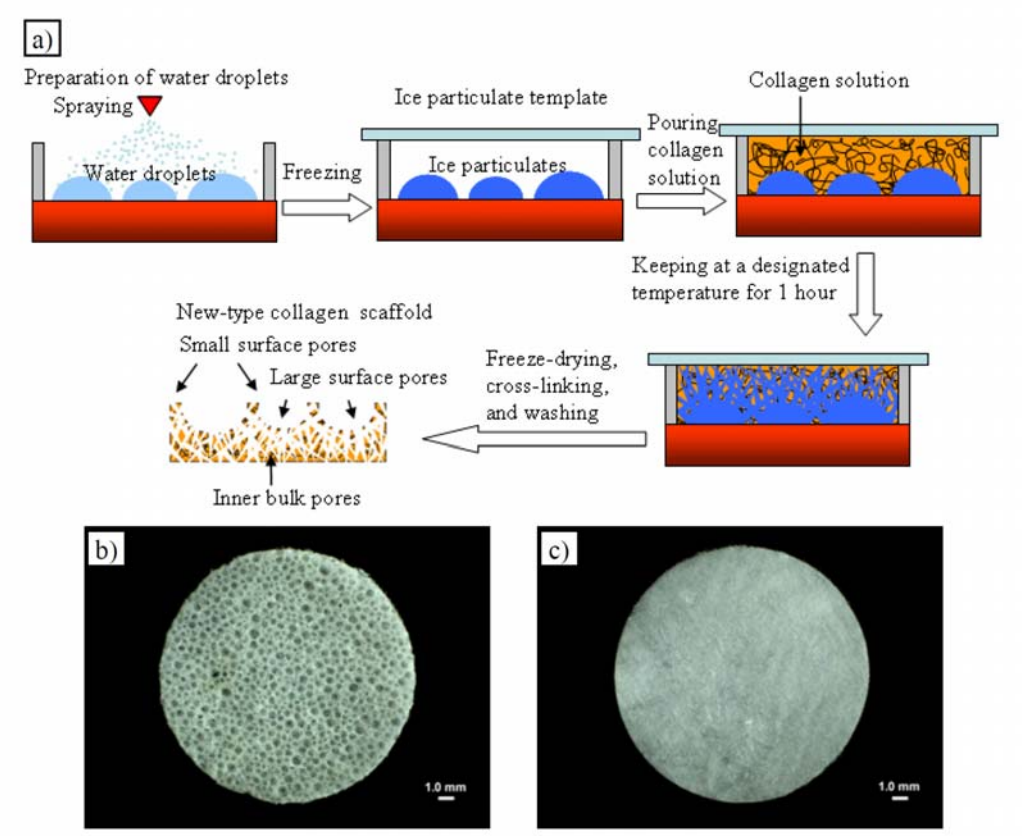

Figure 2.1 Preparation scheme of the funnel-like collagen sponge (a), and photographs of funnel-like collagen sponge prepared with 398 μm-diameter ice particulate template at -3°C (b) and control collagen sponge prepared without use of the ice particulate template at -3°C (c). Scale bars = 1.0 mm.

2.3.8 Statistical analysis

All statistical calculations were performed on KyPlot (KyPlot ver. 2.0, KyensLab Inc.). Each value showed mean ± standard deviation. Significance levels were determined by Student's t-test and one-way ANOVA (analysis of variance) with a post-hoc test by Tukey's method. Statistical significance was considered to be $p < 0.05$.

2.4 Results and discussion

2.4.1 Collagen sponges prepared with ice particulate template

The diameters of embossing ice particulates prepared by spraying pure water 10, 20, and 30 times were 181 ± 43, 398 ± 113, and 719 ± 149 μm, respectively. These ice particulates were used as templates to prepare the new-type collagen sponges. The three sizes of ice particulates were chosen to cover the optimal sizes of surface pores and bulk pores of porous scaffolds for tissue regeneration [17]. Figure 2.1b and c show the collagen sponges prepared with and

without use of the embossing ice particulates. The surface structures of the two types of collagen sponges are different. Large pores are visible and evenly distributed only on the surface of the new-type collagen sponge. The unique structure was somewhat like that of a Büchner funnel. Therefore, a new-type collagen sponge was referred as to a funnel-like scaffold.

2.4.2 Effect of ice particulate dimension on the porous structure of the collagen sponges

The detailed porous structures of the collagen sponges prepared with ice particulates of 181, 398, and 719 μm were observed by a scanning electron microscope. Figure 2.2 shows the morphology of the top surfaces and cross-sections of the new-type collagen sponges and the control collagen sponge. The temperature of the ice particulate template and the freezing temperature were -3°C. The new-type collagen sponge showed a hierarchical porous structure of two layers: a surface porous layer and a bulk porous layer. The surface porous layer consisted of large open pores and some small pores. The sizes of the large surface pores of the new-type collagen sponges prepared with templates of ice particulates of different diameters of 181, 398, and 719 μm were 167 ± 34, 383 ± 75, and 689 ± 198 μm, respectively (Table 2.1). The mean diameters of the large surface pores were almost the same as those of the respective ice particulates used as templates. In effect, the large surface pores were replicas of the embossing ice particulates. The small surface pores among the large surface pores are assumed to be replicas of the newly formed ice crystals that grew among the embossing ice particulates during freezing. The pore sizes of the small surface pores of the new-type collagen sponges shown in Figure 2.2a, c, and e were 50 ± 13, 79 ± 22, and 93 ± 34 μm, respectively (Table 2.1). The pore size of the small surface pores decreased as the size of the ice particulates decreased. This might be because the small ice particulates were more tightly compacted and could transfer heat more quickly than do the large ice particulates.

The bulk porous layer consisted of small pores that were interconnected with the large surface pores and extended into the bulk body of the sponge from the surface pores. The sizes of the inner bulk pores of the new-type collagen sponges prepared with templates of ice particulates of different diameters of 181, 398, and 719 μm were 105 ± 25, 109 ± 26, and 108 ± 30 μm, respectively (Table 2.1). There were no significant differences among the sizes of the inner bulk pores when ice particulates of different sizes were used if the temperature of the ice particulates was the same. In contrast to the new-type collagen sponge, the control collagen sponge prepared without an ice template had irregular surface pores. The mean size of surface pores was 113 ± 33 μm.

Observation of the cross-sections of the collagen sponges further demonstrated the interconnected porous structure of the two porous layers in the new-type collagen sponges (Figure 2.2b, d and f). Semi-spherical surface pores and underlying bulk small pores formed the unique porous structure of the collagen sponge. The large surface pores were replicas of the embossing ice particulates on the template. The size, shape, and density of the large surface pores were directly dependent on the size, shape, and density of the template ice particulates. During freezing process, the ice particulates would serve as nuclei to initiate ice crystallization at the freezing interface between ice particulates and liquid phase collagen solution. This led to growth of ice crystals from the surface of the ice particulates into the bulk aqueous solution. The ice particulates together with the newly formed ice crystal network established the unique porous structure of the new-type collagen sponges. The control collagen sponges did not show any bi-layer porous structure. There were tubelike pores in the control collagen sponge. The tubelike pores should be replicas of the new ice crystals formed during freezing.

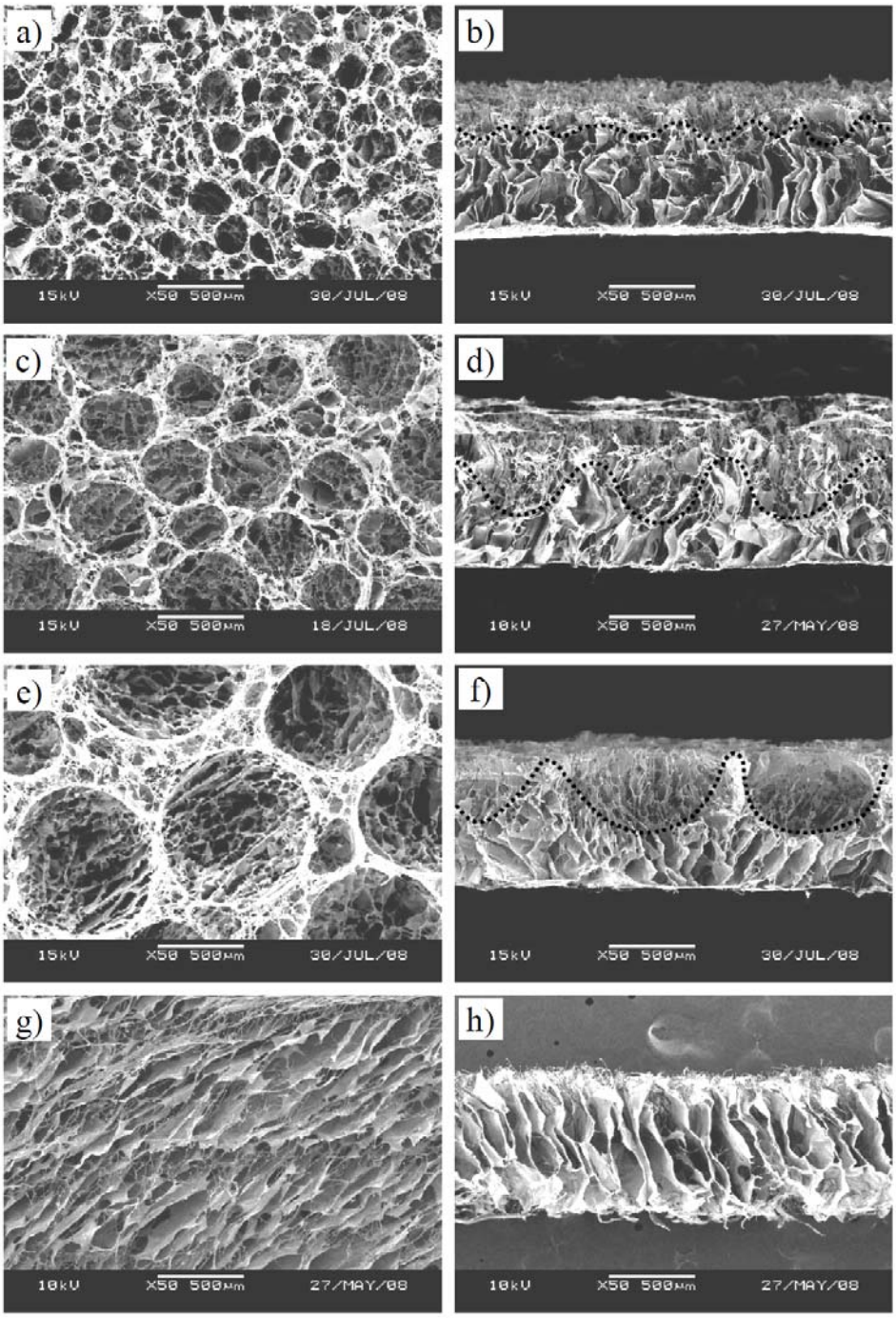

Figure 2.2 SEM photomicrographs of top surfaces (a, c, e) and cross-sections (b, d, f) of the funnel-like collagen sponges prepared by using the embossing ice particulate template with ice particulate diameters of 181 µm (a, b), 398 µm (c, d), and 719 µm (e, f) at -3°C. Top surface (g) and cross-section (h) of control collagen sponge prepared without use of the ice particulate template. The dotted line in b, d, and f outlines the large surface pores. Scale bars = 500 µm.

2.4.3 Effect of freezing temperature on the porous structure of the collagen sponges

The effect of the temperature of the ice particulate template and the freezing temperature on the pore structure of the new-type collagen sponges is shown in Figure 2.3. The template temperature was adjusted to be the same as that of the freezing temperature. Four kinds of collagen sponges were prepared by changing the temperature of the ice particulate template. An ice particulate template having a diameter of 398 μm was used. The pore sizes of the large surface pores of the new-type collagen sponges prepared at -1, -3, -5, and -10°C were 372 ± 81, 383 ± 75, 362 ± 85, and 359 ± 78 μm, respectively (Table 2.2). There was no significant difference among the pore sizes of the large surface pores since ice particulates with the same sizes and shapes were used to prepare these collagen sponges. However, the pore sizes of the inner bulk pores and the small surface pores decreased with a decrease in the temperature of the ice particulates. The inner bulk pores and surface small pores were dense and small when prepared at low temperature, sparse and large when prepared at high temperature. The temperature effect on the porous structure might be explained by the temperature effect on the formation of ice crystal network during freezing process [18-22]. Low temperature results in quick formation of dense, small ice crystals and high temperature results in slow formation of sparse, big ice crystals.

Table 2.1 Pore diameter analysis of the large, top surface pores, the small, top surface pores and the inner bulk pores of the new-type collagen sponges prepared with different ice particulate templates at -3°C, and the top surface pores of control collagen sponge prepared without ice template at -3°C (means ± S.D., n=100 from 5 sponges of each condition)

	Dimension of ice particulates (㎛)			
	Control (without ice particulates)	181	398	719
Large surface pores (㎛)	113±33[a]	167±34[b,c]	383±75[b,c]	689±198[b,c,d]
Small surface pores (㎛)	-	50±13[b,c]	79±22[b,c]	93±34[b,d]
Inner bulk pores (㎛)	-	105±25	109±26	108±30

[a] The datum is the pore size of the top surface of the control collagen sponge. [b] Significant difference with control. [c] Significant difference with that prepared with 181 μm ice particulates. [d] Significant difference with that prepared with 398 μm ice particulates.

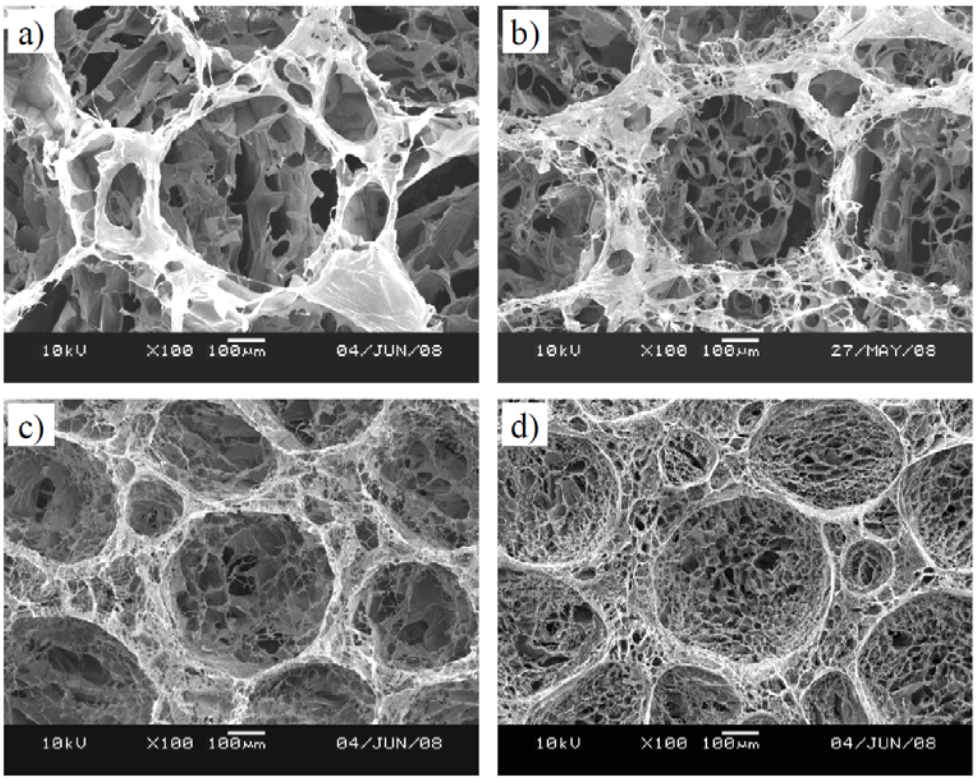

Figure 2.3 SEM photomicrographs of top surfaces (a-d) of funnel-like collagen sponges prepared by using the embossing ice particulate template with ice particulate diameter of 398 µm at different temperatures: -1 (a), -3 (b), -5 (c), and -10°C (d). Scale bars = 100 µm.

Table 2.2 Pore diameter analysis of the large, top surface pores, the small, top surface pores, and the inner bulk pores of the funnel-like collagen sponges prepared at different temperatures with 398 µm ice particulate template (mean ± S.D., n=100 from 5 sponges of each condition)

	Temperature			
	-1℃	-3℃	-5℃	-10℃
Large surface pores (㎛)	372±81	383±75	362±85	359±78
Small surface pores (㎛)	90±25	79±22[a]	54±18[a,b]	32±6[a,b,c]
Inner bulk pores (㎛)	118±30	110±27[a]	74±19[a,b]	35±7[a,b,c]

[a] Significant difference with that prepared at -1 ℃. [b] Significant difference with that prepared at -3 ℃. [c] Significant difference with that prepared at -5 ℃.

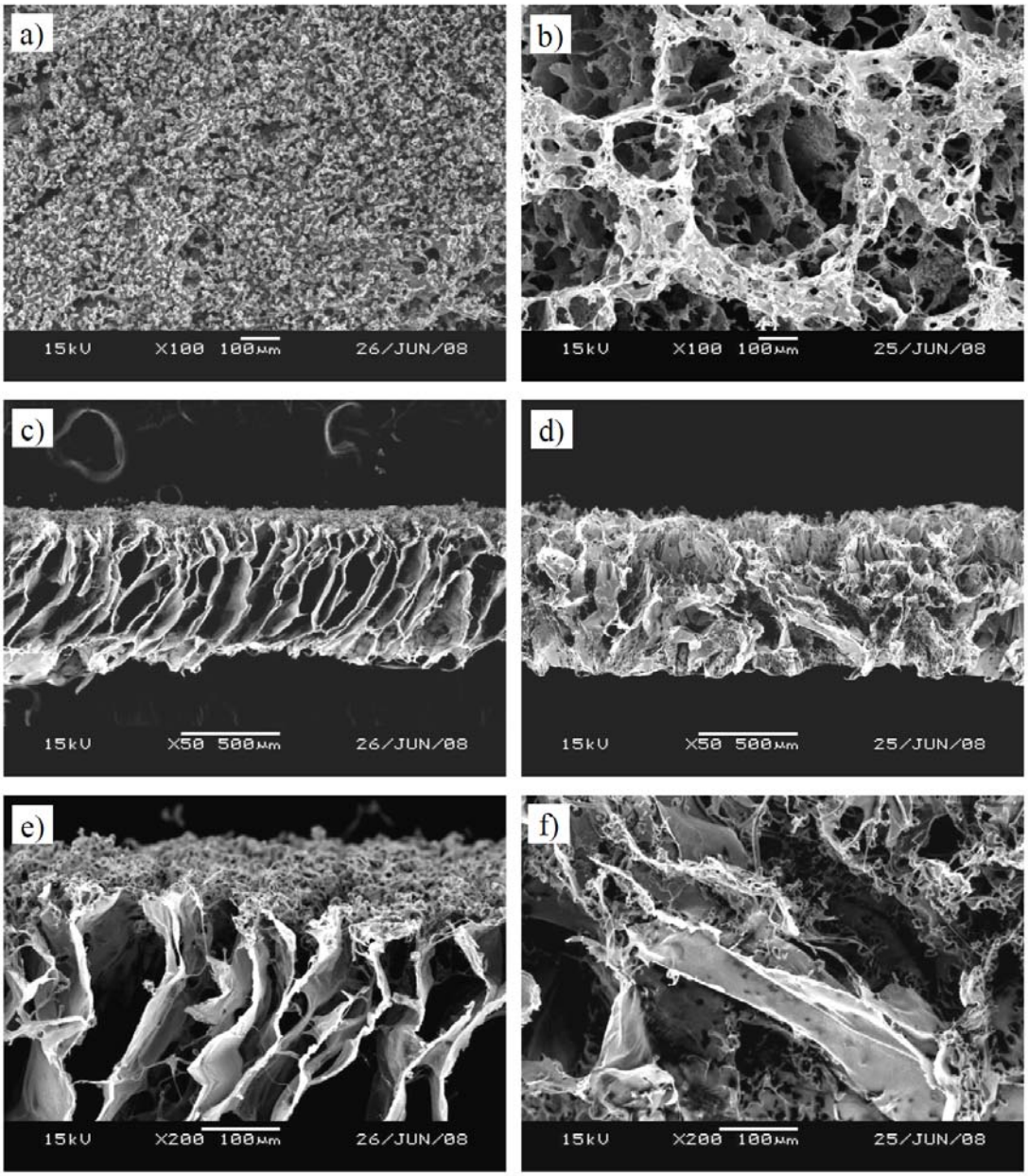

Figure 2.4 SEM photomicrographs of top surfaces (a, b) and cross-sections at low (c, d) and high (e, f) magnifications of control collagen sponge (a, c, e) and funnel-like collagen sponge (b, d, f) after fibroblast culture in the sponges for 1 hour.

2.4.4 Cell adhesion, distribution and tissue formation in the collagen sponges

The new-type collagen sponge prepared with a template of 398 μm-diameter embossing ice particulates at -3°C and the control collagen sponge prepared at -3°C without ice template were used for the cell culture of human dermal fibroblasts. A cell suspension solution of fibroblasts was dropped onto the collagen sponges for cell seeding. The cell suspension solution penetrated into the collagen sponges, delivering the cells into the pores of the sponges. The cell seeding efficiencies of the new-type and control collagen sponges were 93.2 ± 1.0% and 92.1 ± 1.1%, respectively. Both collagen sponges showed high cell seeding efficiency, and there was no significant difference between the two collagen sponges. The distribution of fibroblasts in the collagen sponges was observed by a SEM (Figure 2.4). The fibroblasts were observed both on the top surface and within the inner pores of the new-type collagen sponge. The cells were distributed throughout the new-type collagen sponge. However, the fibroblasts were mostly distributed on the surface and few cells were observed in the inner part of the control collagen sponge. The difference of cell distribution might be caused by the different porous structures of the sponges. The large surface open pores and high interconnectivity of the inner bulk pores of the new-type collagen sponge facilitated cell delivery and penetration into the whole sponge. However, the low ratio of surface open pores and low interconnectivity in the control collagen sponge retarded cell diffusion into the inner part of the sponge.

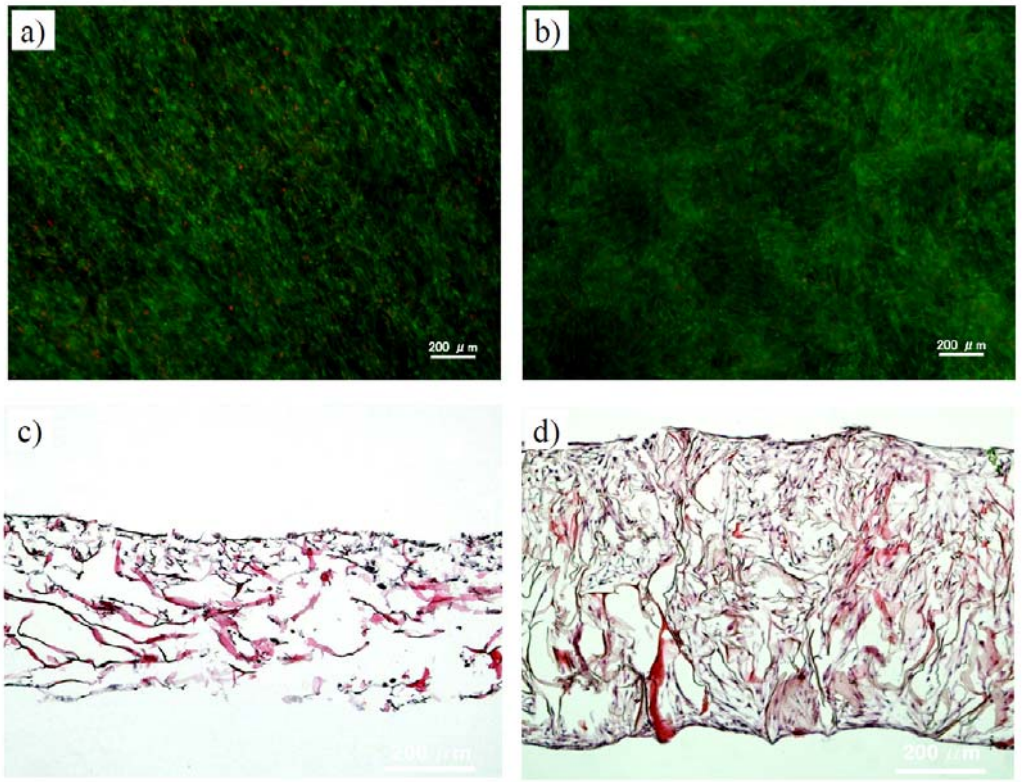

Figure 2.5 Live/dead staining (a, b) and HE staining (c, d) of fibroblasts after culture in control collagen sponge (a, c) and funnel-like collagen sponge (b, d) for 2 weeks.

Cell viability was investigated after the fibroblasts were cultured in the new-type and control collagen sponges for 2 weeks (Figure 2.5a and b). Many red-stained dead cells were detected in the control collagen sponge while few were detected in the new-type collagen sponge. Implanted cells require extra space to spread and grow for normal proliferation [23]. The open surface and interconnected porous structure in the new-type collagen sponge improved cell delivery and distribution, provided enough extra area for cell spreading and proliferation, thus avoiding over cell aggregation and overgrowth. However, in the case of the control collagen sponge, most of the cells were stacked up on the sponge surface, resulting in the accumulation and overgrowth of the fibroblasts that might result in the death of some cells.

After culture in the collagen sponges for 2 weeks, the fibroblasts were stained by hematoxylin and eosin stains (Figure 2.5c, d). More cells were observed on the surface than in the inner bulk part of the control collagen sponge. In contrast, the fibroblasts were distributed homogenously throughout the new-type collagen sponge. Besides the effect of homogeneous cell distribution in the new-type pore structure, the open surface pores and interconnected inner pores might also facilitate transfer of nutrient and metabolites to fibroblasts and lead to rapid formation of dermal tissue.

2.5 Conclusions

A new-type of collagen sponge was prepared by using embossing ice particulates as a template. The collagen sponge had a hierarchical structure of large open pores on the top surface and interconnected small pores in the inner bulk body. The shape, size, and density of the surface large pores were determined by the ice particulates that were used as templates while the interconnected small pores were determined by the freezing temperature. The unique porous structure of the new-type collagen sponge facilitated cell seeding, cell penetration, and distribution throughout the scaffold, and accelerated the regeneration of new tissue. This method is very simple, reproducible, and could easily be applied to other materials. The use of ice particulates as a template will be a useful method for the creation of an open and interconnected porous structure.

2.6 References

1 Sibambo, S. R., Pillay, V., Choonara, Y. E., Du Toit, L. C., Khan, R. A., and Penny, C., Kinetic and structural modeling mechanisms of melatonin transport from an electrolytically regulated salted-out PLGA scaffold. *J Bioact Compat Polym* **24**, 266-296 (2009).

2 Kawazoe, N., Lin, X., Tateishi, T., Chen, G., Three-dimensional cultures of rat pancreatic RIN-5F cells in porous PLGA-collagen hybrid scaffolds. *J Bioact Compat Polym* **24**, 25-42 (2009).

3 Tan, L., Chen, Y., Wang, Y., Zhou, W., Zhu, X., He, X., Su, J., Cui, S., In vivo evaluation of butylene terephthalate-ethylene oxide-DL, lactide polymer as porous scaffolds for tissue engineering. *J Bioact Compat Polym* **24**, 43-55 (2009).

4 Li, H., Zheng, Q., Xiao, Y., Feng, J., Shi, Z., Pan, Z., Rat cartilage repair using nanophase PLGA/HA composite and mesenchymal stem cells. *J Bioact Compat Polym* **24**, 83-99 (2009).

5 Engelmayr, G. C., Cheng, M., Bettinger, C. J., Borenstein, J. T., Langer, R., Freed, L.E., Accordion-like honeycombs for tissue engineering of cardiac anisotropy. *Nature Mater* **7**, 1003-1010 (2008).

6 Kyriakidou, K., Lucarini, G., Zizzi, A., Salvolini, E., Belmonte, M. M., Mollica, F., Gloria, A., Ambrosio, L., Dynamic co-seeding of osteoblast and endothelial cells on 3D polycaprolactone scaffolds for enhanced bone tissue

engineering. *J Bioact Compat Polym* **23**, 227-243 (2008).

7 Zhang, T., Yan, Y., Wang, X., Xiong, Z., Lin, F., Wu, R., and Zhang, R., Three-dimensional gelatin and gelatin/hyaluronan hydrogel structures for traumatic brain injury. *J Bioact Compat Polym* **22**, 19-29 (2007).

8 Tong J.-C. and Yao S.-L., Novel scaffold containing transforming growth factor-ß1 DNA for cartilage tissue engineering. *J Bioact Compat Polym* **22**, 232-244 (2007).

9 Mikos, A. G., Thorsen, A. J., Czerwonka, L. A., Bao, Y., Langer, R., Winslow, D. N., Vacanti, J. P., Preparation and characterization of poly(L-lactic acid) foams. *Polymer* **35**, 1068-1077 (1994).

10 Zhang, H., Hussain, I., Brust, M., Butler, M. F., Rannard, S. P., Cooper, A. I., Aligned two- and three-dimensional structures by directional freezing of polymers and nanoparticles. *Nature Mater* **4**, 787-793 (2005).

11 Faraj, K. A., Kuppevelt, T. H. V., Daamen, W. F., Construction of collagen scaffolds that mimic the three-dimensional architecture of specific tissues. *Tissue Eng* **13**, 2387-2394 (2007).

12 Yang, F., Murugan, R., Ramakrishna, S., Wang, X., Ma, Y. X., Wang, S., Fabrication of nano-structured porous PLLA scaffold intended for nerve tissue engineering. *Biomaterials* **10**, 1891-1900 (2004).

13 Harris, L. D., Kim, B. S., Mooney, D. J., Open pore biodegradable matrices formed with gas foaming. *J Biomed Mater Res* **42**, 396-402 (1998).

14 Meng, W., Kim, S. Y., Yuan, J., Kim, J. C., Kwon, O. H., Kawazoe, N., Chen, G., Ito, Y., Kang, I. K., Electrospun PHBV/collagen composite nanofibrous scaffolds for tissue engineering. *J Biomater Sci Polym Ed* **18**, 81-94 (2007).

15 Mikos, A. G., Bao, Y., Cima, L. G., Ingber, D. E., Vacanti, J. P., Langer, R., Preparation of poly(glyco1ic acid) bonded fiber structures for cell attachment and transplantation. *J Biomed Mater Res* **27**, 183-189 (1993).

16 Sun, W., Starly, B., Darling, A., Gomez, C., Computer-aided tissue engineering: Application to biomimetic modeling and design of tissue scaffolds. *Biotech Appl Biochem* **39**, 49-58 (2004).

17 Oh, S. H., Park, I. K., Kim, J. M., Lee, J. H., In vitro and In vivo characteristics of PCL scaffolds with pore size gradient fabricated by a centrifugation method. *Biomaterials* **28**, 1664-1671 (2007).

18 Zhang, H., Cooper, A. I., Aligned porous structures by directional freezing. *Adv Mater* **19**, 1529-1533 (2007).

19 Sastry, S., Ins and outs of ice nucleation. *Nature* **438**, 746-747 (2005).

20 O'Brien, F. J., Harley, B. A., Yannas, I. V., Gibson, L., Influence of freezing rate on pore structure in freeze-dried collagen-GAG scaffolds. *Biomaterials* **25**, 1077-1086 (2004).

21 Schoof, H., Apel, J., Heschel, I., Rau, G., Control of pore structure and size in freeze-dried collagen sponges. *J Biomed Mater Res B: Appl Biomater* **58**, 352-357 (2001)

22 Doillon, C. J., Whyne, C. F., Brandwein, S., Silver, F. H., Collagen-based wound dressings: control of the pore structure and morphology. *J. Biomed Mater Res* **20**, 1219-1228 (1986).

23 Freyman, T. M., Yannas, I. V., Gibson, L .J., Cellular materials as porous scaffolds for tissue engineering. *Prog Mater Sci* **46**, 273-282 (2001).

Chapter 3

Preparation of chitosan scaffolds with a hierarchical porous structure

3.1 Summary

Development of porous scaffolds with open surface pore structures is required for tissue engineering to deliver cells into the three-dimensional (3D) spaces in the scaffolds and improve cell distribution. This chapter demonstrated a new type of funnel-like chitosan sponge prepared by using ice particulates as a template. The funnel-like chitosan sponges had a hierarchical bi-layer porous structure of a surface layer and an interconnected bulk porous layer. The top surface porous layer consisted mainly of large open pores. The bulk porous layer was beneath the large surface pores and consisted of small pores that were connected with the large surface pores. The large surface pores were dependent on the shape, dimension, and density of the embossing ice particulates while the bulk pores were dependent on the freezing temperature. The large open surface pores and interconnected bulk pores in the funnel-like chitosan sponges facilitated cell seeding and cell distribution from the surface into the inner bulk pores. Cells cultured in the funnel-like chitosan sponges showed high viability, high proliferation, and homogenous tissue formation. Such funnel-like chitosan sponges will be useful for tissue engineering.

3.2 Introduction

The use of porous scaffolds in tissue engineering provides a three-dimensional environment for cell adhesion, proliferation, and differentiation to accelerate new tissue formation [1,2]. Chitosan has been studied for tissue engineering applications because of its biocompatibility, biodegradability, antibacterial property, reactive groups, and structural similarities to glycosaminoglycans [3,4]. Chitosan is a natural cationic polymer (positive charge) that is a linear amino polysaccharide composed of approximately 20% β-1,4-linked N-acetyl-D-glucosamine and approximately 80% β-1,4-linked D-glucosamine prepared by the partial deacetylation of chitin in hot alkali [5]. Chitosan can easily be fabricated into porous sponges, fibers, hydrogels, and microspheres [5-9]. The use of chitosan as a tissue engineering scaffold has been reported for a variety of tissues such as bone, liver, neural tissue, vascular tissue, cartilage, and skin [10-16]. In addition, chitosan has been utilized for its ability to deliver proteins, such as growth factors, in a controlled and stable manner, which may prove beneficial in many tissue engineering targets for the promotion of tissue growth and angiogenesis [17,18]. When porous scaffolds are used for three-dimensional cell culture, an adequate porous structure of the scaffold is very crucial to enable cellular penetration into the construct and full differentiation inside after

transplantation [19]. Many scaffold fabrication techniques have been developed to control the pore structures of porous scaffolds. These include freeze-drying, porogen leaching, gas forming, fiber bonding, electrospinning, thermally induced phase separation, and prototyping [20-27]. However, it has been difficult to control the surface porous structure of scaffolds to ensure large open pores for even cell seeding and uniform cell distribution. In this study, we used embossing ice particulates as a template for the preparation of a novel type of funnel-like chitosan sponge that had a hierarchical porous structure for tissue engineering. The ice particulates caused the formation of the large open pores at the surface that were connected with the underlying bulk pores. The chitosan sponges were used for the culture of human dermal fibroblasts to investigate the effect on cell distribution, viability, and new tissue formation.

3.3 Materials and methods

3.3.1 Materials

Chitosan from crab shells (medium molecular weight: 190000-300000, 75-85% deacetylated, Aldrich) was used as a base material. Chitosan powder is soluble in dilute aqueous acid solution (<pH 6.5). Homogeneous chitosan aqueous solution (1.0 wt%) was prepared with 1.0 wt% acetic acid (99.0%, Wako) and stored at -1°C before use.

3.3.2 Preparation of chitosan sponges

Hierarchically structured chitosan scaffolds were prepared by using the embossing ice particulates as templates to control the pore structure of the top surface. After the ice-particulate template reached the designated temperature (-1, -3, -5, or -10°C) in the low temperature chamber, an aqueous solution of chitosan (1.0 wt%) was poured onto the template to fill the area inside the silicone frame. The surface of the chitosan solution was covered with a glass plate wrapped with polyvinylidene chloride (PVDC) film to flatten the solution surface and ensure the thickness of the aqueous solution to be 1 mm. The chitosan solution and PVDC-wrapped glass plates were stored at -1°C for 24 hours for cooling before being applied to the template. The chitosan solution did not freeze during cooling at -1°C. The manipulations were conducted in the low temperature chamber that was set at a designated temperature (-1, -3, -5, or -10°C). The chitosan solution together with the template were kept in the low temperature chamber for 1 hour to solidify the liquid state of chitosan solution gradually. The ice particulates on the templates initiated ice crystallization and the chitosan solution froze after chitosan solution was applied on the ice particulate template. After 1 hour, the PVDC-wrapped glass plate was detached from the frozen chitosan and the template was moved to a deep freezer (-80°C) for further freezing for 5 hours. Then, the frozen chitosan block was detached from the PFA-wrapped copper plate, silicone frame, and freeze-dried for 24 hours in a freeze-drying machine (VirTis AdVantage Benchtop Freeze Dryers, SP Industries Incorporation). Finally, the freeze-dried sponges were immersed in ethanol (99.5%, Wako) for 3 hours to exchange residual acetic acid. After stabilization, the chitosan sponges were washed three times with pure water to be adjusted to neutral condition and freeze-dried again. Control chitosan sponges were prepared by the same procedure without the use of the ice-particulate template.

3.3.3 Cell culture and seeding

Neonatal human dermal fibroblasts (NHDF, Cascade Biologics Incorporation) were used for cell culture experiments in vitro. The cells were grown in culture dishes (100 mm) with Medium 106 (Cascade Biologics Inc.)

supplemented with 2% (v/v) fetal bovine serum (FBS), 10 ng/ml human recombinant epidermal growth factor (hEGF), 3 ng/ml human recombinant fibroblast growth factor-basic (hFGF-B), gentamicin, and amphotericin (Cascade Biologics Inc.). Cell culture was maintained in an incubator equilibrated with 5% CO_2 at 37°C. The fibroblasts were subcultured once after reaching a confluent cell monolayer. The fibroblasts in confluence were rinsed with N-2-hydroxyethylpiperazine-N'-2-ethanesulfonic acid (HEPES) buffer and detached from the culture dishes using 0.025% (w/v) trypsin and 0.01% (w/v) ethylenediaminetetraacetic acid (EDTA) and neutralized by HEPES solution containing 10% FBS (Kurabo Industries Ltd.). The collected cell suspension was centrifuged and resuspended in the serum medium to a concentration of 5.0 x 10^6 cells/ml. The hierarchically structured chitosan sponge prepared with ice particulates 398 μm in diameter at -3°C and control chitosan sponge were used for cell culture. The samples were cut into disks (diameter: 16 mm) in order to be arranged in cell-culture plates (Micro Plates-24 Well, AS ONE Corporation). The disks were sterilized in 70% ethanol for 30 minutes and then rinsed with phosphate buffered saline (PBS) three times and exchanged with cell culture media. The cell suspension was dropped onto the chitosan sponge disks (200 μL/disk) to seed the cells in each scaffold and incubated for 4 hours. Thereafter, the chitosan sponge disks were transferred to new plates. The cells in the old medium and those that adhered to each well of the old cell-culture plates were collected and counted by a hemocytometer. The number of cells in each well was regarded as the number of unattached cells. The difference between the number of seeded cells and the number of unattached cells was considered as the number of attached cells held by the sponges. The cell seeding efficiency of each sponge was calculated same as previous chapter. To obtain the means and standard deviations, 5 sponge disks were used for the measurements.

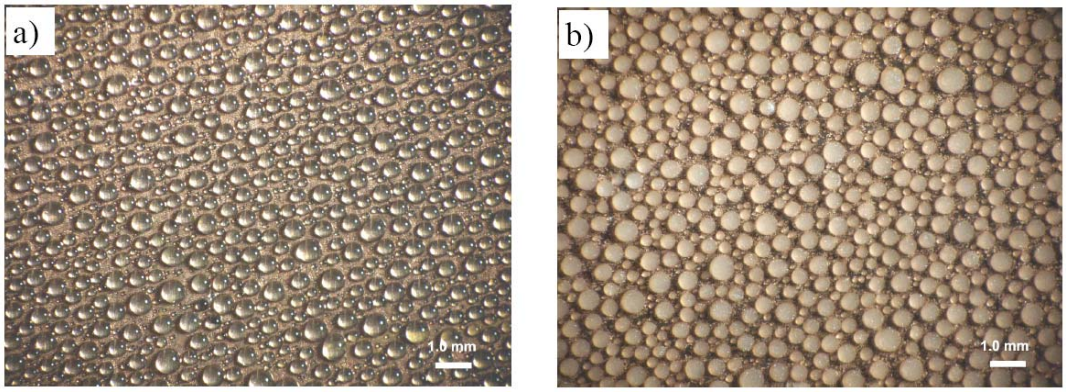

Figure 3.1 Photomicrographs of water droplets (a) and ice particulates (b) for embossing on a template. Scale bars = 1.0 mm.

3.3.4 Evaluation of cell viability and proliferation

Live/dead staining was carried out to evaluate cell viability using Calcein-AM (live: green) and Propidium Iodide (dead: red) staining reagents (Cellstain Double Staining Kit, Dojindo Laboratories). NHDF cells, cultured in the chitosan sponges for 24 hours, were washed by HEPES buffer and incubated in 2 μM Calcein-AM and 4 μM Propidium Iodide solution in HEPES buffer for 30 minutes. Then, the specimens were finally rinsed by HEPES buffer. The submerged specimens were observed under a fluorescence microscope (BX51, Olympus Corp.). Cell proliferation was evaluated using WST-1 reagent (Roche Diagnostics GmbH) that is a colorimetric assay based on the cleavage of WST-1

tetrazolium salt by mitochondrial dehydrogenases by cellular respiration and metabolic rate. After the NHDF cells were cultured in the chitosan sponges for 1, 3, and 5 days, each sponge was moved to a new 24-well plate with fresh media (1000 μl) and further incubated for 1 hour. Then, WST-1 reagent (100 μl) was added to each specimen and incubated for 30 minutes at 37°C in a CO_2 incubator. The culture medium became yellow during the incubation. The media (200 μl) was moved to a 96-well plate by a pipette. The absorbance of each well was measured at 440 nm using a microplate reader (Bio-Rad Benchmark Plus, Bio-Rad Laboratories Inc.)

3.4 Results and discussion

3.4.1 Ice particulate template

The ice particulate template was prepared by freezing water droplets on a copper plate. A copper plate wrapped with PFA film was used as a holder to support the ice particulate formation. Pure water was sprayed onto the PFA membrane surface so water droplets would form on the surface (Figure 3.1a). The dimension of the water droplets could be controlled by the spraying time. The water droplets became larger as the spraying times increased. The copper plate carrying the water droplets was placed in a -30°C freezer to form ice particulates. The set of ice particulates embossed on the PFA film-wrapped copper plate was used as the template. The ice particulates had semi-spherical morphology (Figure 3.1b). Templates of three different dimensions embossed with ice particulates were prepared and used for the scaffold preparation. The mean diameters of the ice particulates of the three types of templates were 181 ± 43, 398 ± 113, and 719 ± 149 μm.

3.4.2 Chitosan sponges

Chitosan sponges were prepared by using ice particulates as a template. The ice-particulate template was moved to a low temperature chamber set at -3°C. After the template temperature was allowed to equalize in the chamber for 1 hour, an aqueous chitosan solution was poured onto the ice particulates. The chitosan solution was frozen after being kept in the chamber for 1 hour. After further freezing at -80°C and freeze-drying, hierarchically structured chitosan sponges were produced. The gross appearance of the chitosan sponge prepared with ice particulates 398 μm in diameter is shown in Figure 3.2a. Large, homogeneous pores were visible on the top surface of the chitosan sponge while not on the control chitosan sponge (Figure 3.2b). The detailed porous structure of the chitosan sponge was observed by a SEM (Figure 3.2i, j, q, r). The chitosan sponge prepared with the ice-particulate template showed a hierarchical porous structure: a top surface layer and a bulk porous structure. The porous top surface layer consisted of large, open pores with some small pores interspersed among the large pores. Under the large surface pores, the bulk porous layer consisted of small pores that were interconnected with the large surface pores. Observation of the cross sections of the chitosan sponges further demonstrated the interconnected porous structure of the two porous layers in the hierarchically structured chitosan sponges. The large pores in the top surface were semispherical in shape and were connected with the bulk small pores. The unique hierarchical structure was somewhat like that of a Büchner funnel same as previous collagen sponges (Figure 3.2c). Therefore, the chitosan sponges prepared with the ice-particulate template were referred as to funnel-like chitosan sponges. However, the control chitosan sponge that was prepared without the use of ice particulates did not show the bi-layer porous structure. The control chitosan sponge contained inclinatory tube-like pores.

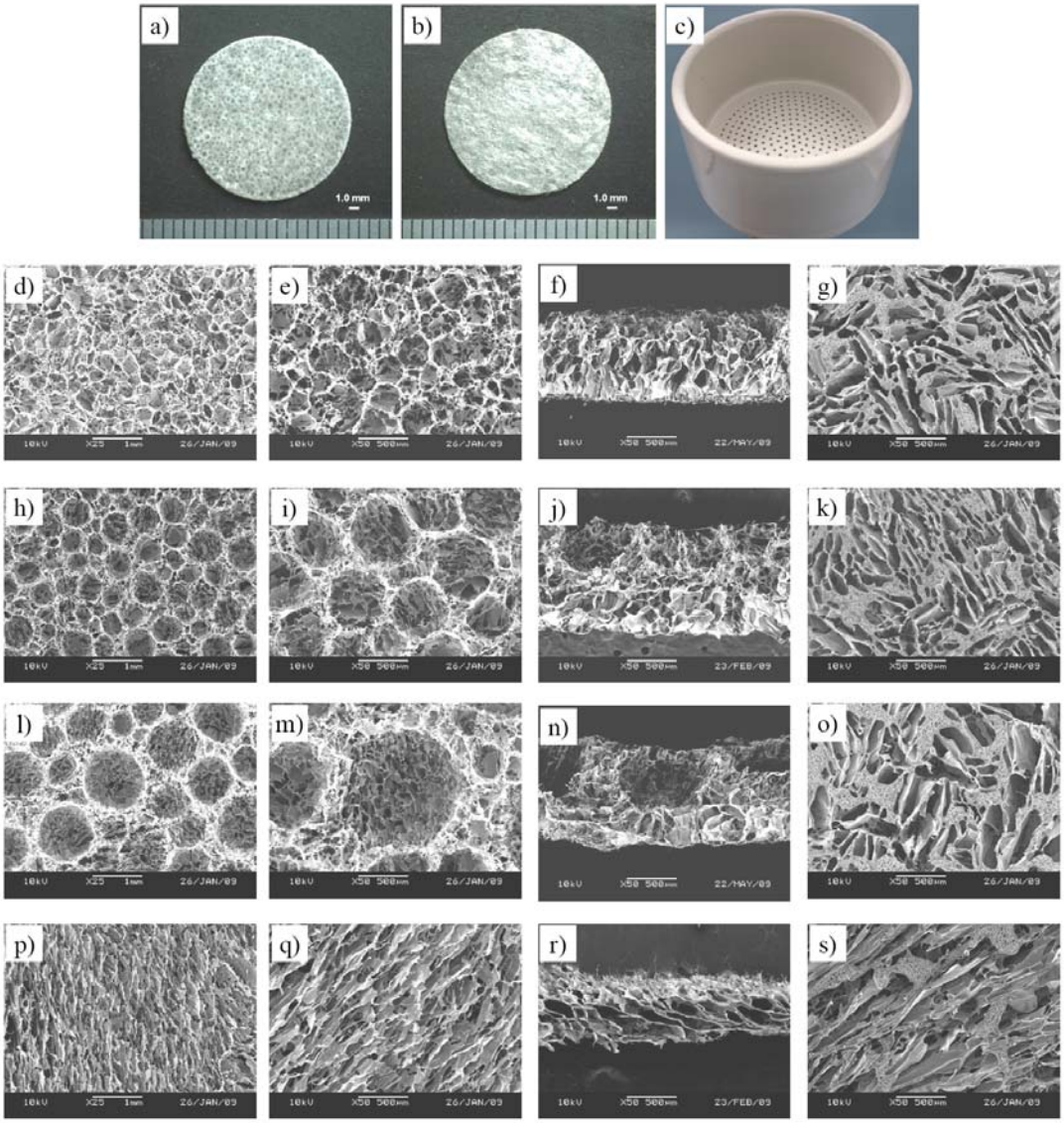

Figure 3.2 Photographs of a funnel-like chitosan sponge prepared with 398 μm-diameter ice-particulate template at -3°C (a), a control chitosan sponge prepared at -3°C without ice-particulate template (b) and a Büchner funnel (c); and SEM photomicrographs of top surfaces (d, e, h, i, l, m), cross sections (f, j, n), and bottom surfaces (g, k, o) of funnel-like chitosan sponges prepared by using templates embossed with ice particulates having diameters of 181-μm (d-g), 398- μm (h-k), and 719- μm (l-o) at -3°C, and the top surface (p, q), cross section (r), and bottom surface (s) of the control chitosan sponge prepared at -3°C without use of the ice-particulate templates. Scale bars in a, b, d, h, l, p = 1000 μm, scale bars in e-g, i-k, m-o and q-s = 500 μm.

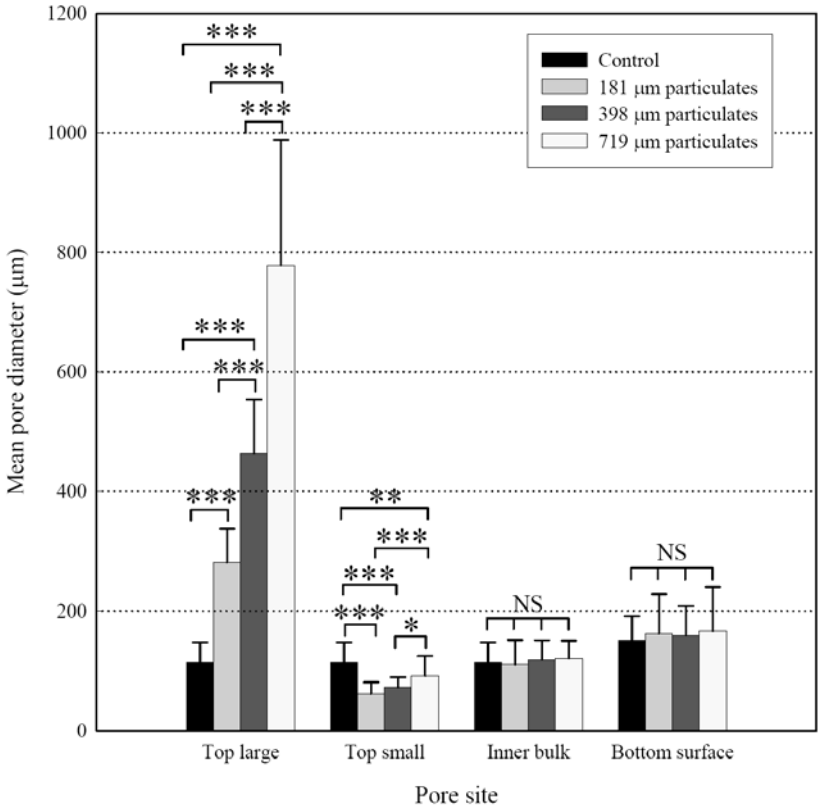

Figure 3.3 Pore diameter analysis of the large, top surface pores, the small, top surface pores, the bulk pores, and the bottom surface pores of the funnel-like chitosan sponges prepared by using templates embossed with ice particulates having diameters of 181 μm, 398 μm, and 719 μm at -3°C and the control chitosan sponge prepared at -3°C without use of the ice-particulate template. Data are mean ± S.D. for n = 30 pores from 5 specimens of each condition. ***$p<0.001$, **$p<0.01$, *$p<0.05$, NS indicates not significant.

3.4.3 Effect of ice particulate dimension

The funnel-like chitosan sponges were prepared with ice particulates of three different diameters: 181, 398, and 719 μm (Figure 3.2d-s). The temperature of the ice-particulate template and low temperature chamber was -3°C during the preparation process. All the chitosan sponges prepared with different ice-particulate templates showed hierarchical pore structures of a top surface porous layer and a bulk porous layer. The top surface porous layer consisted of large, open pores and some small pores. The bulk porous layer consisted of small pores that were interconnected with the large surface pores. The bottom surface had pores of irregular, spindle-like shapes.

The control chitosan sponge showed a top surface and cross structures different from those of the funnel-like chitosan sponge. The surface pores showed random morphology. There were no large pores in the top surface and no hierarchical porous structure in the control chitosan sponge. However, the bottom surface structure of the control chitosan sponge was similar to that of the funnel-like chitosan sponge.

The mean pore diameters of the large, top surface pores, the small, top surface pores, the bulk pores, and the bottom surface pores were analyzed from photomicrographs of each sponge (Figure 3.3). The size of the large, top

surface pores was dependent on the dimension of the ice particulates. The larger ice particulates resulted in larger top surface pores. The smaller ice particulates resulted in smaller top surface pores. The size and density of the large, top surface pores could be controlled by adjusting the size and density of the ice particulates. The mean size of the small, top surface pores of the three types of funnel-like chitosan sponges was significantly different and increased with an increase in the size of the ice particulates. However, the effect of ice particulate dimension on the small, top surface pores was much less than was that on the large, top surface pores. The mean sizes of the bulk pores of the funnel-like chitosan sponge prepared with different ice particulates were in the same range. There was no significant difference among the bulk pore sizes of the funnel-like chitosan sponges. The control chitosan sponge had a similar bulk pore size and bottom surface pore size, as did those of the funnel-like chitosan sponges.

During the preparation of the chitosan sponges, shrinkage in the radial direction was not evident but was very significant in the vertical direction. The thickness of the chitosan sponges should be 1000 μm if there was no shrinkage in the vertical direction. However, the average thickness of the funnel-like chitosan sponges and the control chitosan sponge was about 932±89 and 532±88 μm, respectively. The funnel-like chitosan sponges showed less vertical shrinkage than did the control chitosan sponge. The dimension of the ice particulates showed no effect on the thickness of the funnel-like chitosan sponges.

3.4.4 Effect of freezing temperature

The funnel-like chitosan sponges were prepared at four different freezing temperatures (Figure 3.4). The temperature of the ice particulates and low temperature chamber was set at -1, -3, -5, and -10°C. An ice-particulate template having a diameter of 398 μm was used. The hierarchical structure was observed in all the funnel-like chitosan sponges prepared at these four temperatures. The chitosan aqueous solution froze within 1 hour at all four temperatures. The chitosan solution froze faster at the lower temperature than it did at the higher temperature. The large surface pores showed the same semi-spherical morphology for the funnel-like chitosan sponges prepared at each temperature. The mean diameters of the large, top surface pores in the four different funnel-like chitosan sponges were almost same. The morphology and size of the large, top surface pores were not affected by the freezing temperature. The mean size of the small, surface pores, bulk pores, and bottom surface pores decreased significantly as the freezing temperature decreased (Figure 3.5). The freezing temperature showed a significant effect on the size of these pores.

3.4.5 Cell culture in chitosan sponges

The funnel-like chitosan sponge prepared with 398 μm-diameter ice particulates at -3°C and the control chitosan sponge prepared without ice particulates at -3°C were used for the cell culture of human dermal fibroblasts. The fibroblasts were seeded by dropping a suspension solution of fibroblasts onto the chitosan sponges. The cell seeding efficiencies of the funnel-like and control chitosan sponges were 98.73 ± 0.29% and 98.47 ± 0.65%, respectively. Both the funnel-like and control chitosan sponges showed high cell seeding efficiency. Most of the cells were entrapped in the chitosan sponges.

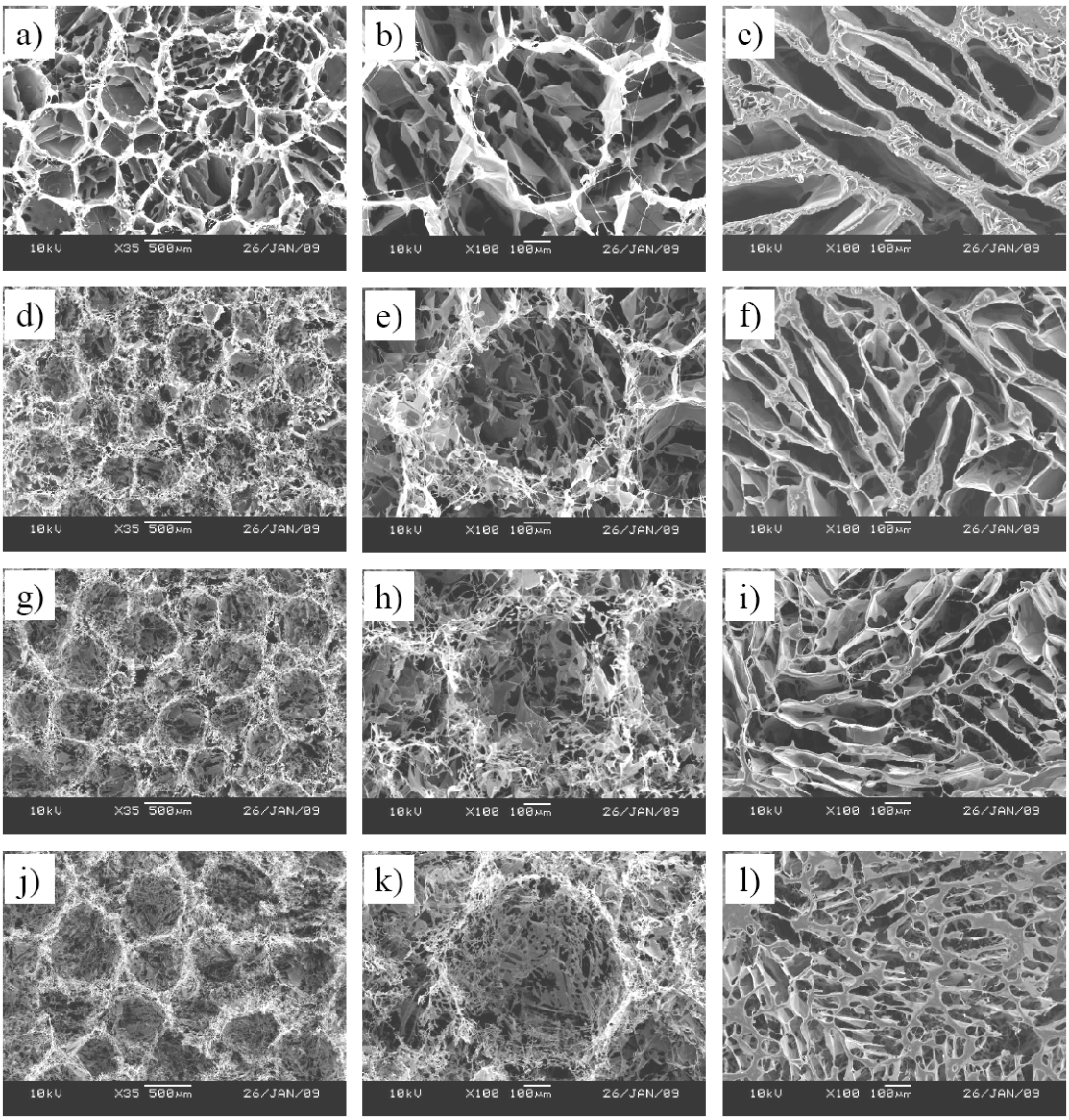

Figure 3.4 SEM photomicrographs of top surfaces (a, b, d, e, g, h, j, k) and bottom surfaces (c, f, i, l) of the funnel-like chitosan sponges prepared with 398 µm-diameter ice-particulate template at different temperatures: -1 (a-c), -3 (d-f), -5 (g-i), and -10°C (j-l). Scale bars in a, d, g, j = 500 µm, scale bars in b, c, e, f, h, i, k, l = 100 µm.

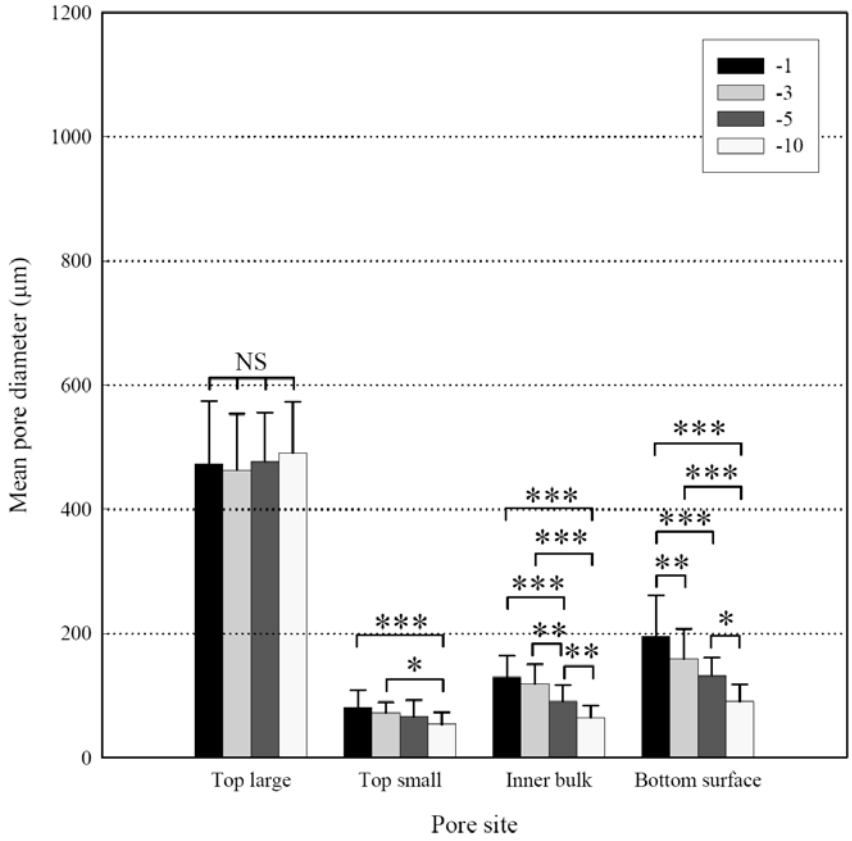

Figure 3.5 Pore diameter analysis of the large, top surface pores, the small, top surface pores, the bulk pores, and the bottom surface pores of funnel-like chitosan sponges prepared with 398 μm-diameter ice-particulate templates at different temperatures of -1, -3, -5, and -10°C. Data are mean ± S.D. for n = 30 pores from 5 specimens of each condition.***p<0.001, **p<0.01, *p<0.05, NS indicates not significant.

Cell distribution in the funnel-like and control chitosan sponges was observed by SEM (Figure 3.6). Cells were observed in the large, top surface pores and bulk pores when cultured in the funnel-like chitosan sponge. The cells were homogeneously distributed in the whole funnel-like chitosan sponge. The cells could be delivered to the bulk pores through the large, top surface pores. Alternatively, cells mostly adhered to the top surface and few cells were observed in the bulk pores when cultured in the control chitosan sponge. The cells were densely distributed on the surface and did not penetrate into the middle of the scaffolds. The less open structure of the top surface pores in the control chitosan sponge retarded the delivery and infiltration of cells into the inner part of the sponge.

3.4.6 Cell viability and histology

Cell viability was investigated after the fibroblasts were cultured in the funnel-like and control chitosan sponges for 24 hours (Figure 3.7a and b). Few red-stained dead cells were detected in the funnel-like chitosan sponge

while many were detected in the control chitosan sponge. The cells cultured in the funnel-like chitosan sponge showed higher viability than did those in the control chitosan sponge. Cell proliferation in the funnel-like and control chitosan sponges was investigated by measuring the activities of mitochondrial dehydrogenases. Fibroblast proliferation was significantly faster in the funnel-like chitosan sponge than it was in the control sponge (Figure 3.7c). The homogeneous distribution of cells in the funnel-like chitosan sponge provided more space for cell spread and occupation, and thus resulted in greater viability and proliferation. The effect became more evident with the increase of culture time.

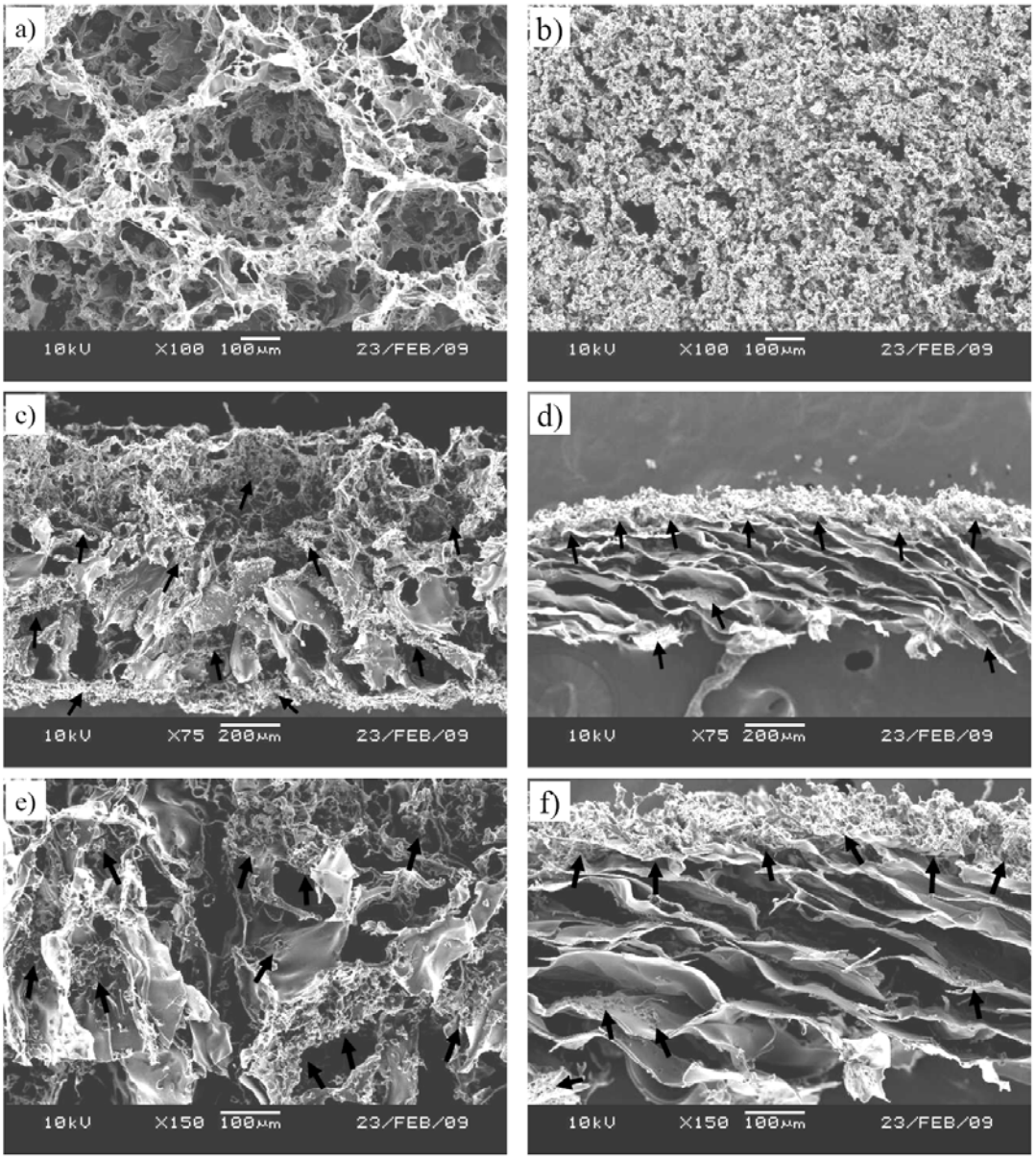

Figure 3.6 SEM photomicrographs of top surfaces (a, b) and cross sections (c-f) of a funnel-like chitosan sponge (a, c, e) and a control chitosan sponge (b, d, f) after fibroblasts were cultured in the sponges for 1 hour. Scale bars in a, b, e, f = 100 μm, scale bars in c, d = 200 μm. Arrows indicate cells.

After the fibroblasts were cultured in the funnel-like and control chitosan sponges for 2 weeks, the cell/sponge constructs were sectioned and stained by hematoxylin and eosin stains (Figure 3.8). The cells were homogenously distributed in the funnel-like chitosan sponge. The cells proliferated three-dimensionally in the sponge. In contrast, the cells were mainly distributed on the top and bottom surfaces of the control chitosan sponge. Few cells were detected in the central part of the control sponge.

Open surface porous structure is very important for three-dimensional scaffolds to facilitate cell seeding, penetration, and distribution in the scaffolds[19]. In this study, ice particulates were used as a template to create an open surface porous structure in chitosan sponges. The funnel-like chitosan sponges prepared using ice-particulate templates showed a unique hierarchical porous structure of an open surface porous layer and an interconnected bulk porous layer. The morphology, size, and density of the large, top surface pores were only dependent on the ice particulates embossing on the template. The freezing temperature showed no effect on the large, top surface pores. The large, top surface pores were, in effect, replicas of the embossing ice particulates. The freezing temperature did not affect the shape of the ice particulates and should have no affect on the formation of the large, top surface pores. Therefore, the properties of the large, top surface pores could be controlled by adjusting the shape, dimension, and density of the ice particulates. Some small pores were among the large surface pores. The small, top surface pores were mostly affected by the freezing temperature. A low freezing temperature resulted in small, top surface pores. The small, top surface pores were replicas of the newly formed ice crystals that grew among the embossing ice particulates during freezing. It has been reported that a low freezing temperature induces quick formation of small ice crystals [28]. The ice-particulate template also showed some effect on the small surface pores. The size of the small surface pores decreased as the dimension of the ice particulates embossed on the template decreased. This might be because the small ice particulates were more tightly compacted and less space was available for the formation of new ice crystals among the small ice particulates.

The bulk porous layer consisted of small pores that were connected with the large, top surface pores and extended into the bulk body of the sponge from the top surface pores. The inner bulk pores had almost the same sizes when the funnel-like chitosan sponges were prepared with ice particulates of different dimensions at the same freezing temperature. The ice particulates did not affect the diameter of the bulk pores. However, the sizes of the inner bulk pores changed with the freezing temperature. The size of the inner bulk pores decreased with a decrease in the temperature of the ice particulates. The inner bulk pores were dense and small when prepared at a low temperature, sparse and large when prepared at a high temperature. The inner bulk pores were replicas of the newly formed ice crystals that were formed when the chitosan solution was frozen. Formation of the ice crystals is affected by the temperature [28,29]. Low temperature results in the quick formation of dense, small ice crystals and high temperature results in the slow formation of sparse, large ice crystals. This might explain the effect of the ice particulate temperature on the porous structure of the inner bulk pores (Figure 3.2-3.5).

Freeze-drying has been used for the preparation of porous scaffolds of collagen, gelatin, chitosan, and collagen-glycosaminoglycan [21,30]. The conventional freeze-drying process for fabricating porous scaffolds creates variable cooling rates throughout the scaffold during freezing, producing a heterogeneous pore matrix structure with large variations in average pore diameters at different locations throughout the scaffold. Porous scaffolds with a homogeneous structure were prepared using a modified method that resulted in more homogeneous freezing by controlling the freezing rate and obtaining more uniform contact between the vessel containing the matrix suspension and the freezing shelf [28]. Although these freeze-drying methods can control the pore structure to some degree, it is difficult to control the surface pore structure. By using pre-prepared ice particulates embossed on a surface as a template, it is easy to control the surface porous structure to make open surface pores. The density, dimension, and morphology of the top surface pores can be tailor-made by designing the ice particulates. The ice particulates could serve as nuclei to initiate ice crystallization at the freezing interface of the liquid phase chitosan solution when the chitosan aqueous

solution is applied to the ice-particulate template (Figure 3.9). The process led to the growth of natural dendritic ice crystals from the surface of the ice particulates into the bulk aqueous solution. The newly formed ice crystals might be somewhat like prickles on a bur. The ice particulates together with the newly formed dendritic ice crystal network determine the unique funnel-like porous structure of the chitosan sponges. In this study, the ice particulates formed on a flat surface were used as template. Ice particulates can also be formed on curved or complicated surfaces and used as templates if the surface curve is not too shape to inhibit the formation of water droplets.

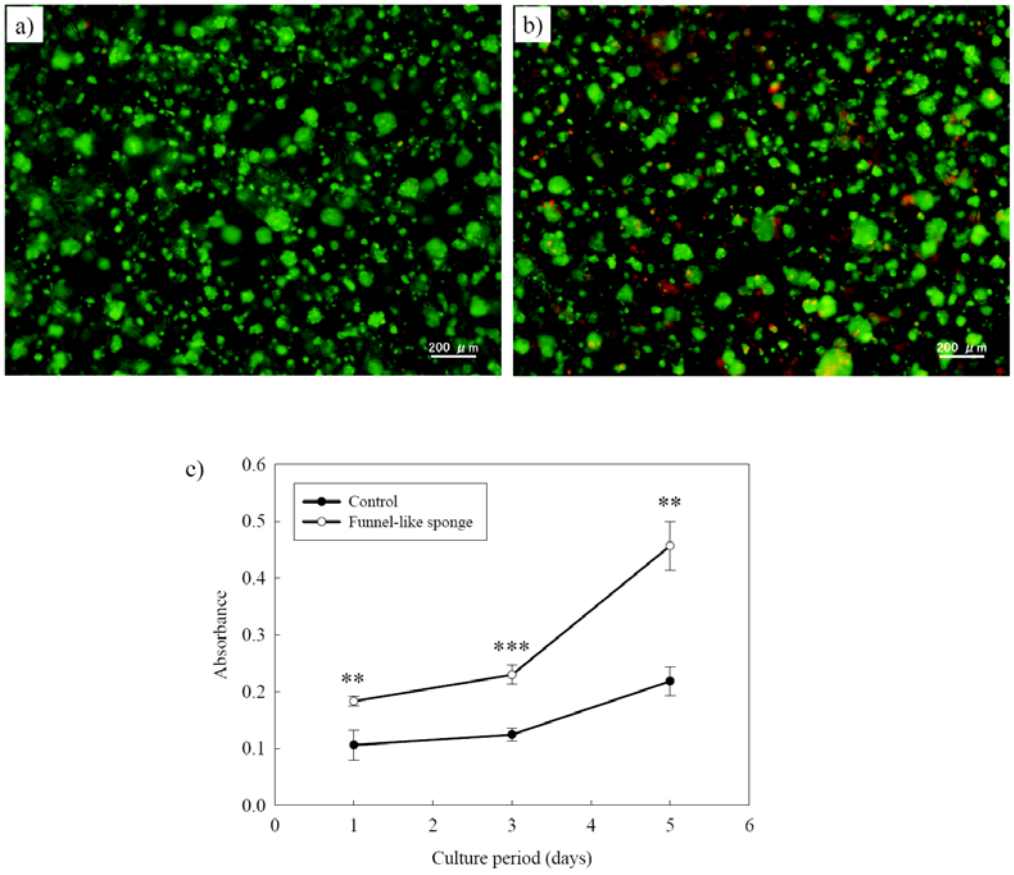

Figure 3.7 Live/dead staining (a, b) of fibroblasts after 24 hour culture in a funnel-like chitosan sponge (a) and a control chitosan sponge (b) and cell proliferation in a funnel-like chitosan sponge and a control chitosan sponge that was analyzed by WST-1 assay after culture in the sponges for 1, 3, and 5 days. Data are mean ± S.D. for n = 3 specimens from each condition. ***p<0.001, **p<0.01.

The funnel-like chitosan sponges showed less shrinkage compared to that of the control chitosan sponge. The stacked tube-like pores were slanted, causing the control sponge to easily shrink in the vertical direction. However, the bulk pores in the funnel-like chitosan sponge were somewhat like the structure of prickles on a bur. The pore structures were well balanced to suppress any sponge shrinkage.

The funnel-like structure of the hierarchical chitosan sponges facilitated cell infiltration and diffusion into the

inner pores of the scaffolds, and improved cell distribution throughout the scaffolds. The fibroblasts were homogeneous distributed in the funnel-like chitosan sponges, showed high viability, and three-dimensional proliferation. However, in the control chitosan sponge, the fibroblasts were mostly distributed on the surface and few cells were observed in the inner part. The cells stayed and proliferated only on the surface of the control chitosan sponge and not in the inner part. The large, top surface open pores and interconnected inner porous structure in the funnel-like chitosan sponges improved cell delivery and distribution and provided enough extra area for cell spreading and proliferation, thus avoiding excess cell aggregation and overgrowth.

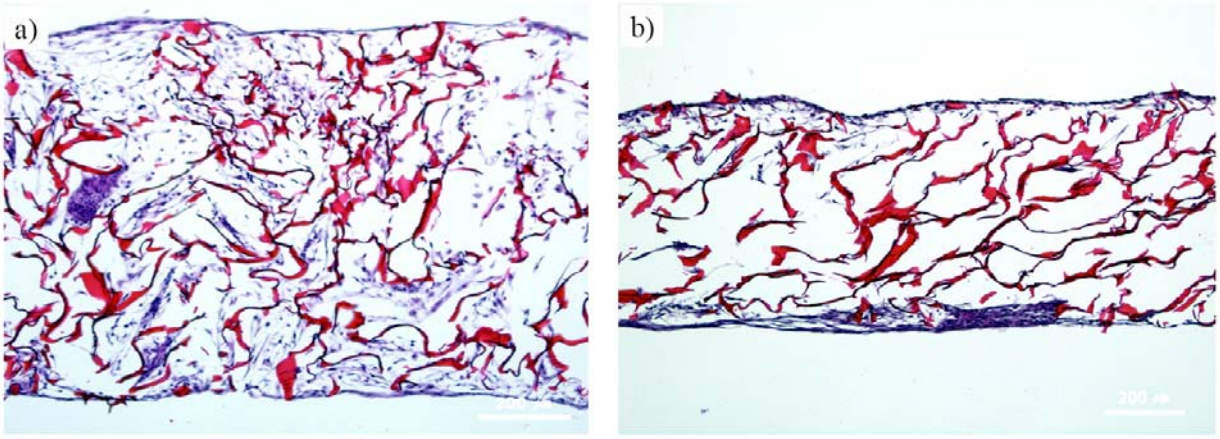

Figure 3.8 HE staining of fibroblasts after culture in a funnel-like chitosan sponge (a) and a control chitosan sponge (b) for 2 weeks.

3.5 Conclusions

Funnel-like chitosan sponges were prepared using an embossing ice template technique. The funnel-like chitosan sponges showed a hierarchical porous structure of large, open pores in the top surface layer and small, interconnected pores in the bulk layer. The characteristics of the large, top surface pores were affected by the shape, dimension, and density of the embossing ice particulates, but not by the freezing temperature. The inner bulk porous structure was affected by the freezing temperature and not the embossing ice particulates. When cultured in the funnel-like chitosan sponge, the cells showed homogenous distribution, high viability, and constructed homogenous tissue. The unique porous structure of the funnel-like chitosan sponge facilitated homogenous cell seeding, improved cell distribution, and therefore promoted homogeneous tissue formation. Such funnel-like scaffolds will be useful for tissue engineering applications. The embossing ice particulate method proved an easy and useful method of controlling the surface pore structure of porous scaffolds.

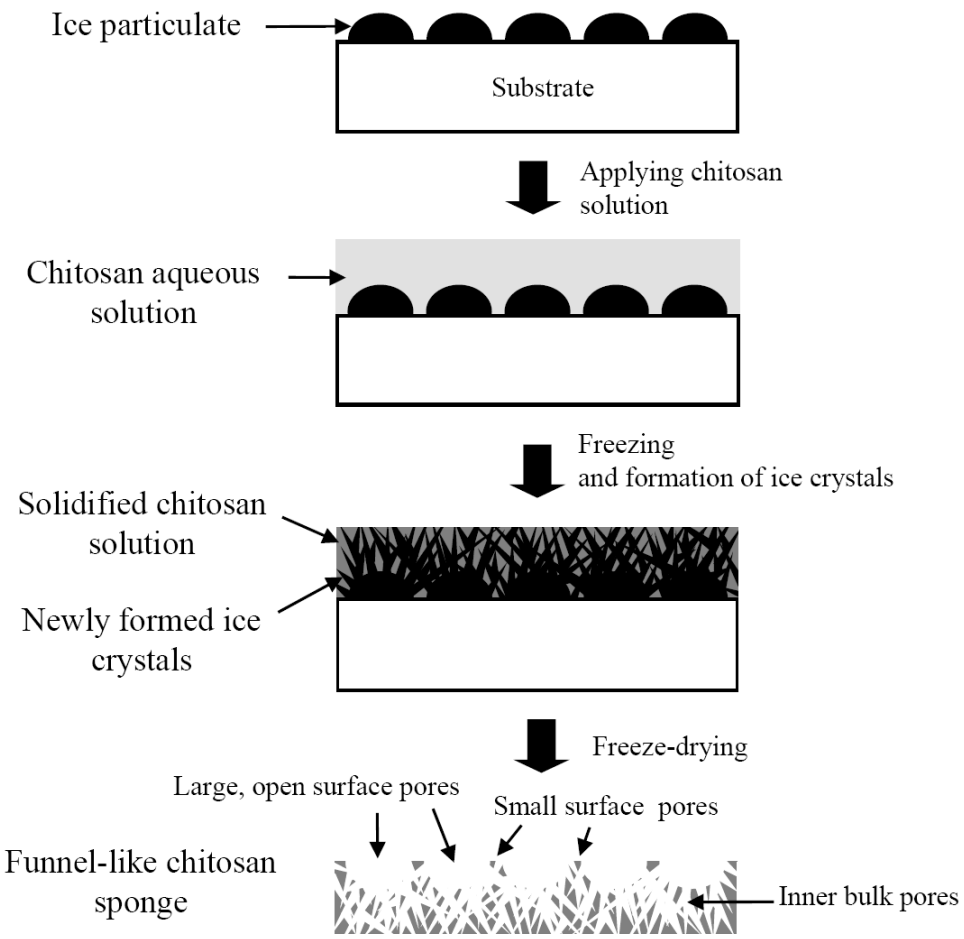

Figure 3.9 Schematic diagram of formation of porous structure in the funnel-like chitosan sponge.

3.6 References

1 Moutos, F. T., Freed, L. E., Guilak, F., A biomimetic three-dimensional woven composite scaffold for functional tissue engineering of cartilage. *Nature Materials* **6**, 162-167 (2007).

2 Engelmayr Jr, G. C., Cheng, M., Bettinger, C. J., Borenstein, J. T., Langer R., Freed, L. E., Accordion-like honeycombs for tissue engineering of cardiac anisotropy. *Nature Materials* **7**, 1003-1010 (2008).

3 Kim, I. Y., Seo, S. J., Moon, H. S., Yoo, M. K., Park, I. Y., Kim, B. C., Cho, C. S., Chitosan and its derivatives for tissue engineering applications. *Biotechnology Advances* **26**, 1-21 (2008).

4 Martino, A. D., Sittinger, M., Risbud, M. V., Chitosan: a versatile biopolymer for orthopaedic tissue-engineering. *Biomaterials* **26**, 5983-5990 (2005).

5 Khor, E., Lim, L. Y., Implantable applications of chitin and chitosan. *Biomaterials* **21**, 1-5 (2009).

6 Madihally, S. V., Matthew, H. W. T., Porous chitosan scaffolds for tissue engineering. *Biomaterials* **20**, 1133-1142 (1999).

7 Choi, S. W., Xie, J., Xia, Y., Chitosan-based inverse opals: three-dimensional scaffolds with uniform pore structures for cell culture. *Adv Mater* **21**, 1-5 (2009).
8 Tan, H., Chu, C. R., Payne, K. A., Marra, K. G., Injectable in situ forming biodegradable chitosan-hyaluronic acid based hydrogels for cartilage tissue engineering. *Biomaterials* **30**, 2499-2506 (2009).
9 Jiang, T., Abdel-Fattah, W. I., Laurencin, C. T., In vitro evaluation of chitosan/poly(lactic acid-glycolic acid) sintered microsphere scaffolds for bone tissue engineering. *Biomaterials* **27**, 4894-4903 (2006).
10 Heinemann, C., Heinemann, S., Bernhardt, A., Worch, H., Hanke, T., Novel textile chitosan scaffolds promote spreading, proliferation, and differentiation of osteoblasts. *Biomacromolecules* **9**, 2913-2920 (2008).
11 Feng, Z. Q., Chu, X., Huang, N. P., Wang, T., Wang, Y., Shi, X., Ding, Y., Gu, Z. Z., The effect of nanofibrous galactosylated chitosan scaffolds on the formation of rat primary hepatocyte aggregates and the maintenance of liver function. *Biomaterials* **30**, 2753-2763 (2009).
12 Yu, L. M. Y., Kazazian, K., Shoichet, M. S., Peptide surface modification of methacrylamide chitosan for neural tissue engineering applications. *J Biomed Mater Res A* **82**, 243-255 (2007).
13 Zhu, C., Fan, D., Duan, Z., Xue, W., Shang, L., Chen, F., Luo, Y., Initial investigation of novel human-like collagen/chitosan scaffold for vascular tissue engineering. *J Biomed Mater Res A* **89**, 829-840 (2009).
14 Jin, R., Moreira Teixeira, L. S., Dijkstra, P. J., Karperien, M., van Blitterswijk, C. A., Zhong, Z. Y., Feijen, J., Injectable chitosan-based hydrogels for cartilage tissue engineering. *Biomaterials* **30**, 2544-2551 (2009).
15 Kasahara, Y., Iwasaki, N., Yamane, S., Igarashi, T., Majima, T., Nonaka, S., Harada, K., Nishimura, S.I., Minami, A., Development of mature cartilage constructs using novel three-dimensional porous scaffolds for enhanced repair of osteochondral defects. *J Biomed Mater Res A* **86**, 127-136 (2008).
16 Ma, L., Gao, C., Mao, Z., Zhou, J., Shen, J., Hu, X., Han, C., Collagen/chitosan porous scaffolds with improved biostability for skin tissue engineering. *Biomaterials* **24**, 4833-4841 (2003).
17 Yilgor, P., Tuzlakoglu, K., Reis, R. L., Hasirci, N., Hasirci, V., Incorporation of a sequential BMP-2/BMP-7 delivery system into chitosan-based scaffolds for bone tissue engineering. *Biomaterials* **30**, 3551-3559 (2009).
18 Zhang, Y., Cheng, X., Wang, J., Wang, Y., Shi, B., Huang, C., Yang, X., Liu, T., Novel chitosan/collagen scaffold containing transforming growth factor-beta1 DNA for periodontal tissue engineering. *Biochem Biophys Res Commun* **344**, 362-369 (2006).
19 Silva, M. M. C. G., Cyster, L. A., Barry, J. J. A., Yang, X. B., Oreffo, R. O. C., Grant, D. M., Scotchford, C. J., Howdle, S. M., Shakesheff, K. M., Rose, F. R. A. J., The effect of anisotropic architecture on cell and tissue infiltration into tissue engineering scaffolds. *Biomaterials* **27**, 5909-5917 (2006).
20 Zhang, H., Hussain, I., Brust, M., Butler, M. F., Rannard, S. P., Cooper, A. I., Aligned two- and three-dimensional structures by directional freezing of polymers and nanoparticles. *Nature Materials* **4**, 787-793 (2005).
21 Faraj, K. A., van Kuppevelt, T. H., Daamen, W. F., Construction of collagen scaffolds that mimic the three-dimensional architecture of specific tissues. *Tissue Eng* **13**, 2387-2394 (2007).
22 Mikos, A. G., Thorsen, A. J., Czerwonka, L. A., Bao, Y., Langer, R., Winslow, D. N., Vacanti, J. P., Construction of collagen scaffolds that mimic the three-dimensional architecture of specific tissues. *Polymer* **35**, 1068-1077 (1994).
23 Harris, L. D., Kim, B. S., Mooney, D. J., Open pore biodegradable matrices formed with gas foaming. *J Biomed Mater Res* **42**, 396-402 (1998).
24 Mikos, A. G., Bao, Y., Cima, L. G., Ingber, D. E., Vacanti, J. P., Langer, R., Preparation of poly(glyco1ic acid) bonded fiber structures for cell attachment and transplantation. *J Biomed Mater Res* **27**, 183-189 (1993).
25 Meng, W., Kim, S. Y., Yuan, J., Kim, J. C., Kwon, O. H., Kawazoe, N., Chen, G., Ito, Y., Kang, I. K., Electrospun PHBV/collagen composite nanofibrous scaffolds for tissue engineering. *J Biomater Sci Polym Ed* **18**, 81-94 (2007).
26 Yang, F., Murugan, R., Ramakrishna, S., Wang, X., Ma, Y. X., Wang, S., Fabrication of nano-structured porous

PLLA scaffold intended for nerve tissue engineering. *Biomaterials* **25**, 1891-1900 (2004).

27 Sun, W., Starly, B., Darling, A., Gomez, C., Computer-aided tissue engineering: application to biomimetic modeling and design of tissue scaffolds. *Biotech Appl Biochem* **39**, 49-58 (2004).

28 O'Brien, F. J., Harley, B. A., Yannas, I. V., Gibson, L., Influence of freezing rate on pore structure in freeze-dried collagen-GAG scaffolds. *Biomaterials* **25**, 1077-1086 (2004).

29 Sastry, S., Water: Ins and outs of ice nucleation. *Nature* **438**, 746-747 (2005).

30 Zhang, H., Cooper, A. I., Aligned porous structures by directional freezing. *Adv Mater* **19**, 1529-1533 (2007).

Chapter 4

Preparation of open porous hyaluronic acid scaffolds for tissue engineering using the ice particulate template method

4.1 Summary

A novel method to fabricate highly interconnected porous hyaluronic acid (HA) scaffolds with open surface pore structures was developed by using embossed ice particulates as a template and their characterization was described in this chapter. HA sponges were cross-linked by water-soluble carbodiimide (WSC) and the optimal cross-linking condition was analyzed by infrared spectroscopy. Cross-linking with 50 mM WSC in a 90% (v/v) ethanol/water solvent mixture assured the highest degree of cross-linking and most stable structure and, therefore, was used to cross-link the HA sponges. Observation with a scanning electron microscope showed that the HA scaffolds had funnel-like porous structures. There were large, open pores on the top surfaces and inner bulk pores under the top surface of the funnel-like HA sponges. The inner bulk pores were interconnected with the large, top surface pores and extended into the whole sponge. The pore morphology and density of the large, top surface pores were dependent on the dimension and density of the ice particulates. The size of the inner bulk pores was dependent on the freezing temperature. The funnel-like pore structures of the HA sponges facilitated cell penetration into the inner pores of the sponges and resulted in homogenous cell distribution in the sponges.

4.2 Introduction

Tissue engineering is a promising approach to regenerate new tissues and organs for implantation by combining a patient's cells with a three-dimensional scaffold and growth factors [1]. It has been applied to almost all types of tissues and organs, and a number of encouraging results have been reported [2–4]. Polymeric porous scaffolds have frequently used in tissue engineering to provide a temporary microenvironment for cell adhesion, proliferation, differentiation and secretion of newly formed extracellular matrix, and to guide the formation of new tissues and organs into the desired shapes. Beside chemical composition and mechanical stability, an adequate porous structure of the matrix is very crucial for enabling cellular penetration into the construct and vascularization inside the scaffolds after transplantation [5]. Although a number of three-dimensional porous scaffolds have been developed from various kinds of biodegradable polymers, not all the scaffolds can ensure regeneration of homogenous tissue formation in the scaffolds. In general, cells are easily allocated and distributed in the peripheral areas and, thus, result in partial tissue regeneration

in the outermost peripheral layers of the scaffolds. Regeneration of homogenous tissues requires smooth cell delivery and distribution into the inner pores of the scaffolds. To solve this problem, a few preparation methods have been developed to increase the interconnectivity of the scaffolds [6–8]. However, precise control of the surface pore structures of the scaffolds has been difficult. We have developed a novel method of controlling the surface pore structure and increasing the interconnectivity between the surface pores and inner bulk pores by using embossed ice particulates as a template. The method has been used to fabricate funnel-like collagen and chitosan sponges that facilitated cell seeding and cell distribution [9].

In this chaper, the ice particulate template method was used for the preparation of funnel-like hyaluronic acid sponges with precisely controlled porous structures. Hyaluronic acid (HA) was used because it is a hydrophilic and natural glycosaminoglycan that is found in human skin, cartilage, intra-articular joint fluid and vitreous humor [10]. It is one of the base connective materials in extracellular matrix. HA has also been shown to play an important role in the lubrication of soft tissues, cushion cells, water absorbance, cell differentiation, migration and cell growth. HA-based scaffolds have been widely used in the tissue engineering of skin, cartilage tissue, bone and soft tissue filler [11–16].

4.3 Materials and method

4.3.1 Materials

Hyaluronic acid (hyaluronic acid potassium salt, from Rooster Comb, HA) and water-soluble carbodiimide (WSC, 1-ethyl-3-(3-dimethylaminopropyl)-carbodiimide and hydrochloride) were purchased from Wako (Osaka, Japan). White HA granules (1.0 wt%) were completely dissolved in pure water at a concentration of 1.0% (w/w). Homogenized HA aqueous solution was adjusted to pH 7.0 and stored at −1◦C before use. WSC was used as a cross-linking agent of HA. Water purified with a Milli-Q Water Purification System (resistivity 18.2 MΩ, TOC 2-5 ppb, Milli-Q Synthesis A10, Millipore) was used to prepare ice particulates and aqueous solutions.

4.3.2 HA scaffold fabrication using an ice particulate template

Open porous HA sponges were prepared by using embossed ice particulate templates with directional ice crystallization and freeze-drying to obtain integral microstructures. At first, hemispheric water droplets were formed by spraying water onto a perfluoroalkoxy (PFA) film-wrapped copper plate. The PFA film was used to increase the contact angle of the water droplets and to facilitate easy detachment of a frozen block from the plate afterward. The water droplets were frozen in a freezer (−30◦C) to obtain ice particulates embossed on the PFA film-wrapped copper plate. The dimensions of the water droplets and ice particulates could be controlled by the spraying times. Embossed ice particulate templates with three different sizes of ice particulates were prepared by spraying pure water 10, 20 and 30 times on the PFA film-wrapped copper plate and freezing [9]. The frozen ice particulate templates were stabilized to a designated temperature of −1, −3, −5 or −10◦C in a low temperature chamber (WT-201, ESPEC) for 1 hour. Subsequently, 1.0% (w/w) HA aqueous solution was poured onto the pre-cooled ice particulate template and covered with a glass plate in the low-temperature chamber, the temperature of which was set at the same temperature as that of the ice particulate template (−1, −3, −5 or −10◦C). The HA solution and ice particulate template were held in the low temperature chamber for 60 minutes to allow the ice particulates to initiate directional ice crystallization into the HA aqueous solution. The frozen HA solution and template were moved to a deep freezer (−80◦C) for further freezing for 5 hours. Then, the frozen HA solution together with the ice particulates were detached from the PFA film and lyophilized

for 24 hours in a freeze dryer under a vacuum of 20 Pa (VirTis-AdVantage Benchtop Freeze Dryer, SP Industries) to form HA sponges. Finally, the lyophilized HA sponges were cross-linked by WSC dissolved in an aqueous solution of ethanol at room temperature for 24 hours. The optimal cross-linking condition was investigated by changing the ethanol/water mixture ratio and WSC concentration. After cross-linking, the HA sponges were rinsed three times with water to remove residual chemicals. The rinsed sponges were frozen at −10◦C for 1 hour and −80◦C for another hour, and lyophilized in a freeze dryer for 24 hours to obtain the HA sponges. Control HA sponges were prepared by the same procedure using the PFA film-wrapped copper plate without the ice particulates.

4.3.3 Determination of cross-linking condition

The HA sponges were cross-linked with different concentrations of WSC dissolved in ethanol/water solvent mixture. The concentration was changed from 1 mM to 100 mM, and the ratio of ethanol to water was changed from 60 to 99.5% (v/v). The degree of cross-linking was analyzed by infrared spectra of each condition by using an attenuated total reflection (ATR) Fourier transformed infrared spectrometer (FT-IR-8400S, Shimadzu). This was done by pressing the HA sponges cross-linked at different conditions onto the surface of a diamond of an ATR attachment (DuraSamplIR II, Smiths Detection). The stability of the cross-linked HA sponges was evaluated by observation of morphology change and shrinkage. The cross-linked HA sponges were incubated in a phosphate buffer solution (PBS) at 37◦C. The morphology of each scaffold was observed after 1, 2 and 3 days incubation.

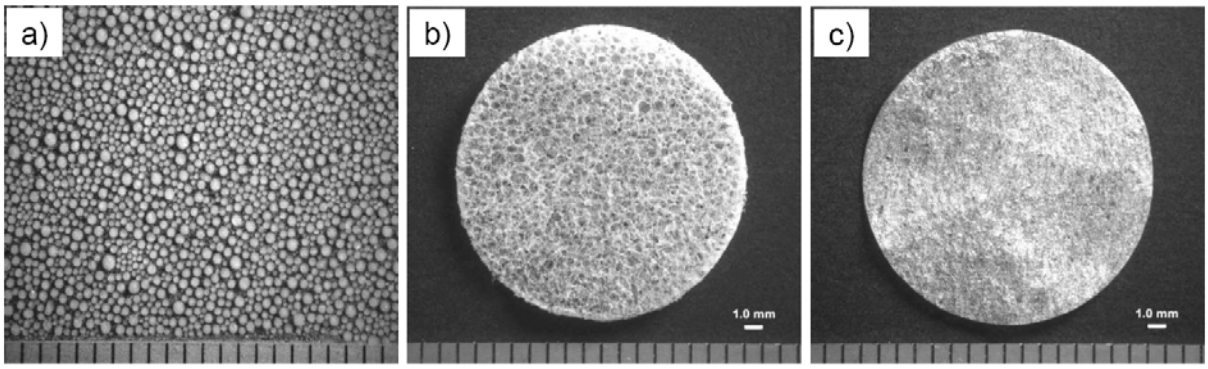

Figure 4.1 Photomicrographs of ice particulates with mean diameter of 398 μm (a), and a HA sponge prepared with the 398-μm diameter ice particulate template at -3°C (b) and a control HA sponge prepared at -3°C without an ice particulate template (c).

4.3.4 Cell culture and evaluation of cell seeding efficiency

The HA sponge scaffolds prepared at −3◦C with a 398-μm diameter ice particulate template were used for cell culture. The scaffolds were cut into round disks (diameter 16 mm) in order to arrange them in cell culture plates (Micro Plates-24 well, As One). The disks were sterilized using 70% ethanol for 30 min and then rinsed three times with PBS and exchanged with cell-culture medium. The side of the HA sponges facing the ice particulate template during preparation was defined as the top surface and the side facing the glass plate was defined as the bottom. The scaffolds were placed in the cell culture plate with the top surface up and the cells were seeded from the top surface. Neonatal

human dermal fibroblasts (NHDF, Cascade Biologics) were used for cell-culture experiments. The cells were grown in culture dishes (100 mm) with medium 106 (Cascade Biologics) supplemented with 2% (v/v) fetal bovine serum (FBS), 10 ng/ml human recombinant epidermal growth factor (hEGF), 3 ng/ml human recombinant fibroblast growth factor-basic (hFGF-B), gentamicin and amphotericin (Cascade Biologics). The cell culture was maintained in an incubator equilibrated with 5% CO_2 at 37◦C. The fibroblasts were subcultured once after reaching a confluent cell monolayer. The fibroblasts in confluence were rinsed with N-2-hydroxyethylpiperazine-N-2-ethanesulfonic acid (HEPES) buffer, detached from the culture dishes using 0.025% (w/v) trypsin and 0.01% (w/v) ethylenediaminetetraacetic acid (EDTA), and neutralized by HEPES solution containing 10% FBS (Kurabo). The collected cell suspension was centrifuged and re-suspended in the serum medium to a concentration of 5.0×10^6 cells/ml. The cells were then seeded onto the top surface of each HA sponge and incubated for 4 hours. Next, the HA sponge disks were transferred to new plates. Finally, the cells in the old medium and those that adhered to each well of the old cell-culture plates were collected and counted by a hemocytometer (Eosinophil Counter, TATAI, SLGC) to calculate cell seeding efficiency same as previous chapters.

4.4 Results and discussion

The design of a porous scaffold structure is one of the crucial factors in tissue engineering to guarantee trouble-free cell seeding, cell penetration, and homogenous cell distribution in the scaffolds to facilitate the expected tissue regeneration [5]. Open surface pores and highly interconnected inner pores of porous scaffolds are essential for uniform three-dimensional cell distribution and tissue formation. HA sponge scaffolds with controlled porous structures were prepared by using ice particulates embossed on a copper plate as a template and by controlling the freezing temperature. The ice particulate template was used as a porogen material due to several advantages. The ice particulate template can initiate the formation of a connected ice crystal network inside the aqueous polymer solution during the freezing process and the ice crystal network can be easily removed by lyophilization. The low temperature manipulation without usage of any organic solvents can preserve the biological activity of functional drugs and proteins incorporated in the scaffolds.

The ice particulates were obtained by freezing water droplets that were formed as a result of spraying pure water onto a hydrophobic surface. Ice particulates with mean diameters of 181 ± 43, 398 ± 113 and 719 ± 149 μm were prepared by spraying pure water 10, 20 and 30 times, respectively. Figure 4.1a shows a micrograph of the embossed ice particulates having a mean diameter of 398 ± 113 μm. The photo of the HA sponge prepared with the 398-μm ice particulate template shows the presence of many large pores on its top surface while few on the surface of the control HA sponge (Figure 4.1b and 4.1c).

4.4.1 Cross-linking of HA scaffolds

Porous scaffolds should be stable and not dissolve during cell seeding and culture. HA is hydrophilic and highly soluble in water. Therefore, the HA sponges should be cross-linked to make them non-dissoluble and stable in aqueous solution and to retard biodegradation in a biological environment for tissue-engineering application. Several cross-linking agents, such as WSC, GA, 1,4-butanediol diglycidyl ether, poly(ethylene glycol) diglycidyl ether, acetic anhydride and photoinitiator Irgacure 2959 (2-hydroxy-1-[4-(2-hydroxyethoxy)phenyl]-2-methyl-1-propanone) for photopolymerization, have been employed to cross-link HA-derived materials [17–20]. WSC was selected as a cross-liking agent in this study because of its efficiency in HA cross-linking and low toxicity [6, 21]. An ethanol and water mixture solvent was used to dissolve WSC while preventing dissolution of the HA sponge during treatment, because ethanol is

water-miscible and a non-solvent for HA. The optimal cross-linking condition was determined by changing the ethanol/water ratio in the solvent and the WSC concentration. At first, the optimal ratio of ethanol to water was determined by fixing the concentration of WSC at 50 mM. The crosslinking was done at room temperature for 24 h. The cross-linked HA sponges were investigated by ATR–FT-IR (Figure 4.2). Only the WSC powder and cross-linked HA sponges had a peak at 1700 cm^{-1}, which was assigned to the carbonyl group of the ester bond. However, both the uncross-linked and cross-linked HA sponges showed nearly the same absorbance at 2938 cm^{-1}, which was assigned to the $–CH_2–$ group [22]. Quantitative analysis of the degree of cross-linking was performed by comparing the peak absorbances at 1700 cm^{-1} and 2938 cm^{-1}, according to Tomihata et al. [19]. The ATR–FT-IR spectra of HA sponges cross-linked with solutions of different ethanol/water ratios containing 50 mM WSC are shown in Figure 4.3a. The absorbance peak assigned to the cross-linking carbonyl group appeared in the HA sponges cross-linked in all the mixture ratios. The absorbance ratios of the peak at 1700 cm^{-1} to that at 2938 cm^{-1} were calculated (Figure 4.3b). The absorbance ratio was high when the mixture ratio of ethanol/water was changed from 60% to 90%. However, when 99.5% ethanol was used, the absorbance ratio decreased. Even though the absorbance ratio was high when 60, 70 or 80% ethanol solution was used, the HA sponge showed partial dissolution in the 60 and 70% ethanol solution, and partial shrinkage in the 80% ethanol solution. The HA sponges showed a high degree of cross-linking, and no evidence of dissolution and shrinkage when the 90% ethanol solution was used. Therefore, a 90% ethanol/10% water (v/v) solution mixture was used to dissolve the WSC for the cross-linking in the following experiment.

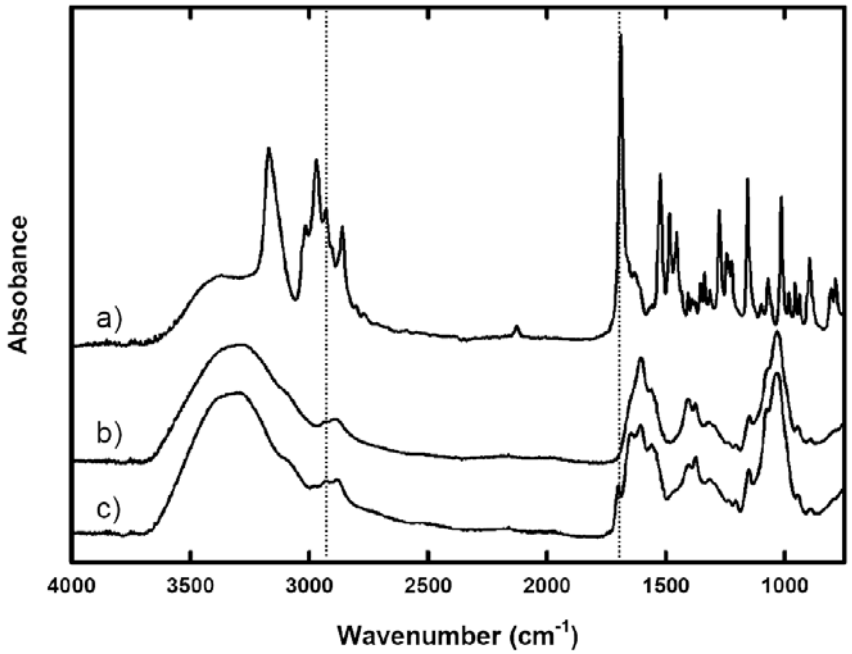

Figure 4.2 ATR-FT-IR spectra of WSC powder (a), uncross-linked HA sponge (b), and cross-linked HA sponge (c).

The optimal WSC concentration was determined by fixing the mixture ratio of ethanol and water at 90:10. The ATR–FT-IR spectra of HA sponges cross-linked at different WSC concentrations are shown in Figure 4.4a. The absorbance peak assigned to the cross-linking carbonyl group was detected from the HA sponges cross-linked at

whatever concentration. The ratio of absorbance at 1700 cm^{-1} to the absorbance at 2938 cm^{-1} increased with increasingWSC concentration. However, the increase became less evident when aWSC concentration greater than 50 mM was used. This result suggests the saturation of cross-linking when WSC concentration was higher than 50 mM. The HA sponges cross-linked with 1 mM and 10 mM WSC were partially deformed and dissolved after immersion in PBS for 1 day. The HA sponges cross-liked with 50 mM and 100 mM of WSC were stable in water, even after incubation in PBS for 3 days. Therefore, 50 mM was selected as the optimal WSC concentration for the cross-linking of the HA sponges. The 90:10 ethanol/water (v/v) solvent mixture containing 50 mM WSC was used for the cross-linking of the HA sponges in the following experiment.

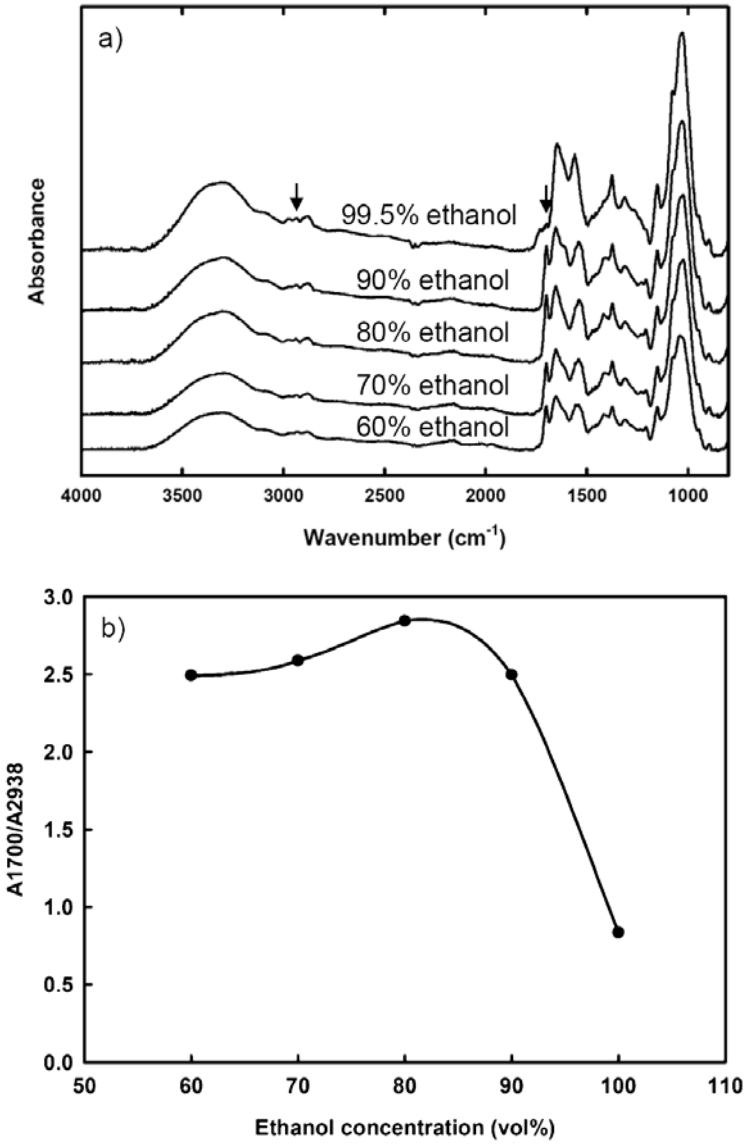

Figure 4.3 ATR-FT-IR spectra of HA sponges cross-linked with 50 mM WSC solution of different ratios of ethanol/water (a) and ratio of ATR-FT-IR absorbance at 1700 cm^{-1} to that at 2938 cm^{-1} against the solvent mixture composition (b).

4.4.2 HA sponges prepared with ice particulates of different dimensions

The HA sponges prepared at −3◦C with templates of 181, 398 and 719-μm diameter ice particulates were observed by SEM (Figure 4.5). The HA sponges prepared with the ice particulate templates showed large open pores on their top surfaces and interconnected inner bulk pore structures. There were two layers in the hierarchically structured scaffolds: a top surface layer and an inner bulk layer. The large open pores on the top surface had semi-spherical shapes that were similar to those of the embossed ice particulates. Observation of the cross-sections demonstrated that the large, open top surface pores were connected with the inner bulk pores. Because the unique pore structure was somewhat like that of a Büchner funnel, the HA sponges prepared with the ice particulate templates were referred to as funnel-like HA sponges. The bottom pores showed a random flake-like structure.

It is likely that the direction and interconnectivity of the bulk pores should be identical to that of the ice crystal network formed during freezing. If the ice crystals were formed in the absence of an external aligned nucleating agent, they would form a spindle-like structure without any specific direction. The control HA sponge prepared without an ice particulate template showed a random flake-like structure. However, the direction of ice growth during freezing is speculated to be controlled by the hemispherical ice particulates when the ice particulate template was used. The embossed ice particulates together with the newly formed ice crystals during freezing determined the pore structure in the funnel-like HA sponges. The thickness of the funnel-like HA sponges was higher than that of the control HA sponge. This might be because the funnel-like HA sponges showed less vertical shrinkage than did the control HA sponge. The dimension of the ice particulates showed no evident effect on the thickness of the funnel-like sponges. The bulk pores in the funnel-like HA sponges were regularly distributed in the vertical direction toward the large, top surface pores, which might be well balanced to suppress any sponge shrinkage. However, the stacked flake-like structures in the HA control sponge were slanted, which might cause the control sponge to easily shrink in the vertical direction.

The sizes of the pores of the funnel-like and control HA sponges were analyzed from their SEM photomicrographs (Figure 4.6). The size of the large, top surface pores was almost in the same range as that of the ice particulates. The size of the top surface pores of the control HA sponge was significantly smaller than that of the large, top surface pores of the funnel-like HA sponges. The mean size of the large, top surface pores of the three types of funnel-like HA sponges was significantly different and increased with an increase in the dimension of the ice particulates. The small, top surface pores were also significantly different among the three types of funnel-like HA sponges. There was no significant difference among the mean sizes of the inner bulk pores of the three types of funnel-like HA sponges, which indicates that the ice particulates size did not affect the pore structure of the inner bulk pores. The sizes of the pores of the bottom surface of the funnel-like HA sponges and control HA sponge were almost the same. These results indicate that the dimension of the ice particulates had a significant effect on the sizes of the large, top surface pores and the small, top surface pores, but no effect on the inner bulk pores and bottom pores.

4.4.3 HA sponges prepared at different temperatures

The effect of freezing temperature on the pore structure of the funnel-like HA sponges was investigated by preparing the funnel-like HA sponges at four different temperatures: −1, −3, −5 and −10◦C. Ice particulates having a diameter of 398 μm were used at all four temperatures. The large, top surface pores were formed at all four temperatures and the pores showed similar semi-spherical morphology. The bottom surface showed random pore structure. The upper row of the illustration in Figure 4.7 indicates the structures of the large, top surface pores and the inner bulk pores formed under them. The large, top surface pores had almost the same dimensions despite the different

freezing temperatures while the inner bulk pores became smaller and denser as the freezing temperature decreased. The mean pore diameters of the large, top surface pores; the small, top surface pores; the inner bulk pores; and the bottom surface pores were analyzed from their SEM photomicrographs (Figure 4.8). The mean diameters of the large, top surface pores in the funnel-like HA sponges were almost the same; there was no significant difference. The sizes of the large, top surface pores were not affected by the freezing temperature. The mean size of the small, top surface pores, inner bulk pores and bottom surface pores decreased as the freezing temperature decreased. The freezing temperature showed a significant effect on the size of these pores.

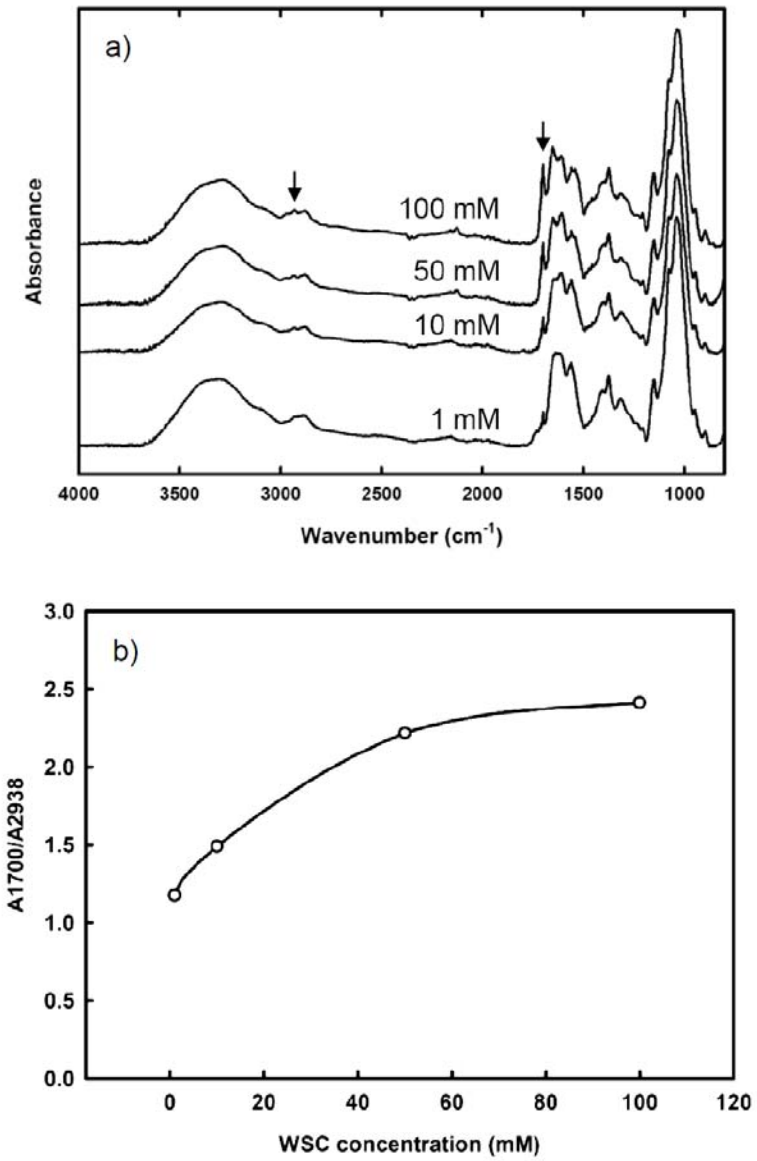

Figure 4.4 ATR-FT-IR spectra of HA sponges cross-linked with different concentrations of WSC prepared with a solvent mixture of 90% ethanol and 10% water (a) and ratio of ATR-FT-IR absorbance at 1700 cm^{-1} to that at 2938 cm^{-1} against the concentration of WSC (b).

The pore structure of the freeze-dried sponge is a replica of the ice crystal morphology in a frozen block during the freezing process. The freezing temperature influences the pore size and ice crystal density because temperature is related to heat transfer and the rate of crystallization in solution. This can be explained by the nucleation and growth of the ice crystals from the liquid to solid phase. Fast crystallization leads to small crystals and slow crystallization leads to large crystals [23–25]. Therefore, the rate of crystallization of an aqueous solution is a critical parameter in the freezing process. When the HA solution was frozen at low temperature, the pores in the scaffolds were small and dense. At a high freezing temperature, the pores were large and sparse. The effects of ice particulate dimension and freezing temperature on the pore structures of the funnel-like HA sponges indicate that the morphology, size and density of the large, top surface pores were only dependent on the ice particulates embossed on the template. The freezing temperature showed almost no effect on the large, top surface pores. The large, top surface pores were, in effect, replicas of the embossing ice particulates. The freezing temperature did not affect the shape of the ice particulates and should have had no effect on the formation of the large, top surface pores. Therefore, the properties of the large, top surface pores could be controlled by adjusting the shape, dimension, and density of the ice particulates. The small, top surface pores were affected by both the ice particulate dimension and freezing temperature. Small ice particulates and a low freezing temperature resulted in small, top surface pores. The small, top surface pores were replicas of the newly formed ice crystals that grew among the embossing ice particulates during freezing. It has been reported that a low freezing temperature induces quick formation of small ice crystals [25]. The small ice particulates might transfer heat more quickly than do the large ice particulates, thus resulting in formation of small ice crystals. The inner bulk porous layer consisted of small pores that were connected with the large, top surface pores and extended into the bulk body of the sponge from the top surface pores. The inner bulk pores were dependent on the freezing temperature, but were not affected by the dimension of the ice particulates.

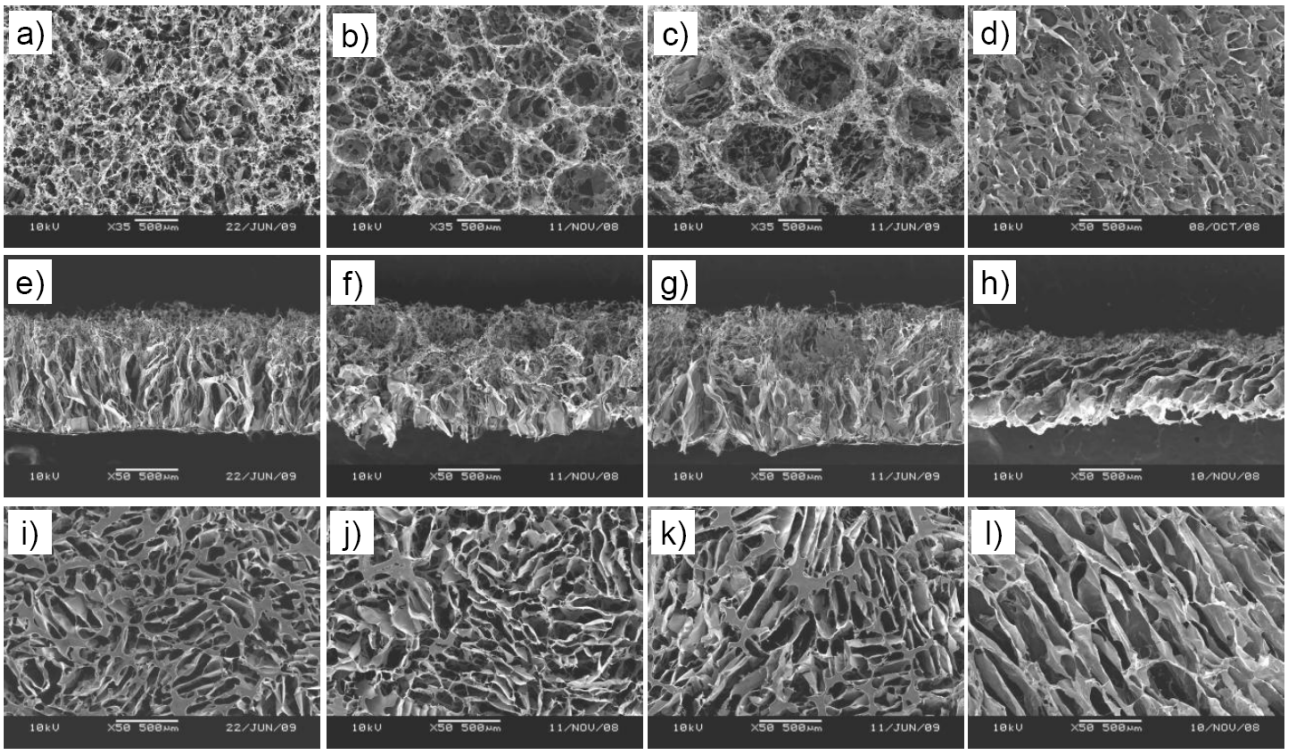

Figure 4.5 SEM photomicrographs of top surfaces (a-d), cross sections (e-h), and bottom surfaces (i-l) of funnel-like HA sponges prepared by using templates embossed with ice particulates having diameters of 181 μm (a, e, i), 398 μm (b, f, j), and 719 μm (c, g, k) and control HA sponge prepared without an ice particulate template (d, h, l). The freezing temperature was -3°C. Scale bars = 500 μm.

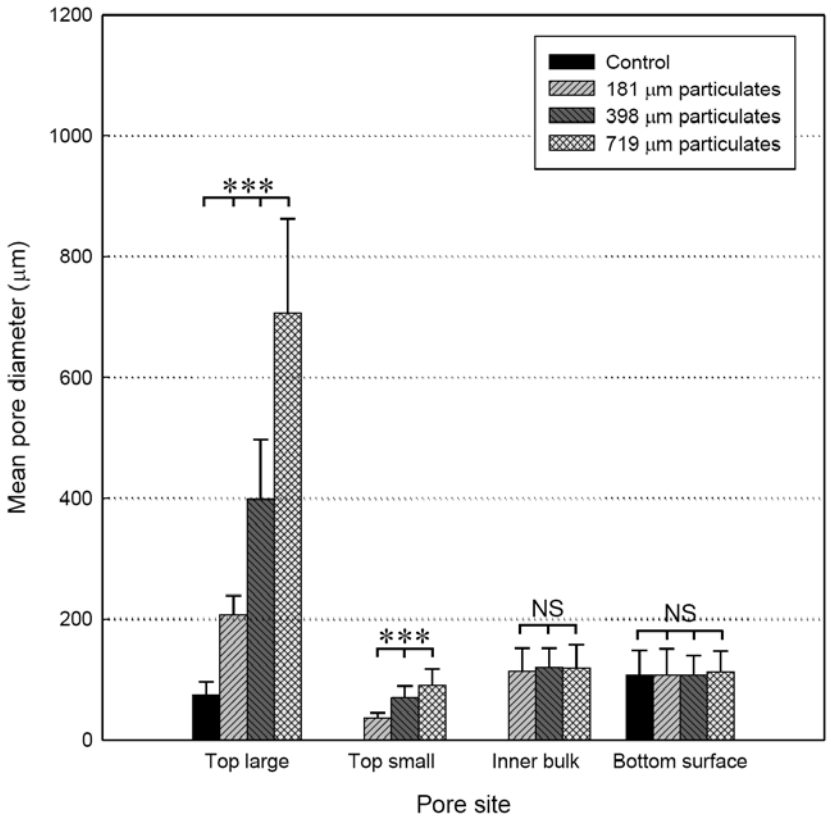

Figure 4.6 Pore diameter analysis of the large, top surface pores; the small, top surface pores; the inner bulk pores; and the bottom surface pores of the funnel-like HA sponges prepared at -3°C with templates embossed with ice particulates having diameters of 181, 398, and 719 μm. Data are mean ± S.D. for n = 100 pores from 3 specimens of each condition. ***$p < 0.001$. NS, not significant.

4.4.4 Cell culture in HA sponges

In vitro cell-culture experiments were performed to examine the effect of pore structure on cell seeding and cell distribution. Neonatal human dermal fibroblasts were seeded in the funnel-like HA sponge prepared at at −3◦C with 398-μm diameter ice particulates, and in the control HA sponge. Cell seeding efficiency was evaluated by counting the number of cells that leaked from the sponges after 4 hours of culture. The cell-seeding efficiency of the funnel-like HA sponge and control HA sponge were 92.8 ± 1.0% and 92.0 ± 2.3%, respectively. Thus, both the control and funnel-like HA sponges showed high cell-seeding efficiency. The cell distribution in the HA sponges was examined by SEM observation (Figure 4.9). The cells were distributed in both the surface pores and inner parts of the funnel-like HA sponge. In contrast, the cells were stacked up on the top surface of the control HA sponge. Only a few cells were detected in the inner pores of the control HA sponge. The funnel-like structure of the HA sponge prepared with ice particulates facilitated cell penetration from the surface into the inner parts of the sponge. The cells could easily pass through the large, top surface pores and enter the interconnected channels of the layer below and become distributed homogenously throughout the sponge.

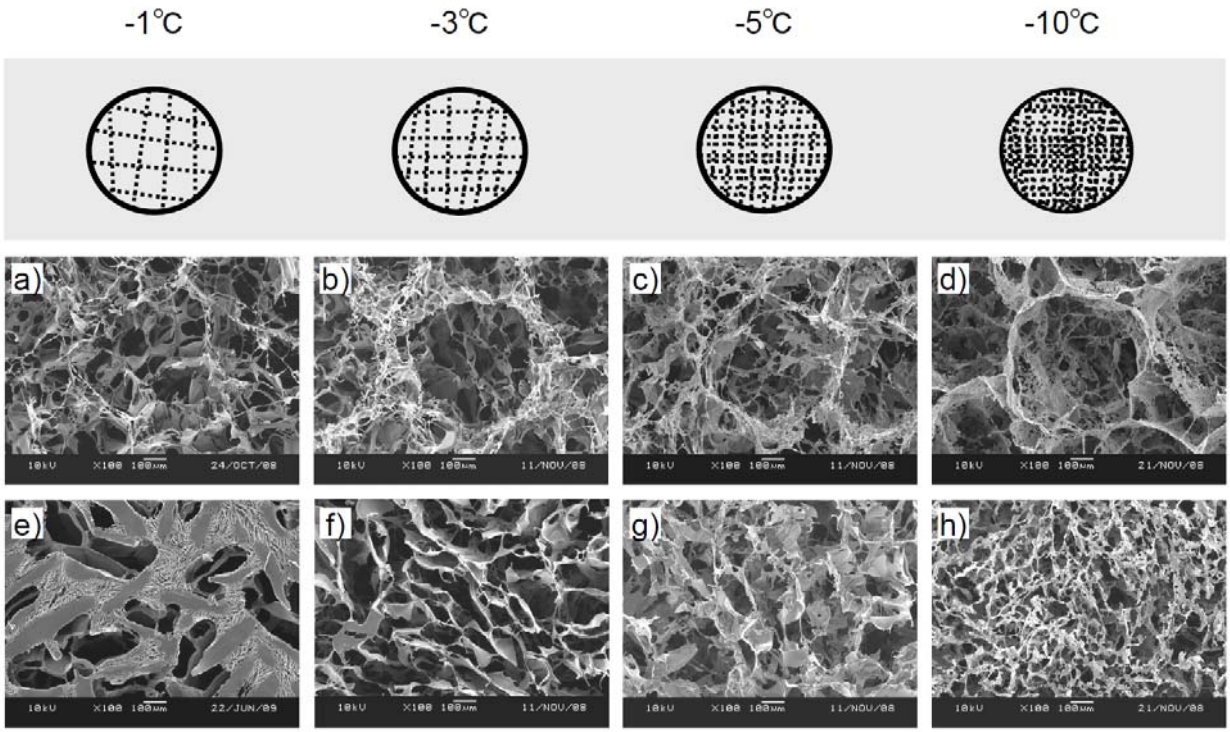

Figure 4.7 SEM photomicrographs of top surfaces (a-d) and bottom surfaces (e-h) of the funnel-like HA sponges prepared with a 398-µm diameter ice particulate template at different temperatures: -1 (a, e), -3 (b, f), -5 (c, g), and -10°C (d, h). Scale bars = 100 µm.

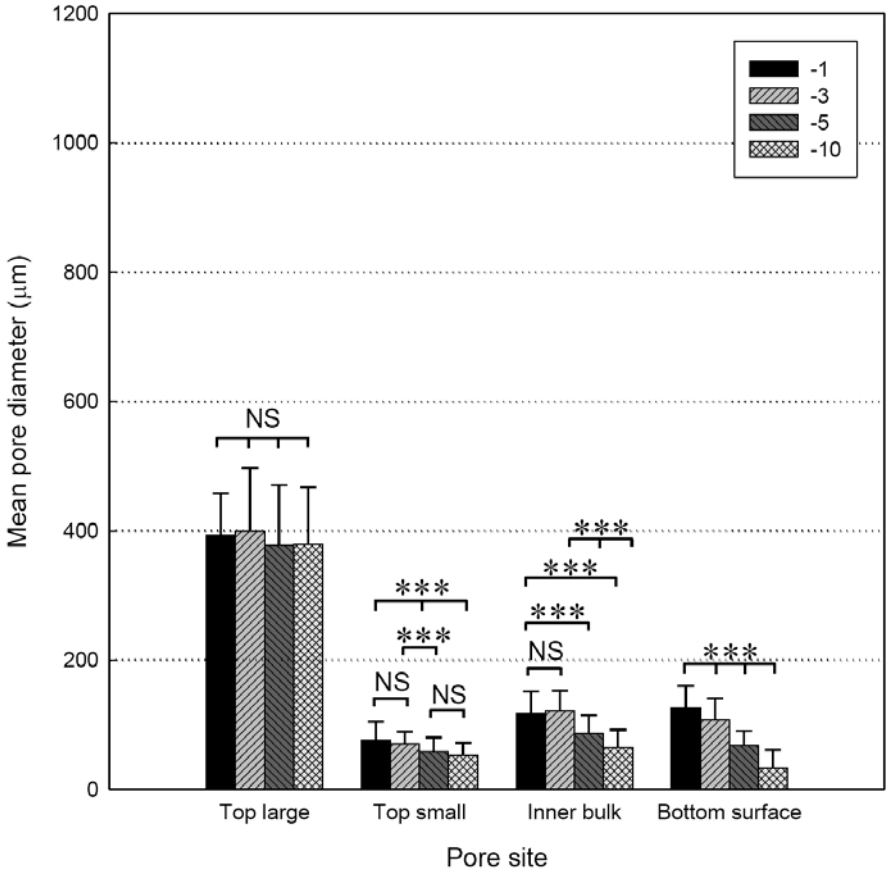

Figure 4.8 Pore diameter analysis of the large, top surface pores; the small, top surface pores; the inner bulk pores; and the bottom surface pores of the funnel-like HA sponges prepared with a 398-μm diameter ice particulate template at different temperatures of -1, -3, -5, and -10°C. Data are mean ± S.D. for n = 100 pores from 3 specimens of each condition. ***$p < 0.001$. NS, not significant.

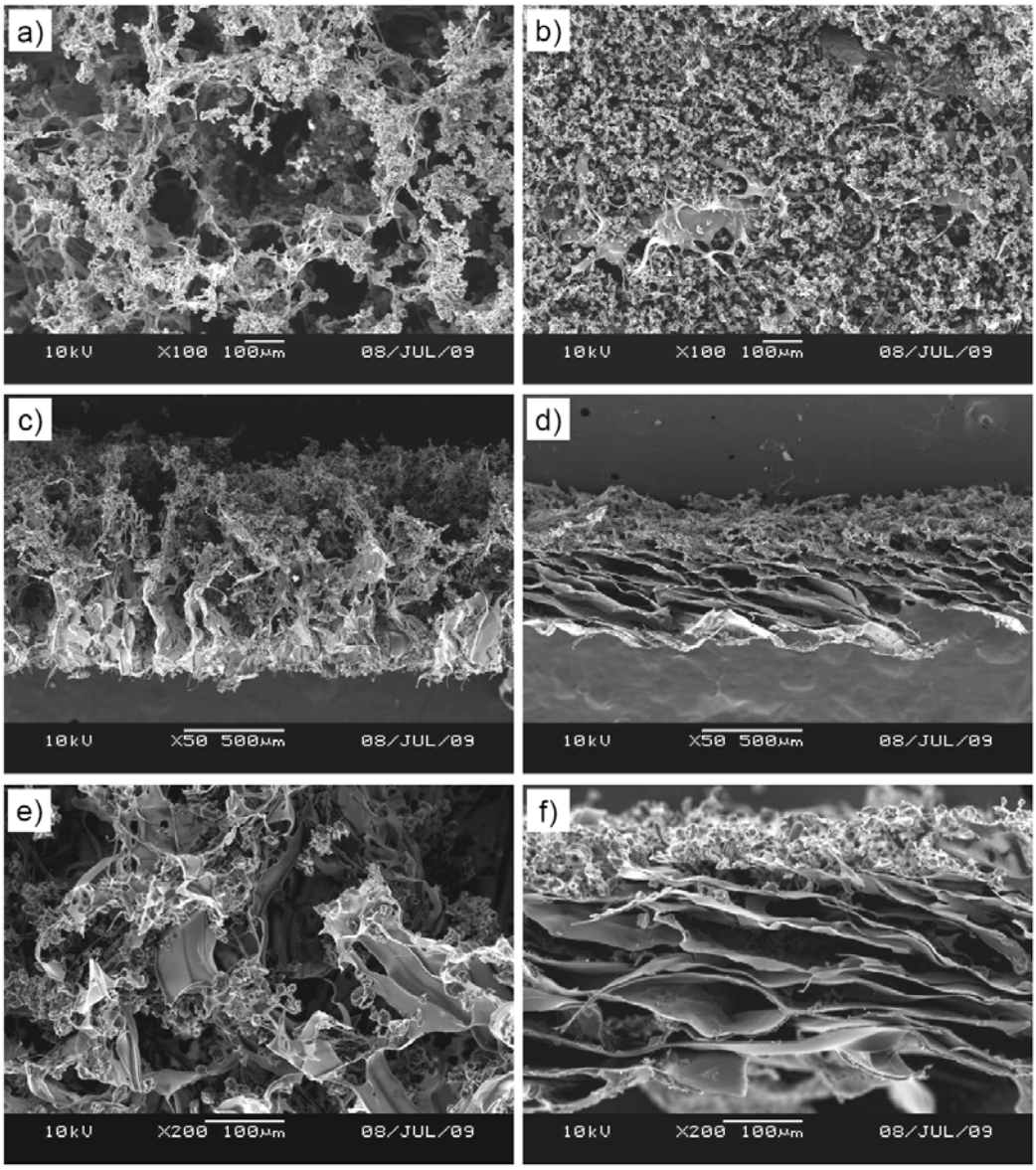

Figure 4.9 SEM photomicrographs of top surfaces (a, b) and cross sections (c-f) of the funnel-like HA sponge (a, c, e) and the control HA sponge (b, d, f) after fibroblasts were cultured in the sponges for 1 hour. Scale bars: a, b, e, f = 100 µm; scale bars: c, d = 500 µm.

4.5 Conclusions

Porous scaffolds of hyaluronic acid were prepared using embossed ice particulates as a template. The HA sponges showed a funnel-like porous structure that had large, top surface pores connected with underlying inner bulk pores. The pore structure of the large, top surface pores were determined by the density and dimension of the ice particulates embossed on the template. The freezing temperature did not affect the large, top surface pores. However, the inner bulk pores under the top surface pores were dependent on the freezing temperature while the ice characteristics of the ice particulates did not affect the structure of the inner bulk pores. The funnellike structure in the HA sponge scaffolds prepared with ice particulates facilitated cell penetration and homogenous distribution in the scaffolds. Such funnel-like HA sponges will be useful for tissue engineering.

4.6 References

1 Langer, R., Vacanti, J. P., Tissue engineering. *Science* **260**, 920 (1993).

2 Seal, B. L., Otero, T. C., Panitch, A., Polymeric biomaterials for tissue and organ regeneration. *Mater Sci Eng* **R34**, 147 (2001).

3 Scuderi, N., Onesti, M. G., Bistoni, G., Ceccarelli, S., Rotolo, S., Angeloni, A., Marchese, C., The clinical application of autologous bioengineered skin based on a hyaluronic acid scaffold. *Biomaterials* **29**,1620 (2008).

4 Chvapil, M., Collagen sponge: Theory and practice of medical applications. *J Biomed Mater Res* **11**, 721 (1977).

5 Dagalakis, N., Flink, J., Stasikelis, P., Burke, J. F., Yannas, I. V., Design of an artificial skin. Part Ⅲ. Control of pore structure. *J Biomed Mater Res* **14**, 511 (1980).

6 Lee, S. J., Kim, S. Y., Lee, Y. M., Preparation of porous collagen/hyaluronic acid hybrid scaffolds for biomimetic functionalization through biochemical binding affinity. *J Biomed Mater Res B* **82B**, 506 (2007).

7 Harris, Leatrese D., Kim B.-S., David J. Mooney, Open pore biodegradable matrices formed with gas foaming. *J Biomed Mater Res* **42**, 396 (1998).

8 Sun, W., Starly, B., Darling, A., Gomez, C., Computer-aided tissue engineering: application to biomimetic modeling and design of tissue scaffolds. *Biotech Appl Biochem* **39**, 49 (2004).

9 Ko, Y.-G., Kawazoe, N., Tateishi, T., Chen, G., Preparation of chitosan scaffold with a hierarchical porous structure. *J Biomed Mater Res B*, In press.

10 Kuo, J.-W., Swann, D. A., Prestwwich, G. D., Chemical modification of hyaluronic acid by carbodiimide. *Bioconjugate Chemistry* **2**, 232 (1991).

11 Campoccia, D., Doherty, P., Radice, M., Brun, P., Abatangelo, G., Williams, D. F., Semisynthetic resorbable materials from hyaluronan esterification. *Biomaterials* **19**, 2101 (1998).

12 Park, S.-N., Lee, H. J, Lee, K. H., Suh, H., Biological characterization of EDC-crosslinked collagen-hyaluronic acid matrix in dermal tissue restoration. *Biomaterials* **24**, 1631 (2003).

13 Km, J., Kim, I. S., Cho, T. H., Lee, K. B., Hwang, S. J., Tae, G., Noh, I., Lee, S. H., Park, Y., Sun, K., Bone regeneration using hyaluronic acid-based hydrogel with bone morphogenic protein-2 and human mesenchymal stem cells. *Biomaterials* **28**, 1830 (2007).

14 Hemmrich, K., von Heimburg, D., Rendchen, R., Bartolo, C. D., Milella, E., Pallua, N., Implantation of preadipocyte-loaded hyaluronic acid-based scaffolds into nude mice to evaluate potential for tissue engineering. *Biomaterials* **26**, 7025 (2005).

15 Borzacchiello, A., Mayol, L., Ramires, P. A., Pastorello, A., Bartolo, C. D., Ambrosio, L., Milell, E., Structural and

rheological characterization of hyaluronic acid-based scaffolds for adipose tissue engineering. *Biomaterials* **28**, 4399 (2007).

16 Halbleib, M., Skurk, T., de Luca, C., von Heimburg, D., Hauner, H., Tissue engineering of white adipose tissue using hyaluronic acid-based scaffolds. I: in vitro differentiation of human adipocyte precursor cells on scaffolds. *Biomaterials* **24**, 3125 (2003).

17 Segura, T., Anderson, B. C., Chung, P. H., Webber, R. E., Shull, K. R., Shea, L. D., Crosslinked hyaluronic acid hydrogels: a strategy to functionalize and pattern. *Biomaterials* **26**, 359 (2005).

18 Masters, K. S., Shah, D. N., Leinwand, L. A., Anseth, K. S., Crosslinked hyaluronan scaffolds as a biologically active carrier for valvular interstitial cells. *Biomaterials* **26**, 2517 (2005).

19 Tomihata, K., Ikada, Y., Crosslinking of hyaluronic acid with water-soluble carbodiimide. *J Biomed Mater Res* **37**, 243 (1997).

20 Tomihata, K., Ikada, Y., Crosslinking of hyaluronic acid with glutaraldehyde. *J Polym Sci A: Polym Chem* **35**, 3553 (1997).

21 Park, S.-N., Park, J.-C., Kim, H. O., Song, M. J., Suh H., Characterization of porous collagen/hyaluronic acid scaffold modified by 1-ethyl-3-(3-dimethylaminopropyl)carbodiimide cross-linking. *Biomaterials* **23**, 1205 (2002).

22 Szymanski, H. A., Erickson, R. E., Infrared band handbook Volume 1. *Plenum Press*, 83 (1970).

23 Mandal, B. B., Kundu, S. C., Cell proliferation and migration in silk fibroin 3D scaffolds. *Biomaterials* **30**, 2956 (2009).

24 Kang, H.-W., Tabata, Y., Ikada, Y., Fabrication of porous gelatin scaffolds for tissue engineering. *Biomaterials* **20**, 1339 (1999).

25 O'Brien, F. J., Harley, B. A., Yannas, I. V., Gibson, L., Influence of freezing rate on pore structure in freeze-dried collagen-GAG scaffolds. *Biomaterials* **25**, 1077 (2004).

Chapter 5

Preparation of collagen-glycosaminoglycan sponges with open surface porous structures using ice particulate template method

5.1 Summary

Porous scaffolds having open surface pores and interconnected bulk pores are essential to promote cell penetration into the porous structure of the scaffold and to facilitate homogeneous spatial cell distribution throughout the scaffold for tissue engineering. Funnel-like sponges of collagen incorporated with glycosaminoglycan (GAG) were prepared by freeze-drying using ice particulates as templates and their characterization was described in this chapter. The porous structures of the funnel-like collagen-GAG sponges were compared with those of funnel-like collagen sponges. The funnel-like collagen-GAG sponges showed similar porous structures to those of funnel-like collagen sponges. The funnel-like collagen-GAG and collagen sponges had one top surface layer and one bulk porous layer. The top surface layer consisted of both large and small pores. The large, top surface pores were determined by ice particulates that were used as templates. The small, top surface pores and inner bulk pores were determined by ice crystals that were newly formed during freezing. The ice particulates affected the diameter of both the large and small, top surface pores, but not the inner bulk pores. When fibroblasts were cultured in the funnel-like sponges, the structures of the sponges facilitated homogenous cell distribution, improved cell viability, and resulted in homogenous tissue formation. Incorporation of GAG increased the mechanical property and cell viability of collagen-GAG sponges.

5.2 Introduction

In the past decade, numerous porous scaffolds have been reported for tissue engineering that provide an ideal temporary support structure for cell adhesion, proliferation, differentiation, extracellular matrix formation, and as guides for the construction of new tissues into a desired shape [1-8]. A suitable pore structure of the scaffold is important for effective cellular penetration into the porous structure and vascularization inside the scaffolds after transplantation [9-15]. Although a number of three-dimensional porous scaffolds have been developed from various types of biodegradable polymers, not all the scaffolds were able to ensure regeneration of the formation of homogenous tissue in the scaffolds. In general, cells easily enter into the peripheral areas of the scaffold, resulting in partial tissue regeneration primarily in the outermost layers [8, 16]. Regeneration of homogenous tissues requires smooth cell delivery and distribution into the inner pores of the scaffolds. To facilitate this difficulty, various methods of scaffold fabrication have been developed to

increase scaffold interconnectivity using phase separation, emulsion freeze-drying, gas forming, fiber bonding, prototyping and porogen leaching methods [17]. However, these methods have encountered some difficulties with undesirable surface pore structures. For this reason, we have developed a new method of controlling the surface pore structure and increasing the interconnectivity between the surface pores and inner bulk pores by using embossed ice particulates as a template [18]. This method has been used to fabricate funnel-like chitosan sponges that had open surface pores and interconnected bulk pores to facilitate homogenous spatial cell distribution.

In this study, the ice particulate template method was used for the preparation of six types of funnel-like collagen and collagen-glycosaminoglycan (GAG) sponges with controlled pore structures. Collagen is a natural polymer that is widely used as a biomaterial [19-21]. GAG was incorporated in a collagen matrix to improve bioactivity and biomechanical properties to better imitate the biological environment because of its role in retaining water, which helps maintain structural integrity, as well as its importance in interacting with proteins in extracellular matrix (ECM) [22]. Chondroitin sulfate is sulfated glycosaminoglycan (GAG) composed of a chain of alternating sugars (N-acetylgalactosamine and glucuronic acid). GAG is usually attached to proteins as a part of a proteoglycan. Collagen scaffolds incorporating GAG have been often used in the tissue engineering of skin, cartilage, and bone tissue engineering [1, 17, 22]. The porous structure of the funnel-like collagen-GAG sponges was investigated and the effect of the composition was evaluated. The sponges were used for the three-dimensional culture of fibroblasts.

5.3 Materials and methods

5.3.1 Preparation of ice particulate templates using an ultrasonic humidifier

Hemispheric water droplets were formed by application of consistent moisture onto a perfluoroalkoxy (PFA) film-wrapped copper plate in a plastic chamber using an ultrasonic humidifier (Iori-Mu, GRE-01, ICC Co., Ltd, Japan). The PFA-wrapped copper plate was attached with a 1-mm thick silicone frame to control the thickness of the loaded polymer solution. The water used in the humidifier was purified with a Milli-Q Water Purification System (resistivity: 18.2 MΩ, TOC: 2-5 ppb, Milli-Q Synthesis A10, Millipore). Three types of water droplets of different dimensions were prepared by controlling the moisture application time for 6, 11, and 21 minutes. The water droplets formed on the PFA-wrapped copper plate were frozen in a freezer at –30°C for 5 hours to prepare the ice particulates. Three types of templates embossed with ice particulates of different dimensions were prepared. The sizes of the embossing ice particulates were measured from their photomicrographs. The frozen ice particulate templates were stabilized at a designated temperature of –3°C in a low temperature chamber (WT-201, ESPEC Corp.) for 1 hour before use.

5.3.2 Preparation of collagen-GAG and collagen sponges

Collagen-GAG sponges were prepared by using the three types of ice particulates as templates. At first, a collagen-GAG mixture solution was prepared. Chondroitin 6-sulfate sodium salt powder (glycosaminoglycan from shark cartilage, 6-sulfate : 4-sulfate=0.33 : 1, Sigma Aldrich) was added to an aqueous solution of collagen type I (from porcine skin, 1.0 wt%, pH 3.0, Nippon Meat Packers, Osaka, Japan) to prepare the collagen-GAG mixture solution. Varying amounts of GAG powder (0.002, 0.005, 0.010, 0.025 and 0.050 g) were added to the aqueous solution of collagen (10 g). The amount ratios of GAG to collagen were 0.02, 0.05, 0.10, 0.25, and 0.50, respectively. The GAG powder did not completely dissolve in the collagen aqueous solution. The collagen-GAG suspension solution was homogenized. The collagen-GAG and collagen solutions were stored at -1°C for 24 hours for cooling before being

poured onto the ice particulate templates. At this temperature, the collagen-GAG and collagen solutions were in supercooled states and did not freeze in the absence of a nucleating agent.

Subsequently, after the ice particulate template was stabilized in the low temperature chamber at -3℃ for 1 hour, the collagen-GAG suspension solution was poured onto the embossed ice template inside the silicone frame. The surface of the collagen-GAG suspension solution was covered with a glass plate wrapped with polyvinylidene chloride film. The collagen-GAG suspension solution and the templates were kept in the low temperature chamber at -3°C for 1 hour to allow the ice particulates to initiate ice crystallization into the suspension. After this initial ice formation, the frozen collagen-GAG suspension on its template was moved to a deep freezer (-80°C) for an additional five hours of freezing. The solidified collagen-GAG block, still containing the ice particulates, was detached from the surface of the PFA film and freeze-dried for 24 hours in a freeze-dryer under a vacuum of 20 Pa (VirTis AdVantage Benchtop Freeze Dryer, SP Industries Inc.) to form the collagen-GAG sponges.

Finally, the freeze-dried collagen-GAG sponges were cross-linked by glutaraldehyde vapor, which was saturated with 25% aqueous glutaraldehyde solution at 37°C in a closed box for 4 hours. After cross-linking, the sponges were immersed in 0.1 M glycine aqueous solution to block any unreacted cross-linking agent. The sponges were then washed three times with pure water and treated at low pressure using a vacuum system to remove any residual chemicals trapped by air bubbles. The washed sponges were instantly frozen at -10°C and freeze-dried again to obtain the collagen-GAG sponges for characterization and cell culture experiments. Collagen sponges were prepared by the same procedure as the collagen-GAG sponges. At the same time, control collagen and control collagen-GAG sponges were prepared by the same procedure using the PFA film-wrapped copper plate without the ice particulates.

5.3.3 Determination of GAG amount in collagen-GAG sponges

The amount of GAG in the collagen-GAG sponges was measured by GAG assay to determine the amount of GAG remaining in the sponges. The collagen-GAG sponges were cut in 5-mm diameter sponge disks. The sponge disks were digested in a papain solution (400 μg/ml, in 0.1 M phosphate buffer, 5 mM L-cysteine, 5 mM EDTA, pH 6.0) at 60°C for 6 hours in a shaking chamber. The amount of GAG was analyzed using Blyscan Sulfated Glycosaminoglycan Assay kit (Biocolor Ltd.). A digested solution of 10 μl was mixed with 90 μl of pure water and reacted with 1000 μl of Blyscan dye solution (1,9-dimethyl-methylene blue in an inorganic buffer containing surfactants and stabilizers). The reacted GAG with dye reagent was centrifuged and the bound dye was dissolved in dissociation reagent. Thereafter, the absorbance was measured at a wavelength of 656 nm using a microplate reader (Bio-Rad Benchmark Plus, Bio-Rad Laboratories, Inc.). The amount of GAG in each sponge disk was calculated using a standard plot of chondroitin sulfate in the range of 0-100 μg/ml.

5.3.4 Mechanical test

Dried collagen-GAG and collagen sponges were used for static tensile mechanical tests (TMI UTM-10T; Toyo Baldwin Co., Ltd., Tokyo, Japan). The length and width of the sponges used for the mechanical test were 16.0 mm and 5.0 mm, respectively. The thickness of the sponges was measured by a vernier caliper. The sponges were pulled to failure at a rate of 1.0 mm/minutes. Load-deformation curves were obtained from a chart recorder. Young's modulus was determined from the load-deformation curves and the dimensions of each sample. The average values were calculated from three measurements.

5.3.5 Cell culture in collagen-GAG and collagen sponges

The collagen-GAG and collagen sponges were cut into round disks (diameter: 16 mm and 5 mm) in order to arrange them in cell culture plates (24-well Microplates, As One Corp. and 96-well plates, F96, PolySorp, Nunc). The disks were sterilized using 70% ethanol for 30 minutes, rinsed three times with phosphate buffered saline (PBS), and exchanged with media. Air bubbles in the scaffolds were removed by 10 minutes of low pressure treatment in a sterile condition. The scaffolds were placed in the cell culture plate with the top surface up and the cells were seeded from the top surface. Neonatal human dermal fibroblasts (NHDF, Cascade Biologics, Inc.) were used for cell culture experiments. The cells were grown in culture flasks (75 cm^2) with Medium 106 (Cascade Biologics Inc.) supplemented with 2% (v/v) fetal bovine serum (FBS), 10 ng/ml human recombinant epidermal growth factor (hEGF), 3 ng/ml human recombinant fibroblast growth factor-basic (hFGF-b), gentamicin, and amphotericin (Cascade Biologics, Inc.). The cell culture was maintained in an incubator equilibrated with 5% CO_2 at 37°C. The fibroblasts were subcultured once after reaching a confluent cell monolayer. The fibroblasts in confluence were rinsed with N-2-hydroxyethylpiperazine-N'-2-ethanesulfonic acid (HEPES) buffer, detached from the culture flasks using 0.025% (w/v) trypsin and 0.01% (w/v) ethylenediaminetetraacetic acid (EDTA), and neutralized by HEPES solution containing 10% FBS (Kurabo Industries, Ltd.). The collected cell suspension was centrifuged and resuspended in the serum medium to a concentration of 5.0 x 10^6 cells/ml. The cells were then seeded onto the top surface of each sponge and cultured in an incubator equilibrated with 5% CO_2 at 37°C.

Table 5.1 Mixing ratio and remained GAG amount in the collagen-GAG sponges

Samples	Initial ratio of GAG to collagen	Ratio of GAG to collagen in collagen-GAG sponges	Percentage of remained GAG to the initial GAG (%)
C100/G0 sponge	0.0 : 100	0.0 : 100	-
C100/G2 sponge	2.0 : 100	1.6±0.6 : 100	80.6±28.3
C100/G5 sponge	5.0 : 100	2.4±1.1 : 100	48.9±22.9
C100/G10 sponge	10.0 : 100	4.7±1.1 : 100	47.4±10.6
C100/G25 sponge	25.0 : 100	10.1±4.2 : 100	40.2±16.7
C100/G50 sponge	50.0 : 100	16.0±2.7 : 100	32.0± 5.4

5.3.6 Analysis of cell distribution

After one hours of culture, the sponges were washed three times with PBS and fixed with 2.5% glutaraldehyde aqueous solution at room temperature for 1 hour. The sponges were then washed three times with pure water and freeze-dried for 24 hours. The freeze-dried samples were cross-sectioned and coated with platinum for SEM observation to examine cellular distribution on the surfaces of the scaffolds. In addition, after 24 hours culture, cell-seeded sponges were washed with PBS and fixed in 10% neutral buffered formalin. Cell-scaffold constructs were dehydrated by a series of ethanol solutions, finally replaced with Lemosol A (Wako Pure Chemical Industries, Ltd.) for paraffin embedding, and sectioned (10 μm) using a rotary microtome (RM2245, Leica Microsystems Nussloch GmbH).

The sectioned cell-sponge constructs were stained with 4',6'-diamino-2-phenylindole (DAPI, Vector Laboratories, Inc.) to visualize nuclei. Stained sections were observed under a fluorescence microscope equipped with a digital imaging system (BX51 with DP70, Olympus Corp.).

5.3.7 Analysis of cell viability

Live/dead staining was performed to evaluate cell viability using calcein-AM (live: green) and propidium iodide (dead: red) staining reagents (Cellstain Double Staining Kit, Dojindo Laboratories). NHDF cells cultured in the collagen-GAG and collagen sponges for 24 hours were washed with HEPES buffer and incubated in 2 μM calcein-AM and 4 μM propidium iodide solution in HEPES buffer for 30 minutes. After being rinsed with HEPES buffer, the submerged specimens were observed with a fluorescence microscope.

Cell viability was also evaluated using WST-1 reagent (Roche Diagnostics GmbH), a colorimetric assay based on the cleavage of WST-1 tetrazolium salt by mitochondrial dehydrogenases by cellular respiration and metabolic rate. For the WST-1 assay, the funnel-like sponges were cut into 5-mm diameter disks. After sterilization and pre-wetting of the sponges, 5.0 x 10^5 cells/scaffold were seeded on each sponge disk. NHDF cells were cultured in the funnel-like collagen and collagen-GAG sponges for 14 days. Thereafter, each sponge disk was moved to a new plate with fresh media (1000 μl) and further incubated for one hour. Then, WST-1 reagent (100 μl) was added to each specimen, which was then incubated for 30 minutes at 37°C in a CO_2 incubator. The culture medium turned yellow during the incubation. The yellow-colored media by reaction with each cell-sponge construct was moved to a 96-well plate by pipette (200 μl). The absorbance of each well was measured at 440 nm with a reference wavelength of 650 nm using a microplate reader (Bio-Rad Benchmark Plus, Bio-Rad Laboratories Inc.). To obtain the means and standard deviations, three sponge disks were used for the measurements.

5.4 Results and discussion

5.4.1 Ice particulate template and determination of incorporated GAG

The design of a porous scaffold structure is important in tissue engineering to induce efficient cell seeding, good cell penetration, and homogenous cell distribution in the scaffolds to facilitate the desired tissue regeneration [8, 16, 23]. Open surface pores and highly interconnected inner pores of porous scaffolds are essential for uniform three-dimensional cell distribution and tissue formation. Controlled porous structure scaffolds composed of collagen and GAG were prepared by freeze-drying using size-controlled ice particulate templates. The ice particulates were prepared by freezing water droplets that were formed on a hydrophobic PFA film-wrapped copper plate. The water droplets were formed by the accumulation of micron-sized mist generated by an ultrasonic humidifier on the surface of the PFA film [24]. The PFA film was used to increase the contact angle of the water droplets and to facilitate easy detachment of a frozen block from the copper plate. The copper plate was used as a substrate of the ice particulates to maintain a cold temperature with high thermal conductivity. Three types of ice particulates were prepared by controlling the duration of moisture application. The diameters of ice particulates prepared with moisture application durations of 6, 11, and 21 minutes were 199 ± 36, 401 ± 84, and 801 ± 371 μm, respectively. Thus, the size of the ice particulates could be controlled by changing the duration of moisture application.

To determine the optimal ratio of GAG to collagen in an aqueous solution for creating tissue engineering scaffolds, five collagen-GAG mixture solutions were prepared and used for scaffold preparation by changing the ratio of GAG to collagen in the mixture solution from 0.02 to 0.50 (Table 5.1). GAG aggregated in the mixture solution and

became more evident as the ratio of GAG increased. The C100/G25 and C100/G50 mixtures were heterogeneous slurry, while the C100/G2, C100/G5, and C100/G10 mixtures were semi-transparent suspensions. The five collagen-GAG mixtures were used for preparation of collagen-GAG sponges. The diameter of the ice particulates used as templates were 401 μm and the freezing temperature was controlled at –3°C. The porous structures of the five types of collagen-GAG were observed by SEM (Figure 5.1). There were large, open pores on the top surface of the collagen-GAG sponges. The large, open pores had semi-spherical shapes that were similar to those of the ice particulates. The large, open pores were clearly observed for the C100/G2, C100/G5, and C100/G10 sponges. However, the top surface pores were partially collapsed for the C100/G25 and C100/G50 sponges. Under the top surface large pores, there were inner bulk pores, which were connected with the top surface large pores. The inner bulk pores of the C100/G2, C100/G5, and C100/G10 sponges had structures that were oriented perpendicular to the top surface. However, the orientation of the inner bulk pores became less evident as the GAG content increased. The thickness of the sponges decreased as the GAG content increased. The pores in the sponges with high GAG content seemed partially collapsed and the sponges shrank.

The amount of GAG in each sponge was analyzed by GAG quantification. The amount of GAG remaining in the collagen-GAG sponges was from 1.61 ± 0.57 to 16.00 ± 2.72%. The final amount of GAG in each sponge was much lower than the initial incorporation amount, indicating that the GAG molecules were only partially fixed during the cross-linking treatment. The non-cross-linked GAG molecules were removed during washing. The percentage of GAG remaining was inversely related to the initial feed ratio of GAG. The partial cross-linking of GAG in the collagen-GAG sponges and removal of the non-cross-linked GAG might affect the porous structures of collagen-GAG sponges containing the high initial feed content of GAG. The pores in the C100/G25 and C100/G50 sponges were partially collapsed and the sponges shrank after cross-linking and washing. The collagen-GAG mixture of C100/G10 was chosen for the following experiments because the C100/G10 sponge showed a stable porous structure and had a definite amount of GAG remaining in the sponge.

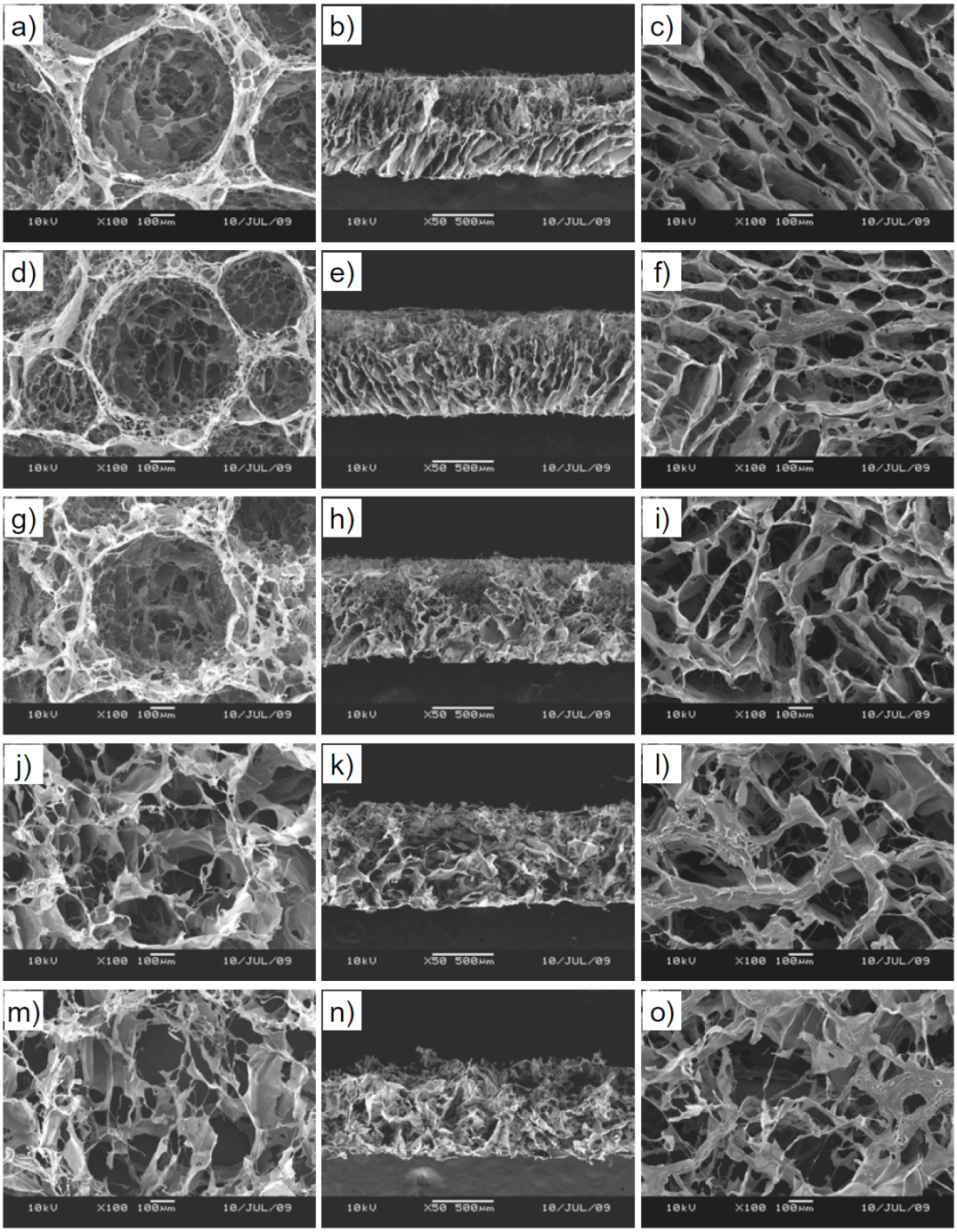

Figure 5.1 SEM photomicrographs of funnel-like sponges of C100/G2 (a-c), C100/G5 (d-f), C100/G10 (g-i), C100/G20 (j-l), and C100/G50 (m-o) using the 401 μm diameter ice particulate template at –3°C. Images of top surfaces (a, d, g, j, m), cross sections (b, e, h, k, n), and bottom surfaces (c, f, i, l, o). Scale bars in b, e, h, k, n and others = 500 μm and 100 μm, respectively.

5.4.2 Collagen-GAG and collagen sponges prepared with ice particulates of different dimensions

Three types of templates having different diameters of ice particulates of 199, 401, and 801 μm were used to prepare C100/G10 and collagen sponges. C100/G10 and collagen control sponges were also prepared without the ice particulate templates. From the gross appearance (Figure 5.2), the control sponges showed a dense, flat surface, while large pores were evident on the surfaces of the sponges prepared with the ice particulates. The microstructures of the C100/G10 and collagen sponges were observed by SEM (Figure 5.3). The sponges prepared with ice particulate templates had two layers of porous structures: a top surface layer and an inner bulk layer. The top surface layer contained both large and small pores. The inner bulk layer contained pores that were connected with the surface pores. The large, open pores on the top surface had semi-spherical shapes that were similar to those of the embossed ice particulates. The sponges prepared with the ice particulate templates were referred to as funnel-like sponges because their unique pore structures were somewhat like that of a Büchner funnel. The bottom pores showed a random flake-like structure. The funnel-like C100/G10 and collagen sponges showed similar porous structures. In contrast to the funnel-like sponges, the control sponges prepared without ice particulates did not have a bilayer porous structure.

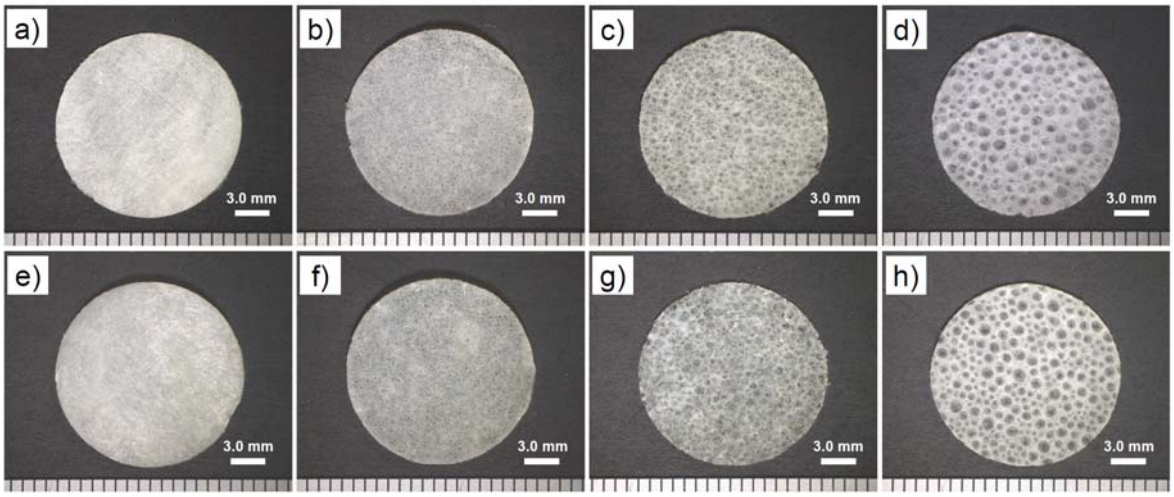

Figure 5.2 Photographs of collagen (a-d) and collagen-GAG (e-h) sponges prepared without ice particulate templates (a, e) and with 199 (b, f), 401 (c, g), and 801 μm (d, h) diameter ice particulate templates at -3°C. Scale bars = 3.0 mm.

The direction and interconnectivity of the bulk pores would be expected to be identical to that of the ice crystal network formed during freezing [25]. If the ice crystals were formed in the absence of an external aligned nucleating agent, they would form a plate-like structure [26]. The control collagen and collagen-GAG sponges prepared without ice particulate templates showed a flake-like microstructure, which was not controllable. It could be vertical or parallel to the top surface. On the other hand, directional growth of ice branches during freezing is considered to be controlled by the hemispherical ice particulates when ice particulates are used as templates. During the freezing process, the embossed ice particulates together with the newly formed ice crystal branches determined the pore morphology of the funnel-like sponges. The bulk pores in the funnel-like sponges were mostly in the vertical direction toward the large, top

surface pores. During the scaffold fabrication process, the vertical orientation and regular distribution of the inner bulk pores might prevent the compression of the sponge from deformation of the sponge thickness.

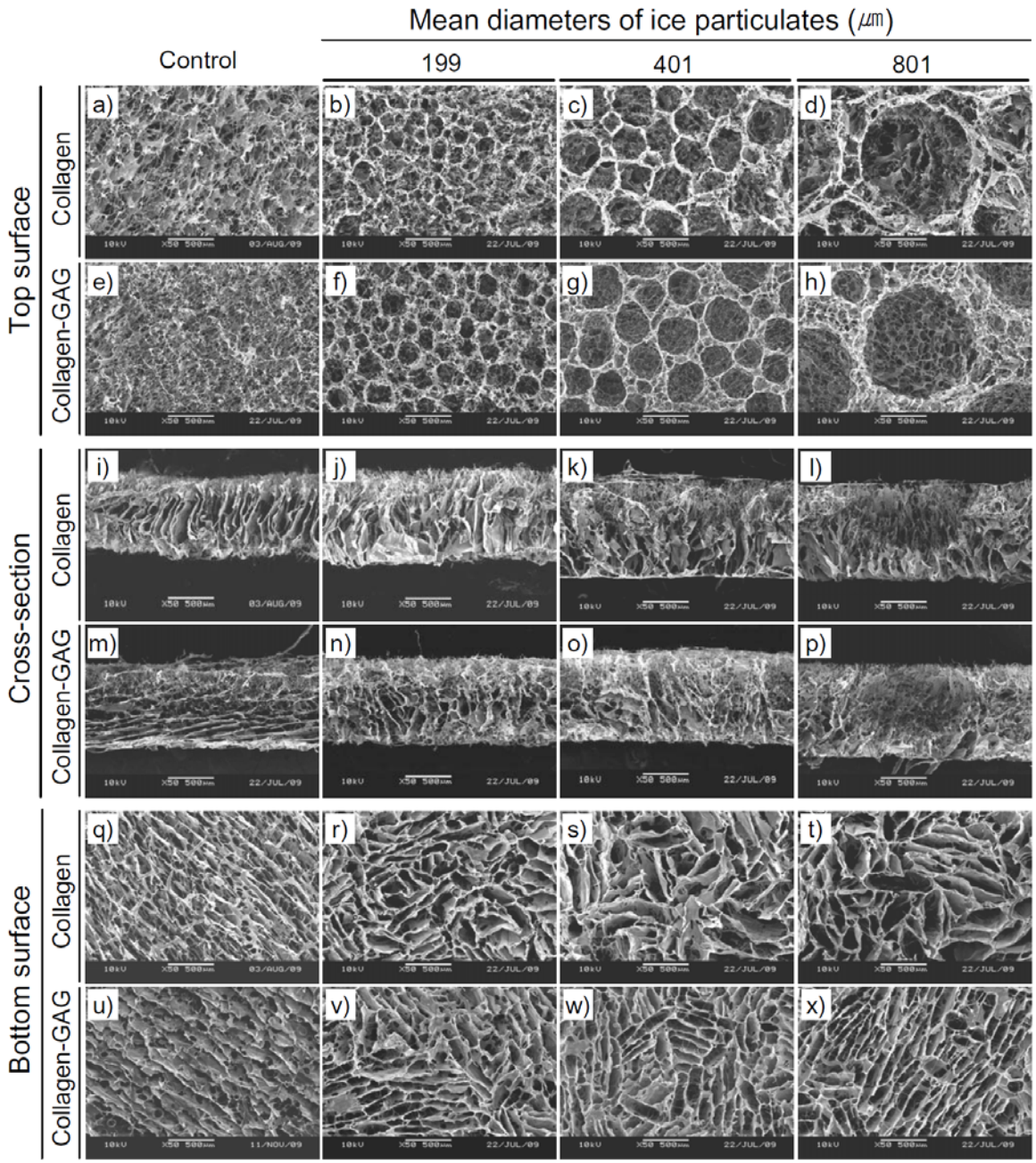

Figure 5.3. SEM photomicrographs of control collagen (a, i, q) and control collagen-GAG (e, m, u) sponges prepared without ice particulate templates. SEM photomicrographs of top surfaces (b-d, f-h), cross sections (j-l, n-p), and bottom surfaces (r-t, v-x) of funnel-like collagen and collagen-GAG sponges prepared by using templates embossed with ice particulates having diameters of 199 μm (b, f, j, n, r, v), 401 μm (c, g, k, o, s, w), and 801 μm (d, h, l, p, t, x). The freezing temperature was -3°C. Scale bars = 500 μm.

The mean pore sizes of the funnel-like and control sponges of C100/G10 and collagen were analyzed using image analysis software with their SEM photomicrographs (Figure 5.4). The pore sizes of the funnel-like collagen sponges were similar to those of the funnel-like C100/G10 sponges when the same ice particulate templates were used. The mean diameters of the large, top surface pores of the funnel-like collagen sponges or C100/G10 sponges were in the same range as those of the respective ice particulates used as templates. The mean diameters of the large, top surface pores of the three types of funnel-like collagen sponges or C100/G10 sponges were significantly different and increased with an increase in the dimension of the ice particulates. The small, top surface pores were also significantly different among the three types of funnel-like collagen or C100/G10 sponges. The diameters of the small, top surface pores increased as larger ice particulates were used as templates. In contrast, there was no significant difference among the sizes of the inner bulk pores of the three types of funnel-like collagen or C100/G10 sponges, which indicates that the size of the ice particulates did not affect the pore structure of the inner bulk pores. There also was no significant difference among the sizes of the bottom surface pores of the funnel-like collagen or C100/G10 sponges. In a comparison of the funnel-like sponges with the control sponges, the mean diameter of the top surface pores of the collagen or C100/G10 control sponges was significantly smaller than the diameters of the large, top surface pores of the funnel-like collagen or C100/G10 sponges. The mean diameters of the bottom surface pores of the collagen sponges were also smaller than were those of the funnel-like sponges.

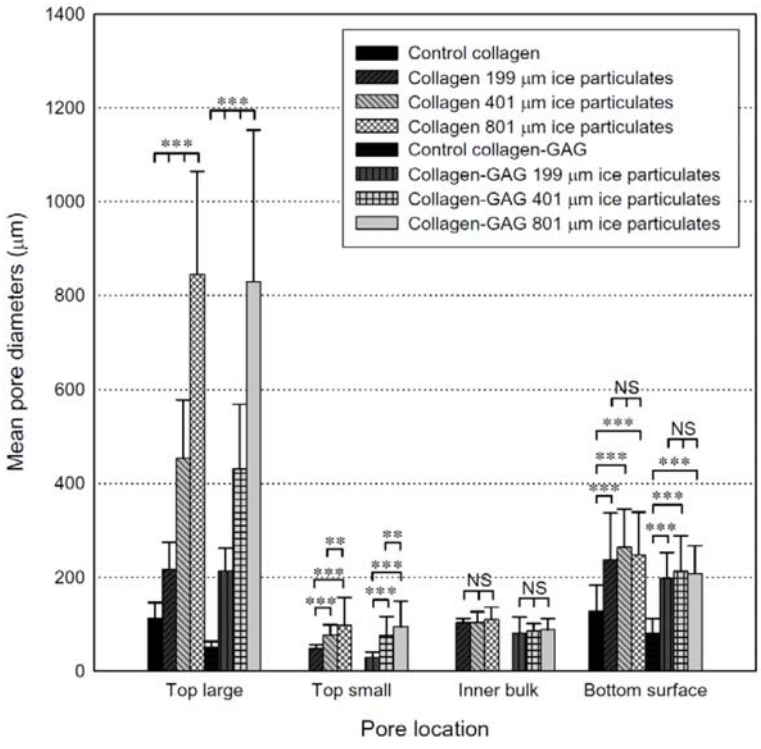

Figure 5.4 Pore diameter analysis of large, top surface pores; small, top surface pores; inner bulk pores; and bottom surface pores of the following sponges: control collagen (CC), funnel-like collagen (FC), control collagen-GAG (CCG), and funnel-like collagen-GAG (FCG) prepared at –3°C with 199, 401, 801 μm diameter ice particulate templates. Data are mean ± S.D. for n = 100 pores from 3 specimens of each condition. NS indicates not significant. ***$p<0.001$, **$p<0.01$, NS indicates not significant.

The results indicate that the dimension of the ice particulates significantly affected the sizes of the large, top surface pores and the small, top surface pores, but not the inner bulk pores and bottom pores. The effect of the ice particulates on the surface pore structure of the collagen-GAG and collage sponges was the same as that on funnel-like chitosan scaffolds reported in our previous study. Except for the effect of the embossing ice particulates, the temperature of freezing also affected the porous structure of the small, top surface pores and the inner bulk pores. A lower freezing temperature resulted in smaller pores [18].

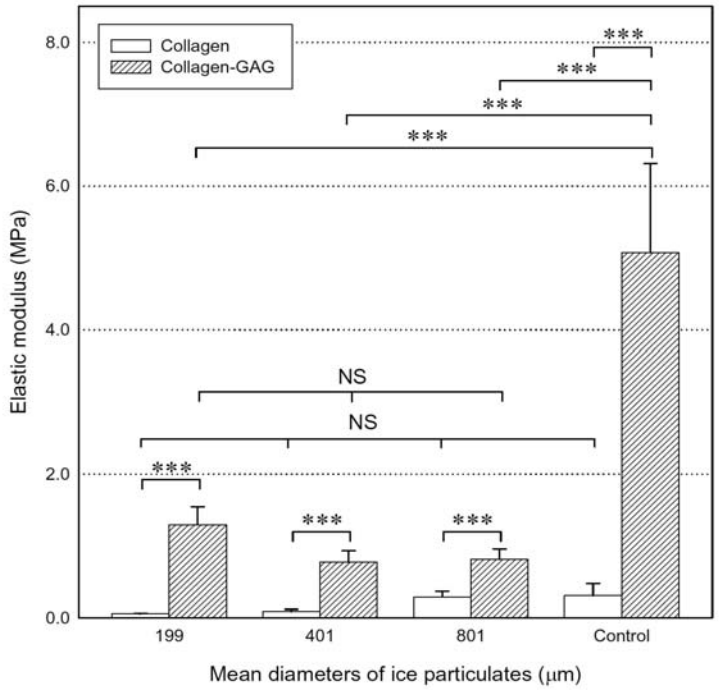

Figure 5.5 Young's moduli of funnel-like collagen-GAG sponges prepared with 199, 401, 801 μm diameter ice particulate templates. Data are mean ± S.D. of 3 samples. *** indicates a significant difference of $p < 0.001$.

5.4.3 Mechanical strength of collagen-GAG and collagen sponges

Young's moduli of the funnel-like and control sponges of C100/G10 and collagen were measured by a static tensile test (Figure 5.5). The C100/G10 sponges showed significantly higher tensile strength than did their respective collagen sponges. Incorporation of GAG in the collagen sponges increased the mechanical property. The C100/G10 control sponge had significantly higher mechanical property than did the funnel-like C100/G10 sponges. There were no significant differences in Young's moduli among the funnel-like C100/G10 sponges prepared with 199, 401, and 801 μm ice particulates. The collagen control sponge and funnel-like collagen sponge prepared with 801 μm ice particulates had significantly higher Young's moduli than did the funnel-like collagen sponges prepared with 199 and 401 μm ice particulates. Introduction of a funnel-like porous structure decreased the tensile strength of the collagen-GAG and collagen sponges. The effect of the dimension of the ice particulates on Young's moduli of the funnel-like sponges was

complicated. There was no effect of ice particulate dimension on the tensile strength of the funnel-like collagen-GAG sponges, but the tensile strength of the funnel-like collagen sponge increased when 801 μm ice particulates were used.

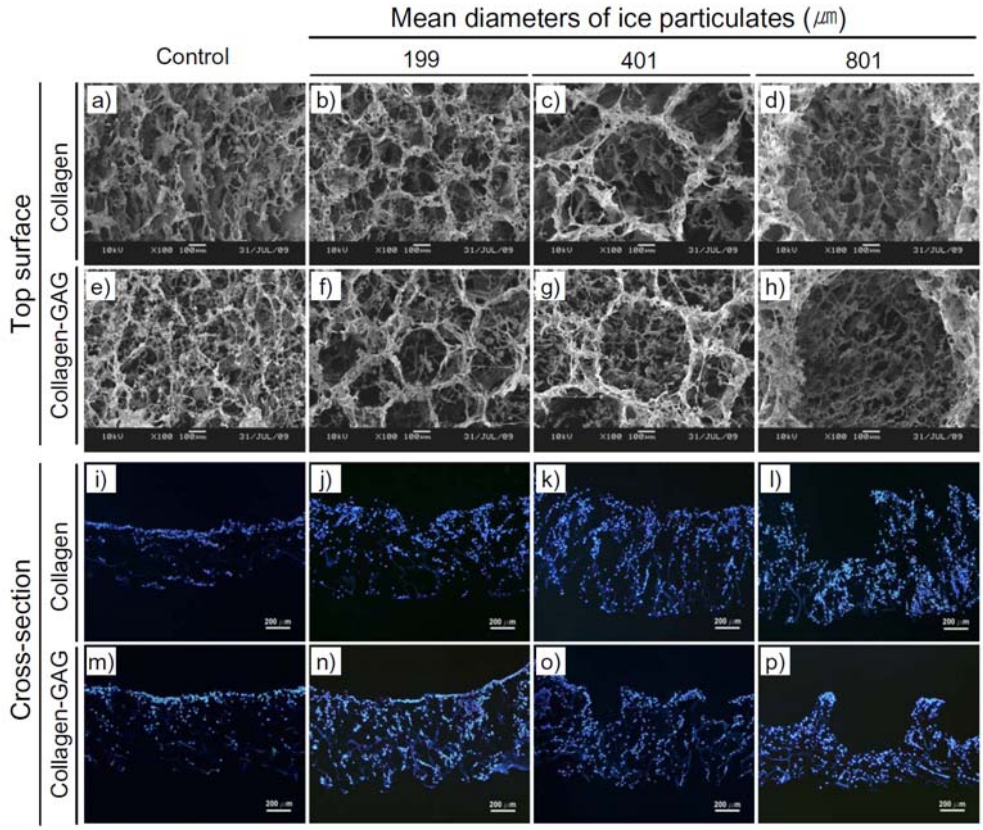

Figure 5.6 SEM photomicrographs (a-h) of top surfaces of control (a, e) and funnel-like (b-d, f-h) sponges of collagen (a-d) and collagen-GAG (e-h) and fluorescence photomicrographs of DAPI-stained cross sections of control (i, m) and funnel-like (j-l, n-p) sponges of collagen (i-l) and collagen-GAG (m-p) after fibroblasts were cultured in the sponges for 1 hour (a-h) and 24 hours (i-p).

5.4.4 Cell distribution and viability in the funnel-like sponges

In vitro cell culture experiments were performed to investigate the effect of pore structure and GAG addition on cell distribution and viability. Cell adhesion and distribution on the top surfaces of the control and funnel-like collagen and C100/G10 sponges were observed by SEM after four hours cell culture (Figure 5.6a-h). The fibroblasts adhered to the top surfaces of all the sponges and there was no evident difference among the sponges. After culture for 24 hours, the sponges were cross-sectioned and the cross-sections were stained with DAPI to visualize the presence of cellular nuclei. Observation with a fluorescence microscope demonstrated that cells were distributed in both the top surface and inner parts of the funnel-like sponges while mostly distributed only on the top surface of the control sponges (Figure 5.6i-p). The open pores on the top surface and the interconnected inner bulk pores facilitated cell penetration and improved spatial distribution in the funnel-like collagen-GAG and collagen sponges. The dense surface

pores and partially interconnected pores in the control sponges inhibited cell penetration into the inner part of the control sponges.

Cell viability was examined after fibroblasts were cultured in the funnel-like sponges for 24 hours using live/dead staining assay (Figure 5.7). The green colored objects indicate live cells and the red colored objects indicate dead cells. Fibroblasts showed good cell viability in all of the funnel-like collagen-GAG and collagen sponges. On the other hand, many dead cells were detected in the collagen-GAG and collagen control sponges. The spatially homogenous cell distribution in the funnel-like sponges prevented the stacking up of cells on the surface layer and thus increased cell viability.

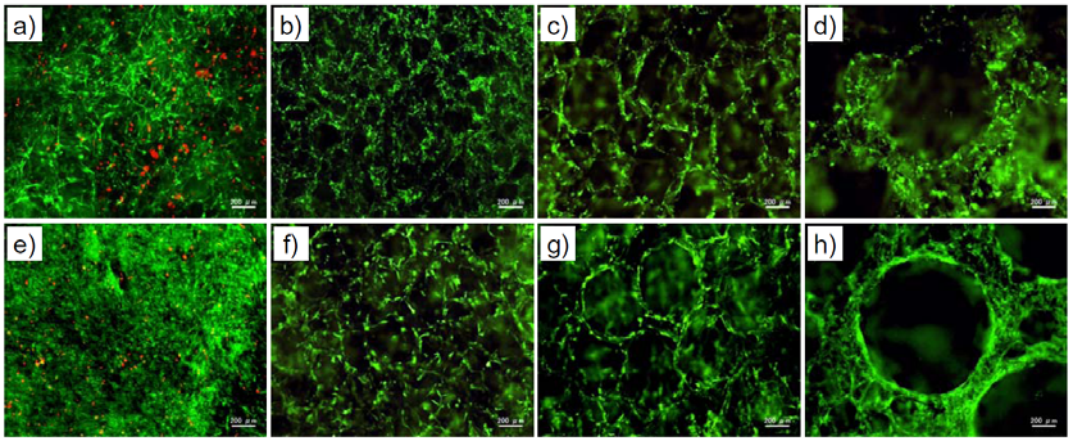

Figure 5.7 Fluorescence photomicrographs of live/dead stained fibroblasts after 24 hour culture in collagen (a) and collagen-GAG (e) control sponges, funnel-like collagen (b-d) and collagen-GAG (f-h) sponges prepared with templates embossed with ice particulates having diameters of 199 (b, f), 401 (c, g) and 801 μm (d, h). Scale bars = 200 μm.

The viability of fibroblasts after culture in the funnel-like collagen-GAG and collagen sponges was evaluated by WST-1 assay (Figure 5.8). The cells cultured in the GAG-incorporated scaffolds showed significantly higher viability than did the cells cultured in the collagen sponges. The results indicate that the incorporated GAG could maintain high cell viability.

5.4.5 Histological evaluation

After culture for two weeks, tissue formation was confirmed by histological staining (Figure 5.9). The cells cultured in the funnel-like sponges showed more homogenous tissue formation than did those cultured in the control sponges. The funnel-like sponges facilitated homogenous tissue formation. By comparing the funnel-like sponges prepared with ice particulates of 199, 401, and 801 μm in diameter, those prepared with 401 μm diameter ice particulates showed the least amount of void space and demonstrated the most homogeneous tissue formation. The funnel-like sponges prepared with 199 μm diameter ice particulates showed some aggregation of cells on their top surfaces because of the relatively small pores on the top surface. The funnel-like sponges prepared with 801 μm diameter ice particulates had sunken pores on the top surface that were too big.

In this study, GAG was introduced into collagen sponges to improve cell activation and mechanical properties. As expected, the GAG-introduced scaffolds showed higher tensile mechanical property and higher cell viability than did the collagen scaffolds. Introduction of GAG into collagen gel can increase the strength and stiffness of the gel [27]. The effect of the presence of GAG in collagen sponge has been reported to promote cell proliferation and migration [28, 29]. In the present study, a small amount of GAG significantly helped promote tissue formation within a short period.

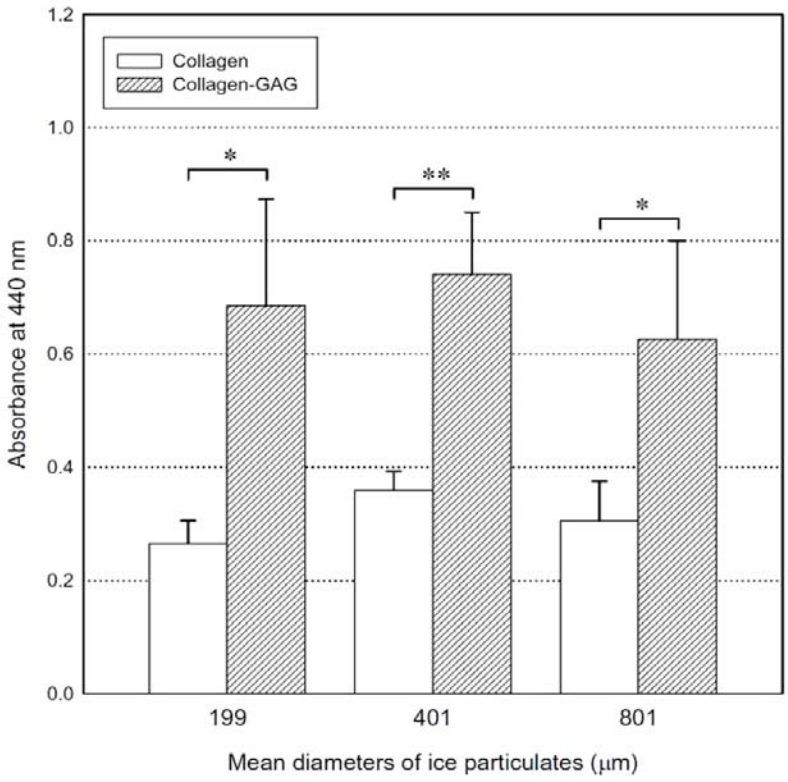

Figure 5.8 Cell viability evaluated by WST-1 assay after fibroblasts were cultured in funnel-like sponges for 14 days. Data are mean ± S.D. of 3 samples. * indicates a significant difference of $p < 0.05$; ** indicates a significant difference of $p < 0.01$.

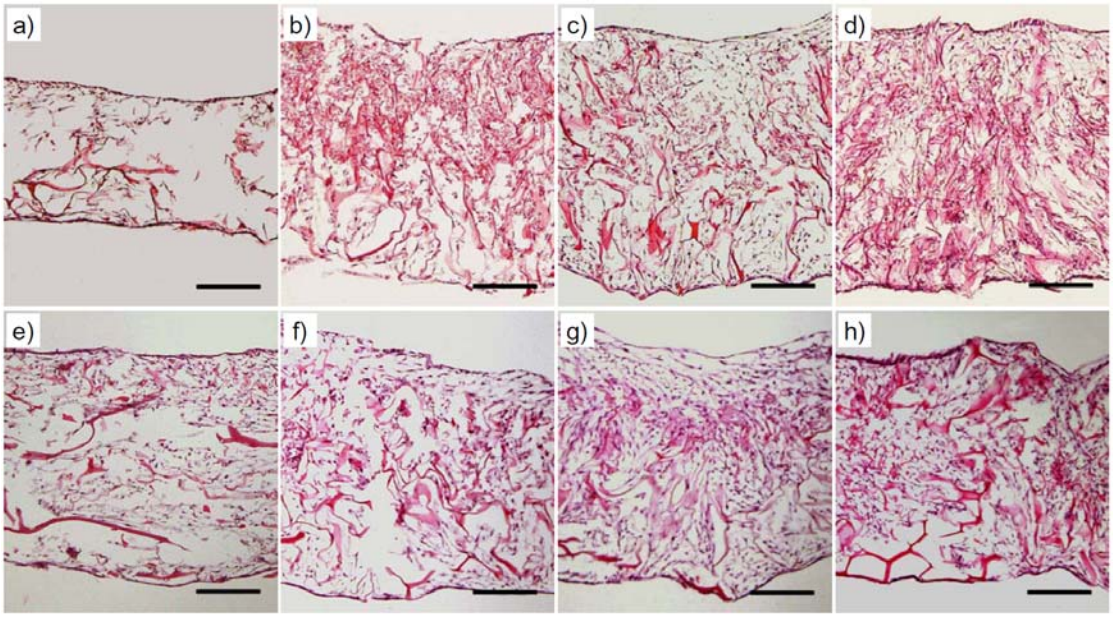

Figure 5.9 HE staining of fibroblasts after 14 days culture in collagen (a) and collagen-GAG (e) control sponges, funnel-like collagen (b-d), and collagen-GAG (f-h) sponges prepared with templates embossed with ice particulates having diameters of 199 (b, f), 401 (c, g), and 801 μm (d, h). Scale bars = 200 μm.

5.5 Conclusions

Open porous collagen-GAG scaffolds were prepared using embossed ice particulate templates. The open porous scaffolds showed a funnel-like porous structure that had large, top surface pores connected with inner bulk pores. The density and dimension of the ice particulates embossed on the template determined the structure of the large, top surface pores but did not affect the structure of the inner bulk pores. The funnel-like porous structure of the collagen-GAG scaffolds facilitated cell penetration and homogenous distribution within the scaffolds with good cell viability in contrast to poor cell penetration in the control scaffold. The incorporation of GAG in collagen scaffolds improved tensile mechanical properties and increased cell viability. The funnel-like collagen-GAG sponges will be useful for tissue engineering applications.

5.6 References

1 O'Brien, F. J., Harley, B. A., Yannas, I. V., Gibson, L. J., The effect of pore size on cell adhesion in collagen-GAG scaffolds. *Biomaterials* **26**, 433-441 (2005).

2 Harley, B. A. C., Kim, H. D., Zaman, M. H., Yannas, I. V., Lauffenburger, D. A., Gibson, L. J., Microarchitecture of three-dimensional scaffolds influences cell migration behavior via junction interactions. *Biophysic J* **95**, 4013-4024 (2008).

3 Lu, Q., Ganesan, K., Simionescu, D. T., Vyavahare, N. R., Novel porous aortic elastin and collagen scaffolds for

tissue engineering. *Biomaterials* **25**, 5227-5237 (2004).

4 Yannas, I. V., Burke, J. F., Gordon, P. L., Huang, C., Rubenstein, R. H., Design of an artificial skin. Ⅱ. Control of chemical composition. *J Biomed Mater Res* **14**, 107-131 (1980).

5 Dagalakis, N., Flinkt, J., Stasikelis, P., Burke, J. F., Yannas I. V. Design of an artificial skin. Part Ⅲ. Control of pore structure. *J Biomed Mater Res* **14**, 511-528 (1980).

6 Hiraoka, Y., Kimura, Y., Ueda, H., Tabata, Y., Fabrication and biocompatibility of collagen sponge reinforced with poly(glycolic acid) fiber. *Tissue Eng* **9**, 1101-1112 (2003).

7 Lee, M., Dunn, J. C. Y., Wu, B. M., Scaffold fabrication by indirect three-dimensional printing. *Biomaterials* **26**, 4281-4289 (2005).

8 Lee, S. J., Kim, S. Y., Lee, Y. M., Preparation of porous collagen/hyaluronic acid hybrid scaffolds for biomimetic functionalization through biochemical binding affinity, *J Biomed Mater Res B* **82B**, 506-518 (2007).

9 Lien, S. M., Ko, L. Y., Huang, T. J., Effect of pore size on ECM secretion and cell growth in gelatin scaffold for articular cartilage tissue engineering. *Acta Biomater* **5**, 670-679 (2009).

10 Salem, A. K., Stevens, R., Pearson, R. G., Davies, M. C., Tendler, S. J. B., Roberts, C. J., et al., Interactions of 3T3 fibroblasts and endothelial cells with defined pore features. *J Biomed Mater Res* **61**, 212-217 (2002).

11 Hsu, S. H., Yen, H. J., Tseng, C. S., Cheng, C. S., Tsai, C. L., Evaluation of the growth of chondrocytes and osteoblasts seeded into precision scaffolds fabricated by fused deposition manufacturing. *J Biomed Mater Res B* **80B**, 519-527 (2007).

12 Woodfield, T. B. F., Malda, J., de Wijn, J., Peters, F., Riesle, J., van Blitterswijk, C. A., Design of porous scaffolds for cartilage tissue engineering using a three-dimensional fiber-deposition technique. *Biomaterials* **25**, 4149-4161 (2004).

13 Chen, G., Sato, T., Ohgushi, H., Ushida, T., Tateishi, T., Tanaka, J., Culturing of skin fibroblasts in a thin PLGA-collagen hybrid mesh. *Biomaterials* **26**, 2559-2566 (2005).

14 Kumbar, S. G., Nukavarapu, S. P., James, R., Nair, L. S., Laurencin, C. T., Electrospun poly(lactic acid-co-glycolic acid) scaffolds for skin tissue engineering. *Biomaterials* **29**, 4100-4107 (2008).

15 Hollister, S. J., Porous scaffold design for tissue engineering. *Nature Mater* **4**, 518-590 (2005).

16 Atthoff, B., Aulin, C., Adelöw, C., Hilborn, J., Polarized protein membrane for high cell seeding efficiency. *J Biomed Mater Res B* **83B**, 472-480 (2007).

17 Lanza, R., Langer, R., Vacanti, J., editors., Principles of tissue engineering-3rd ed. MA:*Elsevier Academic Press*: 309-320 (2007).

18 Ko, Y.-G., Kawazoe, N., Tateishi, T., Chen, G., Preparation of chitosan scaffolds with a hierarchical porous structure. *J. Biomed. Mater. Res. B*, in press.

19 Lee, C. H., Singla, A., Lee, Y., Biomedical applications of collagen. *Internat J Pharm* **221**, 1-22 (2001).

20 Faraj, K. A., Kuppevelt, T. H. V., Daamen, W. F., Construction of collagen scaffolds that mimic the three-dimensional architecture of specific tissues. *Tissue Eng* **13**, 2387-2394 (2007).

21 Chvapil, M., Collagen sponge: Theory and practice of medical applications. *J Biomed Mater Res* **11**, 721-741 (1977).

22 Atala, A., Lanza, R., editors., Methods of tissue engineering. California:*Academic Press* (2002).

23 Zeltinger, J., Sherwood, J. K., Grahan, D. A., Műeller, R., Griffith, L. G., Effect of pore size and void fraction on cellular adhesion, proliferation, and matrix deposition. *Tissue Eng* **7**, 557-572 (2001).

24 Rodes, C., Smith, T., Crouse, R., Ramachandran, G., Measurements of the size distribution of aerosols produced by ultrasonic humidification. *Aerosol Sci Technol* **13**, 220-229 (1990).

25 Kang, H. W., Tabata Y., Ikada, Y., Fabrication of porous gelatin scaffolds for tissue engineering. *Biomaterials*

20,1339-1344 (1999).

26 Schoof, H., Apel, J., Heschel, I., Rau, G., Control of pore structure and size in freeze-dried collagen sponges. *J Biomed Mater Res B* **58**, 352-357 (2001).

27 Saddiq, Z. A., Barbenel, J. C., Grant, M. H., The Mechanical strength of collagen gels containing glycosaminoglycans and populated with fibroblasts. *J Biomed Mater Res A* **89**, 697-706 (2009).

28 Pieper, J. S., Oosterhof, A., Dijkstra, P. J., Veerkamp, J. H., van Kuppevelt, T. H., Preparation and characterization of porous crosslinked collagenous matrices containing bioavailable chondroitin sulphate. *Biomaterials* **20**, 847-858. (1999).

29 Pieper, J. S., van Wachem, P. B., van Luyn, M. J. A., Brouwer, L A., Hafmans, T., Veerkamp, J. H., van Kuppevelt, T. H., Attachment of glycosaminoglycans to collagenous matrices modulates the tissue response in rats. *Biomaterials* **21**, 1689-1699 (2000).

Chapter 6

Concluding remarks and future prospects

6.1 Concluding remarks

This thesis demonstrated a novel fabrication method of open porous polymeric scaffolds using an ice particulate template for tissue engineering. Porous scaffolds of collagen, chitosan, hyaluronic acid and collagen-glycosaminoglycan (GAG) were prepared by this method and their porous structures were characterized.

Chapter 1 introduces background and basic conception of tissue engineering with main factors of cells, scaffolds and growth factors. Design of a three-dimensional scaffold, methods of scaffold fabrication and cell culture technique are discussed. The existing preparation methods of three-dimensional porous scaffolds are summarized by comparing their advantages and drawbacks. Development of a new method for the preparation of scaffolds with controlled porous structures is motivated.

Chapter 2 describes the development of ice particulate template method and fabrication of open porous collagen scaffolds by adjusting various parameters. This chapter explains general process of ice crystallization and freeze-drying. A new-type of collagen sponge was prepared by using embossing ice particulates as a template. The collagen sponge had a hierarchical structure of large open pores on the top surface and interconnected small pores in the inner bulk body. The shape, size, and density of the surface large pores were determined by the ice particulates that were used as templates while the interconnected small pores were determined by the freezing temperature. Open porous collagen scaffolds were compared to control collagen scaffolds in regard to cell seeding efficiency, cell distribution and tissue formation. The unique porous structure of the new-type collagen sponge facilitated cell seeding, cell penetration, and distribution throughout the scaffold, and accelerated the regeneration of new tissue. The use of ice particulates as a template will be a useful method for the creation of an open and interconnected porous structure.

Chapter 3 describes the fabrication of open porous chitosan scaffolds using ice particulate templates. Various parameters were examined for homogeneous chitosan scaffolds. Scaffolds that prepared using ice particulate template method were compared to control chitosan scaffolds. Funnel-like chitosan sponges were prepared using an embossing ice template technique. The funnel-like chitosan sponges showed a hierarchical porous structure of large, open pores in the top surface layer and small, interconnected pores in the bulk layer. The characteristics of the large, top surface pores

were affected by the shape, dimension, and density of the embossing ice particulates, but not by the freezing temperature. The inner bulk porous structure was affected by the freezing temperature and not the embossing ice particulates. When cultured in the funnel-like chitosan sponge, the cells showed homogenous distribution, high viability, and constructed homogenous tissue. The unique porous structure of the funnel-like chitosan sponge facilitated homogenous cell seeding, improved cell distribution, and therefore promoted homogeneous tissue formation.

Chapter 4 describes the fabrication of open porous hyaluronic acid scaffolds using ice particulate template technique. Hyaluronic acid was very weak and easy to degrade in aqueous solution. To retard biodegradation of hyaluronic acid sponges, optimal crosslinking reagent and condition were investigated. In addition, pore size and structure of hyaluronic acid scaffold were analyzed. And cell distribution profile was evaluated by cell seeding of human dermal fibroblasts. Porous scaffolds of hyaluronic acid were prepared using embossed ice particulates as a template. The HA sponges showed a funnel-like porous structure that had large, top surface pores connected with underlying inner bulk pores. The pore structure of the large, top surface pores were determined by the density and dimension of the ice particulates embossed on the template. The freezing temperature did not affect the large, top surface pores. However, the inner bulk pores under the top surface pores were dependent on the freezing temperature while the ice characteristics of the ice particulates did not affect the structure of the inner bulk pores. The funnel-like structure in the HA sponge scaffolds prepared with ice particulates facilitated cell penetration and homogenous distribution in the scaffolds.

Chapter 5 describes the fabrication and establishment of open porous collagen-GAG scaffolds. Open porous collagen-GAG scaffolds were prepared using embossed ice particulate templates. The open porous scaffolds showed a funnel-like porous structure that had large, top surface pores connected with inner bulk pores. The density and dimension of the ice particulates embossed on the template determined the structure of the large, top surface pores but did not affect the structure of the inner bulk pores. The funnel-like porous structure of the collagen-GAG scaffolds facilitated cell penetration and homogenous distribution within the scaffolds with good cell viability in contrast to poor cell penetration in the control scaffold. The incorporation of GAG in collagen scaffolds improved tensile mechanical properties and increased cell viability.

In conclusion, a novel method has been developed to prepare porous scaffolds using ice particulates as a template. The method has been used to prepare funnel-like porous scaffolds of collagen, chotosan, hyaluronic acid and collagen-GAG. The funnel-like scaffolds had open surface pores and interconnected inner porous structures. The open surface pores were controlled by the dimension, shape and density of ice particulates. The inner bulk pores were affected by freezing temperature. The funnel-like porous scaffolds facilitated homogeneous cell distribution, improved cell viability and resulted in homogeneous tissue formation. The use of ice particulates as a template will be a useful method for the creation of an open and interconnected porous structure. The funnel-like porous scaffolds will be useful for tissue engineering.

6.2 Future prospects

This research provided a novel method for fabrication of open porous scaffolds and elucidated advantages of the open surface pores with high interconnectivity. Further study is required for conventional applications in tissue engineering.

First, design of precious structure is needed to regenerate uniform tissues and thickness scale upped sponges are challenged while keeping the advantages of open surface pore structures. To realize this issue, we could introduce patterned ice particulates that made by a robotic dispensing machine controlled by computer-aided design (CAD) system. And to scale up thickness, improvement of thermal transfer of an ice particulate template and large ice particles should be incorporated. Another approach is incorporation of ice particulates inside of collagen solution.

Second, biomechanical property should be investigated. Cells may induce contraction of cell-scaffold construct during culture. It causes deformation of expected dimension of engineered tissues. To solve this issue, hybridization with other mechanical strong materials should be applicable.

Third, cell differentiation experiment is needed using various types of cells for co-culture system.

Finally, induction of vascularisation and examination of metabolic transportation ability are necessary for future clinical application.

List of publications

1. Young-Gwang Ko, Naoki Kawazoe, Tetsuya Tateishi, Guoping Chen, Preparation of chitosan scaffolds with a hierarchical porous structure, Journal of Biomedical Materials Research Part B: Applied Biomaterials, In press.

2. Young-Gwang Ko, Hwan Hee Oh, Naoki Kawazoe, Tetsuya Tateishi, Guoping Chen, Preparation of open porous hyaluronic acid scaffolds for tissue engineering using the ice particulate template method, Journal of Biomaterials Science: Polymer Edition, In press.

3. Young-Gwang Ko, Naoki Kawazoe, Tetsuya Tateishi, Guoping Chen, Preparation of collagen sponges using an ice particulate template, Journal of Bioactive and Compatible Polymers, In press.

4. Young-Gwang Ko, Sarah Grice, Naoki Kawazoe, Tetsuya Tateishi, Guoping Chen, Preparation of collagen-glycosaminoglycan sponges with open surface porous structures using ice particulate template method, Macromolecular Bioscience, Accepted.

5. Hongxu Lu, Young-Gwang Ko, Naoki Kawazoe, Guoping Chen, Cartilage tissue engineering using funnel-like collagen sponges prepared with embossing ice particulate templates, Biomaterials, Submitted

Acknowledgements

I would like to acknowledge my sincere gratitude to my supervisor, Professor Guoping Chen for the guidance in this laboratory and advice on research and life in Japan. It is good opportunity to work with him these three years. And special thanks would be given to Dr. Naoki Kawazoe for detail supports and encouragement on my study.

I would also like to acknowledge the continuous assistance of every other member of the Polymeric Biomaterials Group, Professor Tetsuya Tateishi, Mrs. Setsuko Tsukamoto, and Mrs. Harue Nagata who helped me life in Japan and research. I would also like to acknowledge, Dr. Aiko Okamura, Dr. Xiaoming He, Dr. Taiyo Yoshioka, Dr. Michal Jerzy Wozniak, Dr. Takashi Hoshiba, Dr. Wenda Dai, Dr. Hongxu Lu who instructed me in laboratory skills and life of a researcher. And I would like to acknowledge, my colleges Mrs. Xiaoting Lin, Mr. Kazuyuki Sugiyama, Mr. Hiroyuki Kobayashi, Ms. Chieko Inoue, Ms. Tomoe Yamada, Ms. Fumiko Kamada, Mr. Michiyuki Yurugi, Mr. Kouki Hagiwara, Mr. Hwan Hee Oh, Mr. Wei Song, Ms. Sarah Grice, Ms. Akari Tanaka who helped me about many valuable things.

I would like to acknowledge thesis committee members, Professor Takao Aoyagi, Professor Shuichi Miyazaki, Professor Tetsushi Taguchi.

This work was performed at the Biomaterials Center on the National Institute for Materials Sciences (NIMS), Tsukuba. The work was sponsored by the NIMS-Tsukuba University doctoral program. I would like to acknowledge the financial support of the Doctoral Program in Materials Science and Engineering of Graduate School of Pure and Applied Science, the University of Tsukuba and the National Institute for Materials Science, Japan, without whose support this thesis would not have been possible. Thank you.

Lastly, I would like to thank my family, my father who has inspired me without any advice, and my mother and sister who supported me during study abroad, without whose help I may not have been able to complete my study.

Sincerely,
Young-Gwang Ko
January 2010